INTERIM REPORT

on

Grant NGL-10-005-089

(NASA-CR-142019) RESEARCH ON FISSION FRAGMENT EXCITATION OF GASES AND NUCLEAR PUMPING OF LASERS Interim Report (Florida Univ.) 181 p HC $7.00 CSCL 20E G3/36

N75-15972

Unclas 07774

RESEARCH ON FISSION FRAGMENT EXCITATION OF GASES AND NUCLEAR PUMPING OF LASERS

University of Florida

Professor R.T. Schneider
R. N. Davie
J. F. Davis
J. L. Fuller
R. R. Paternoster
G. R. Shipman
D. E. Sterritt

In Cooperation with

H. H. Helmick
Los Alamos Scientific Laboratory
(pages 4-19)

December, 1974

TABLE OF CONTENTS

INTRODUCTION		1
1.	Fission Fragment Excitation of Gases	2
	A. Experiments Performed at the Godiva Facility, Los Alamos Scientific Laboratory	4
	B. Description of the University of Florida Experiments	19
2.	Population Inversions in Fission Fragment Excited Helium	29
3.	Direct Nuclear Pumping of a Helium-Xenon Laser	40
4.	Nuclear Augmentation of Gas Lasers	48
5.	Measurements of a Repetitively Pulsed High-Power CO_2 Laser	57
6.	Measurement of Thermodynamic Properties of UF_6 and UF_6/He Mixtures (Ballistic Piston Compression Experiments)	128
7.	Nuclear Waste Disposal Utilizing a Gaseous Core Reactor	138

INTRODUCTION

This report summarizes the work done under grant NGL10-005-089 during the fiscal year 1974. Some of this work was done in cooperation with the Los Alamos Scientific Laboratory.

Some of the work reported herein has been previously presented in scientific meetings and journals.

Much of the reported work is presently in progress and a final evaluation of all the data has not yet been made. Therefore this report should be understood as an intermediate progress report on on-going research.

INVESTIGATION OF FISSION FRAGMENT EXCITED GASES

by

John F. Davis
G.R. Shipman
Robert N. Davie
H.H. Helmick*

ABSTRACT

A spectroscopic investigation of fission fragment produced plasma was performed. Described are the experimental apparatus at the Los Alamos Scientific Laboratory and also at the University of Florida. A variety of gases and gas mixtures were studied including He, Ar, Xe, CF_4, UF_6-He, He-Xe, Ar-Xe. Gross light emission as well as spectroscopic information was obtained.

*Los Alamos Scientific Laboratory principal investigator under NAS contract W13,761.

INVESTIGATION OF FISSION FRAGMENT EXCITED GASES

Introduction

The spectroscopic analysis of the radiation produced in gases by ionizing radiation is a valuable tool in understanding the processes involved. Despite efforts of researchers over the past several years, the interaction of charged particles with gases is not fully understood.

The emitted radiation from the gas is directly a result of the charged particle interaction but is also dependent upon the interaction processes in the gas itself. The problem may be divided into three important parts: (1) energy loss by the incident particle $(\frac{dE}{dx})$ through excitation of the stopping gas; (2) effects taking place within the pure gas after the excitation has been produced; and (3) subsequent effects resulting from the presence of small quantities of impurities.

The purpose of this research was to investigate the processes involved in the fission fragment excitation of gases as follows: (1) to investigate the spatial distribution of excitation caused by fission fragments emerging from a planar source and (2) to study the interaction processes of a primary gas with impurities under excitation by fission fragments. A basic understanding of the processes occurring within the gas itself can provide the foundation for the development of a direct nuclear (fission fragment) pumped laser.

Experiments Performed at the Godiva Facility, Los Alamos Scientific Laboratory*

Description.--The objective of the experiment described is to perform spectroscopic studies of the emission spectra in the visible and ultraviolet of ultra pure gases and gas mixtures under irradiation by a cylindrical or planar source of fission fragments. Several gases and gas mixtures at different pressures will be studied.

A general schematic of the experiment at LASL is shown in Figure 1. The fission fragments are furnished by the interaction of a 10 micron 93% enriched Uranium foil mounted coaxially in the test cell and the neutrons furnished by the fast-pulsed reactor assembly, Godiva IV.

Godiva IV is a bare reactor capable of reproducible super-prompt critical bursts. A typical reactor burst will produce approximately 10^{16} neutrons in a pulse about 100 usec wide (full width at half maximum). The bare reactor is 6.9 inches in diameter and 5.7 inches high and weighs 64 kilograms. The reactor was mounted on a stand that could be easily rolled up to the experimental apparatus. This versatility of the reactor had a tremendous advantage of eliminating radiation exposure of personnel and test equipment when major work was performed upon the test equipment. The reactor was rolled up to the test section during reactor operation. The aluminum test section was approximately three feet long and 1.5 inches in diameter. A two-inch thick polyethylene neutron moderator was placed around the test section. One end of the section was sealed by a quartz window used for viewing the fission fragment plasma via closed circuit television for laser alignment of optics and as a light entry point for the Mercury calibration lamp. The other end of the test section was sealed by a two-inch diameter ten-inch focal length quartz lens. The cylindrical Uranium foil, 16 inches long and 1.5 inches in diameter, was mounted in the test section such that the center of the foil was approximately

*Cooperative effort with Los Alamos Scientific Laboratory (H.H. Helmick, Principal Investigator of NASA Contract W13,761).

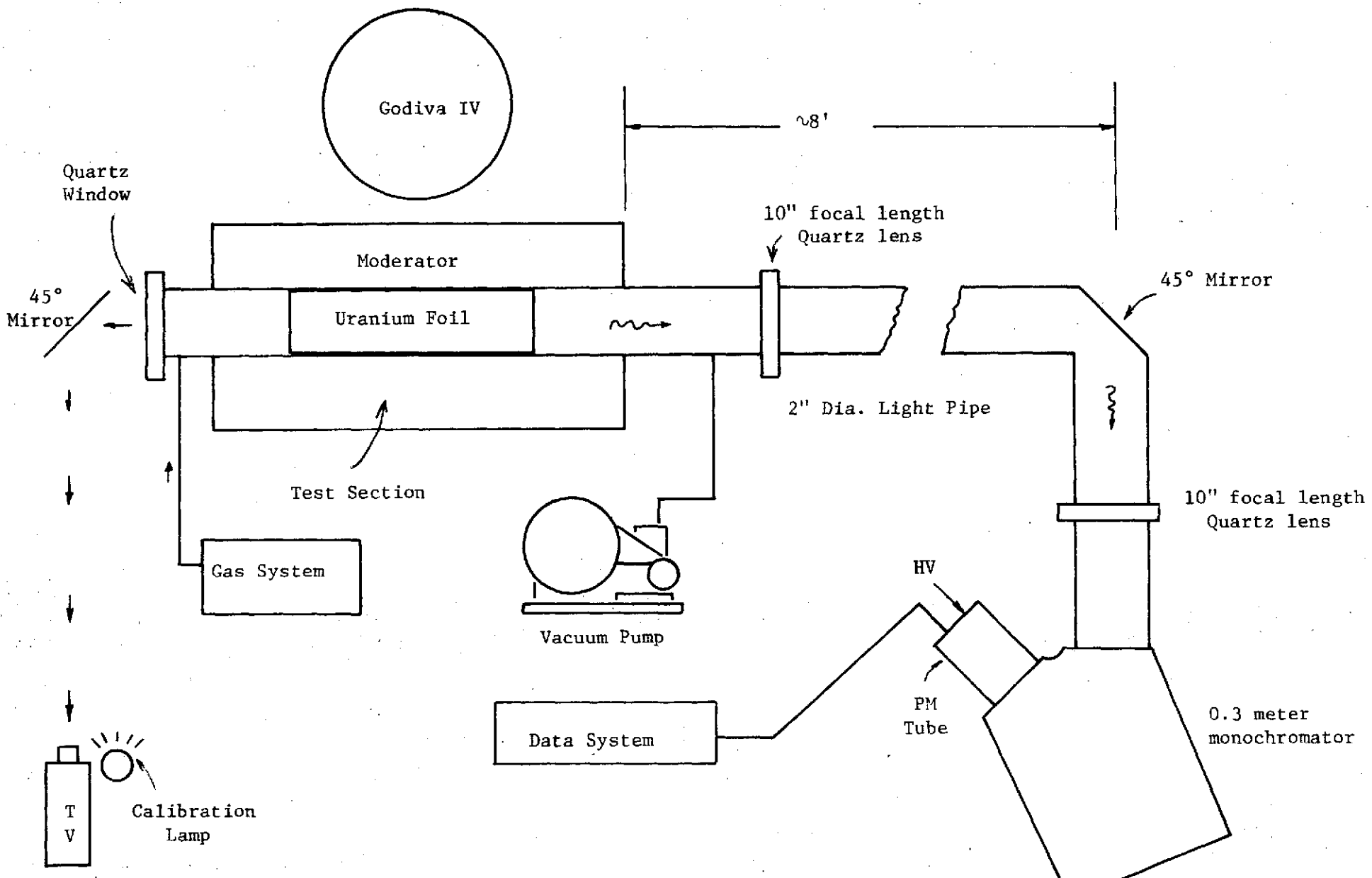

Figure 1. General Schematic.

one focal length (10 inches) from the quartz lens. Thus the test gases and fission fragments were confined to the test section.

The reactor and experimental apparatus was housed in a reactor assembly building (Kiva III) situated approximately 1200 feet from the main control building. This made it necessary that the reactor, spectrograph, calibration lamp, and gas handling apparatus be remotely controlled. A schematic of the gas handling system is shown in Figure 2. A variety of gases of gas mixtures could be leaked into the test cell by remotely controlled air-activated valves. The test gas pressure was monitored remotely in the control room by a closed circuit television system. Of special interest were the requirements in the gas handling system for UF_6. The vapor pressure of UF_6 is 100 torr at STP. Therefore, for tests involving higher UF_6 pressures, the UF_6 bottle, gas handling system, and test section had to be heated. To prevent condensation in the system the test section and has handling system had to be heated to a higher temperature than the UF_6 bottle. This was accomplished through the use of heating tapes and asbestos insulation. The UF_6 bottle, cold trap, and test section's temperature were monitored continuously with thermocouples and a four track strip chart recorder. Since UF_6 reacts with water vapor or hydrogen bearing compounds to form HF which is detrimental to rubber seals and quartz optics, the system was healium leak tested and evacuated for several days to clean the system out of water and water vapor. Only research grade gases were used to prevent the introduction of impurities into the system. Since the UF_6 attacks the oil in the roughing pump, a trap consisting of 75% soda lime and 25% activated Al was connected in the vacuum system in front of the roughing pump.

Data was taken by two methods. A secondary method was via observation of the closed circuit television. The primary system consisted of a light pipe

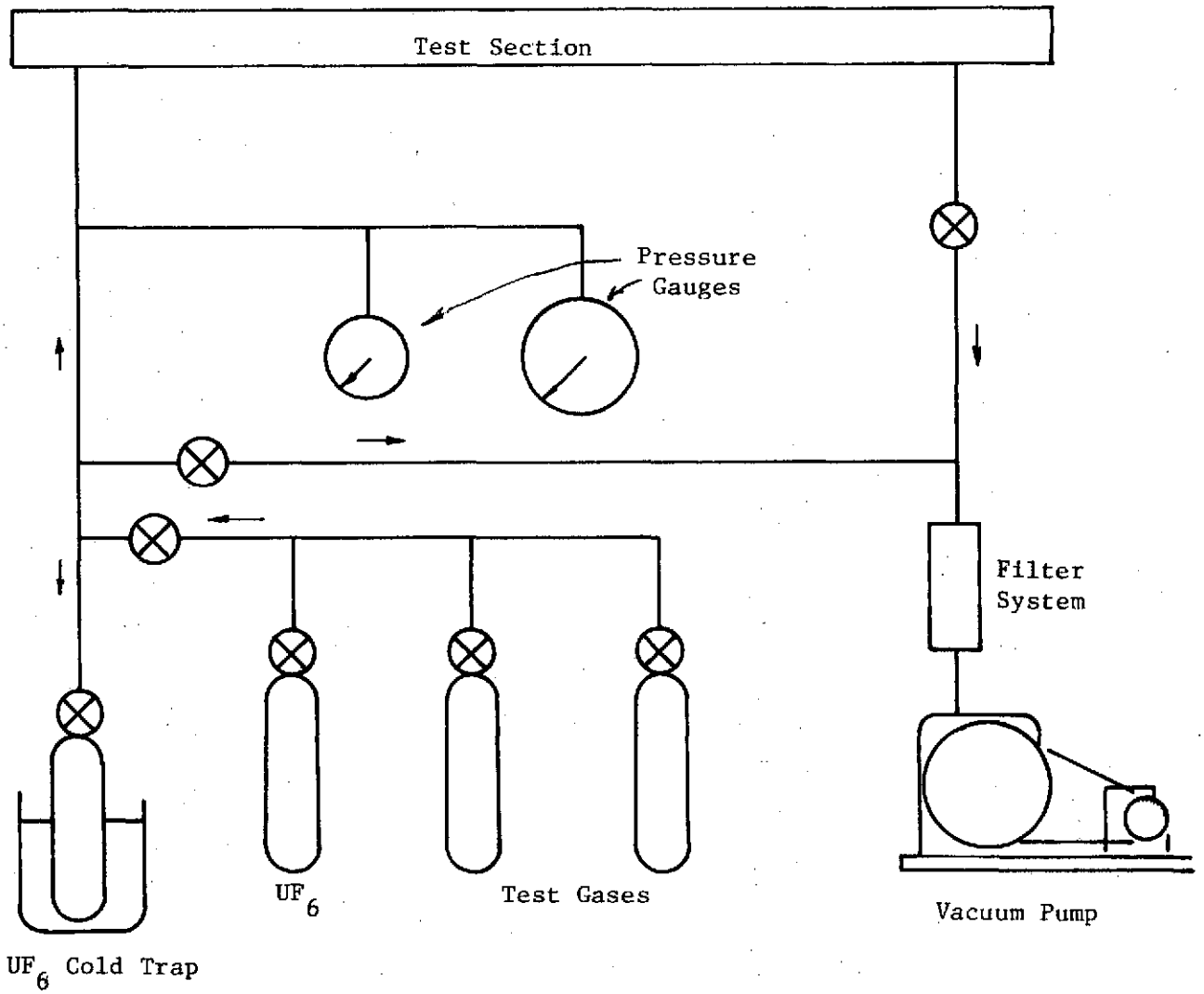

Figure 2. Gas System.

connected to the test section, lenses mounted in the light pipe, a monochromator and a photomultiplier tube. A general schematic of the optical arrangement can be seen in Figure 1. Two lenses were mounted in the light pipe as shown in the figure. Both lenses were quartz, two inches in diameter, and had ten-inch focal lengths. One lens was mounted at the end of the test section approximately one focal length from the center of the Uranium foil. The other lens was mounted in the light pipe one focal length from the monochromator entrance slit. This condensing lens had a f# of 5.7 which closely matched the monochromator f# of 5.3. System alignment was accomplished with a Helium-Neon alignment laser and calibration spectra were taken with a Mercury Oscram lamp. The monochromator used was a 0.3 meter McPherson Model 218 with interchangeable gratings. For the present experiments, a 1200 line/mm grating blazed at 3000 Å and a 2400 line/mm grating balzed at 1500 Å were used. The grating drive was connected to a stepping motor controlled by the Data Acquisition System. The grating drive mechanism established the grating driving rate at 4 steps per Å with the 1200 line/mm grating and 8 steps per Å with the 2400 line/mm grating. The monochromator entrance and exit slits were set at 100 microns. The photomultiplier tube used was a EMI with a S20Q cathode. The characteristics of this tube are shown in Figure 4. The high noise level produced from the interaction of reactor gamma rays with the PM tube made it necessary to use extensive shielding. The shield consisted of 2 x 4 x 8 inch lead bricks, cadmium sheets, borated polyethylene and lo-inch thick concrete. Inside this massive assembly was housed the monochromator and attached PM tube.

A schematic of the data acquisition system is shown in Figure 3. The output of the PM tube went into a line driver which provided the signal to an analog computer mounted 1200 feet away in the main control room. The analog computer was programmed to provide signal gain, RC filtering, and signal matching

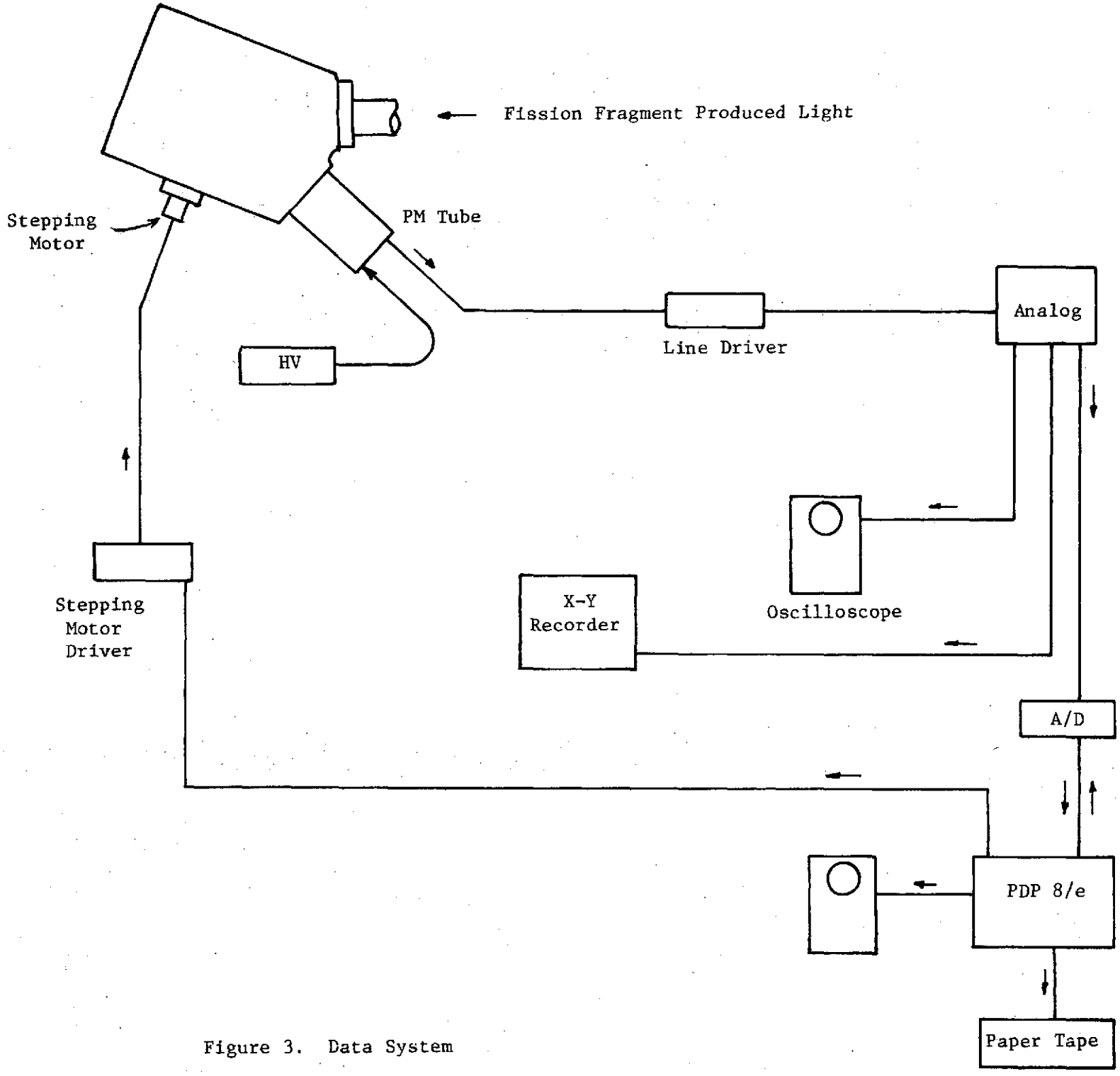

Figure 3. Data System

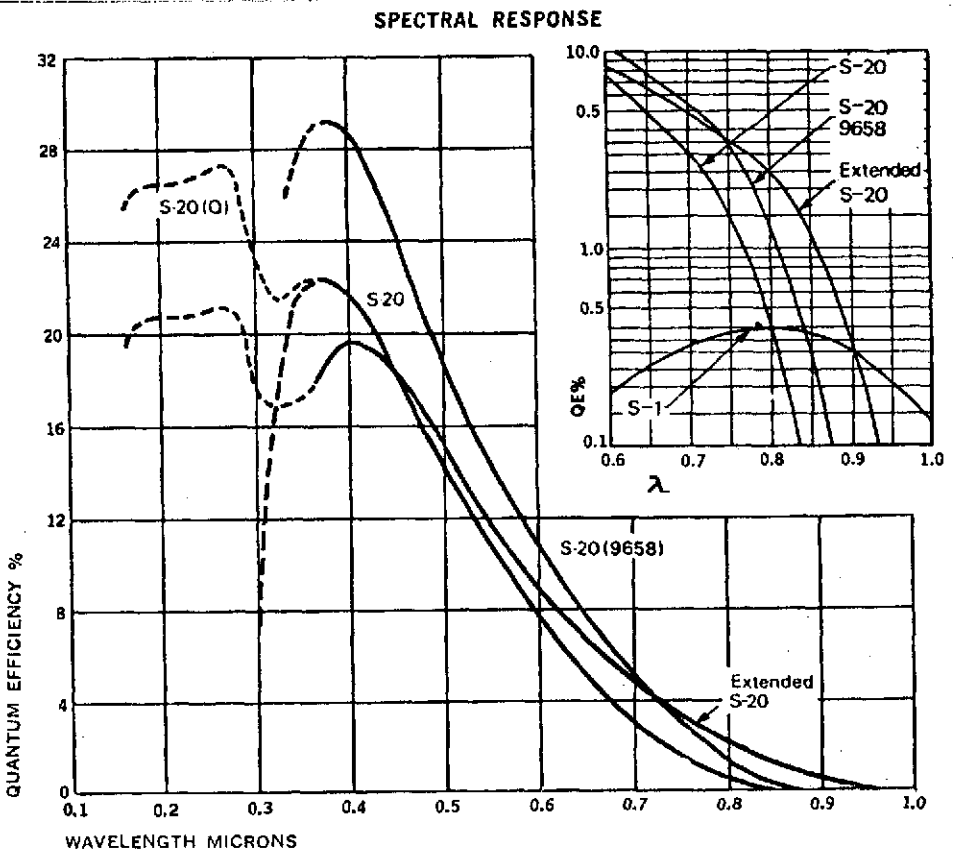

FIG 4. EMI 9558 PM Tube, S20Q Response Curve

to the analog-to-digital converter (ADC). The output of the ADC was sent to a Digital PDP8/e central processing unit which provided signal averaging, data acquisition rate, data storage on paper tape and controlled the stepping motor grating drive on the monochromator.

Data storage was accomplished by three methods. Data from reactor bursts was recorded by photographing oscilloscope traces, and directly by an X-Y recorder. Data taken during steady state reactor operation was taken on an X-Y recorder and by paper tape output from the control processing unit. The paper tape output could be analyzed by a storage oscilloscope on site or further analyzed by the central computer facility at LASL which provided computer digital printout and graphical display on 35 mm film.

Experimental Results

He, Ar, Xe.--All experiments were performed with the experimental setup as described above. Initial experiments were tried with Helium and Xenon with minimum shielding. The reactor was operated steady state at 8 kilowatts with gas pressure a variable between 10 torr to one standard atmosphere (3.5 psi). In the initial experiments, no significant light signal could be distinguished above the high noise level produced by gamma ray interaction with the PM tube. Due to this high noise level, more massive shielding was installed. This reduced noise significantly but not enough so that we could produce spectral scan data of any value with Helium, Xenon, or Argon.

Some interesting observations were noted when using Xenon gas: (1) for steady state reactor power at 8 kW and Xe pressure at approximately 280 torr the glow observed on the television screen began to die away after 1.5 to 2 minutes. (2) with the reactor at a steady state power of 8 kW, as the Xe pressure was increased from zero to 70 torr the signal on the PM tube increased

very rapidly, but no apparent glow could be seen on the television. As the pressure was increased to 200 torr, a glow began to appear on the television monitor, but the PM tube signal did not increase. At 230 torr the signal was peaked on television and also on the PM tube. As the pressure was increased above 230 torr, the fission fragment plasma no longer filled the entire test section volume and began to recede towards the walls, with subsequent loss of signal. This would indicate that there is a shift of spectral output with pressure. No other significant information could be gathered at this time.

UF_6 + Ar, UF_6 + He.--Relative light intensity measurements were made with UF_6 + Ar and UF_6 + He by using the PM tube signal and scanning across zero order with the monochromator. At a steady state reactor power of 8 kW, 6 torr UF_6 and 160 torr Argon produced a 1.0 volt signal above noise. A 20 torr UF_6 and 180 torr Argon mixture produced a 0.8 V signal above noise. For UF_6 alone, no signal was observed from 0 to 160 torr. In all cases, as the percent of UF_6 increased the light output decreased. For a 4 torr UF_6 and 60 torr He mixture, the signal was 0.8 V above noise and as the He or UF_6 pressure was increased, the signal decreased.

CF_4 Studies.-- Scintillation studies at the University of Florida using CF_4 gas stimulated by a Cf^{252} source indicated significantly more light emission than by the noble gases and tremendous light multiplication with a HV field applied. Therefore, the test section at Los Alamos was modified to accommodate a Tungsten 10 mil center wire to provide a concentric electrode configuration. A series of experiments were run with variable reactor power, CF_4 pressure and voltage on the center wire. Only the total light output was monitored with the monochromater in zero order or scanning across zero order. These results can be seen in Figures 5, 6, 7, and 8. Significantly more light output was observed with CF_4 than with previous gases.

Figure 5. INTENSITY vs. REACTOR POWER

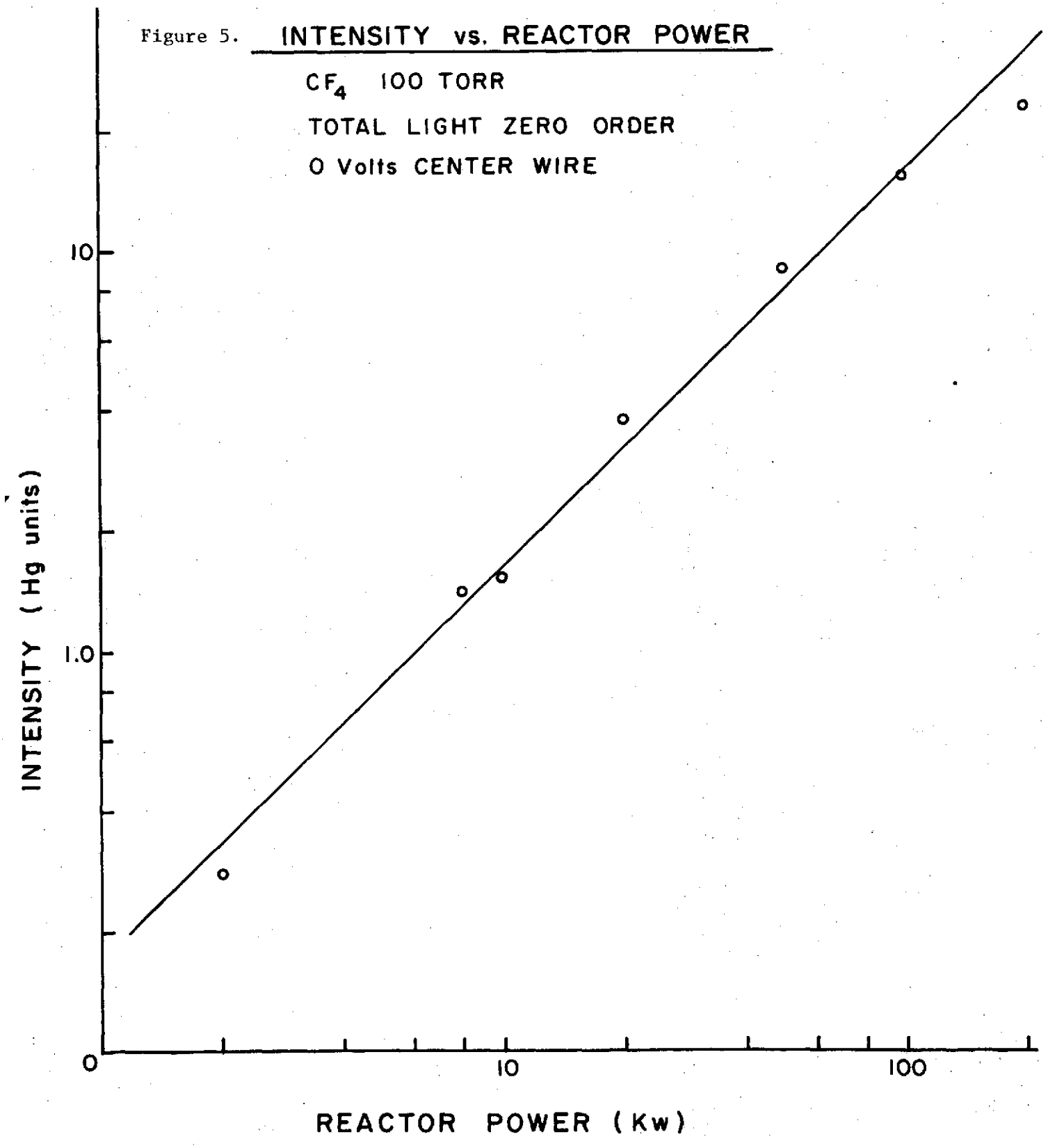

Figure 6. NEUTRON FLUX IN CAVITY

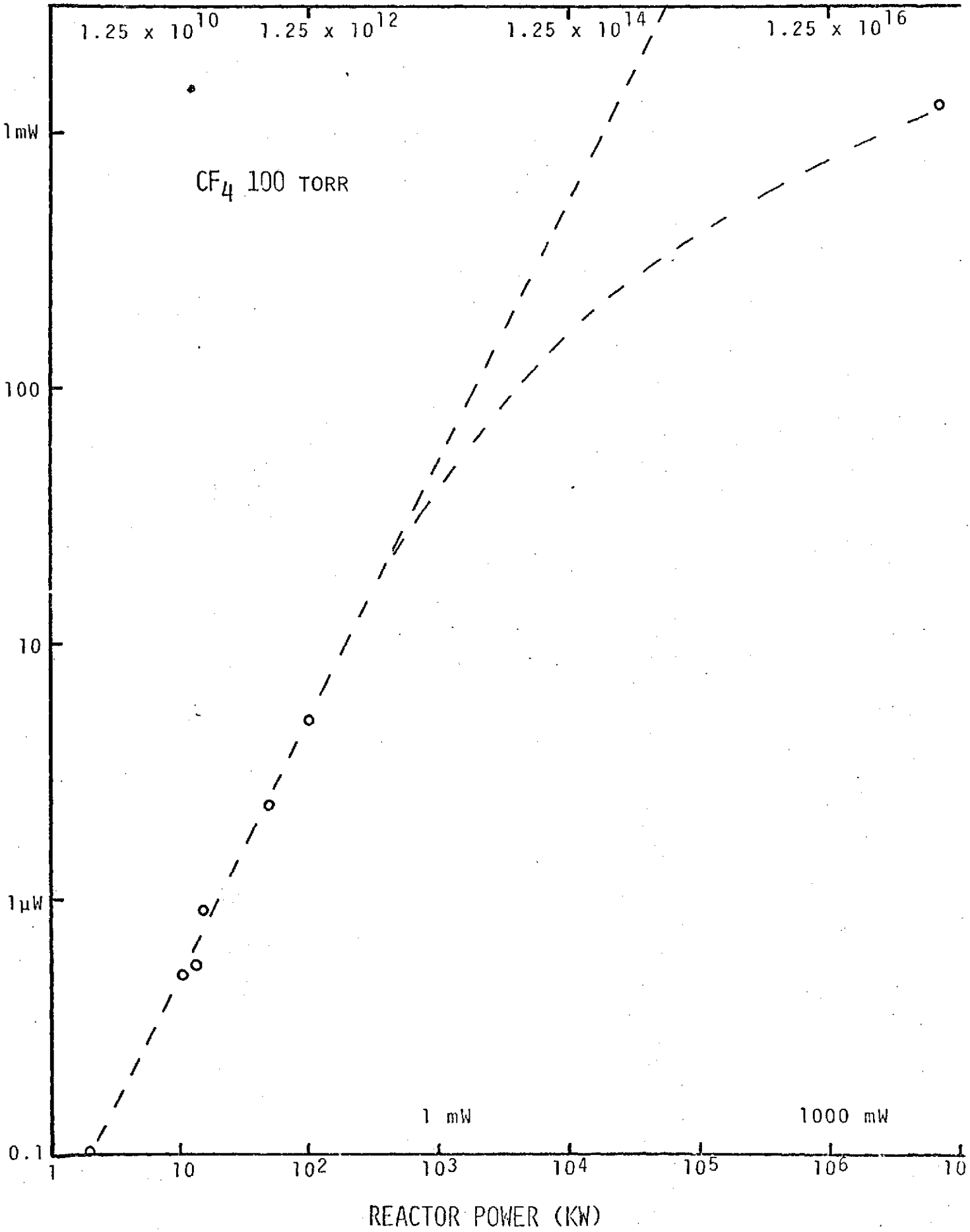

Figure 7

LIGHT OUTPUT FROM 100 TORR CF_4

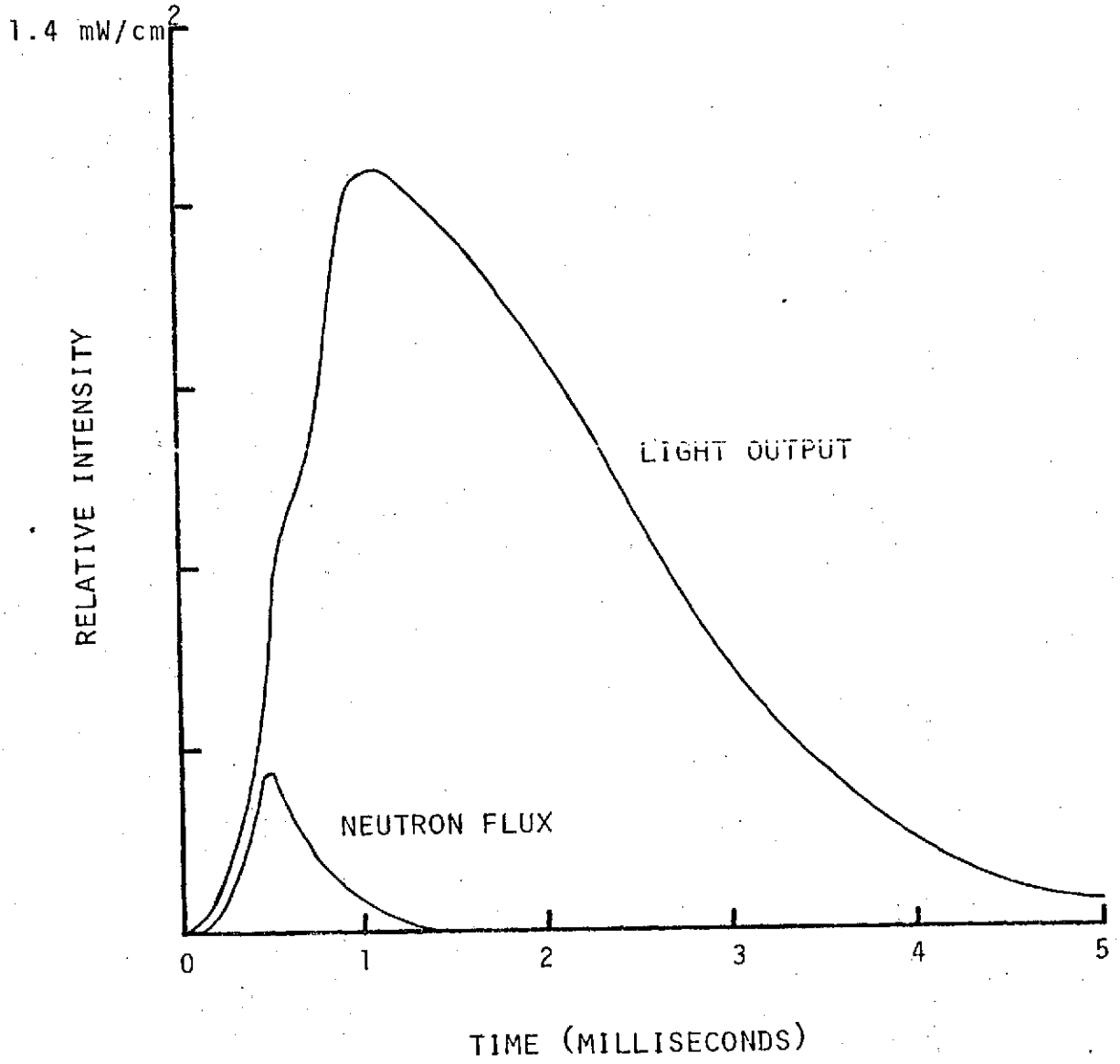

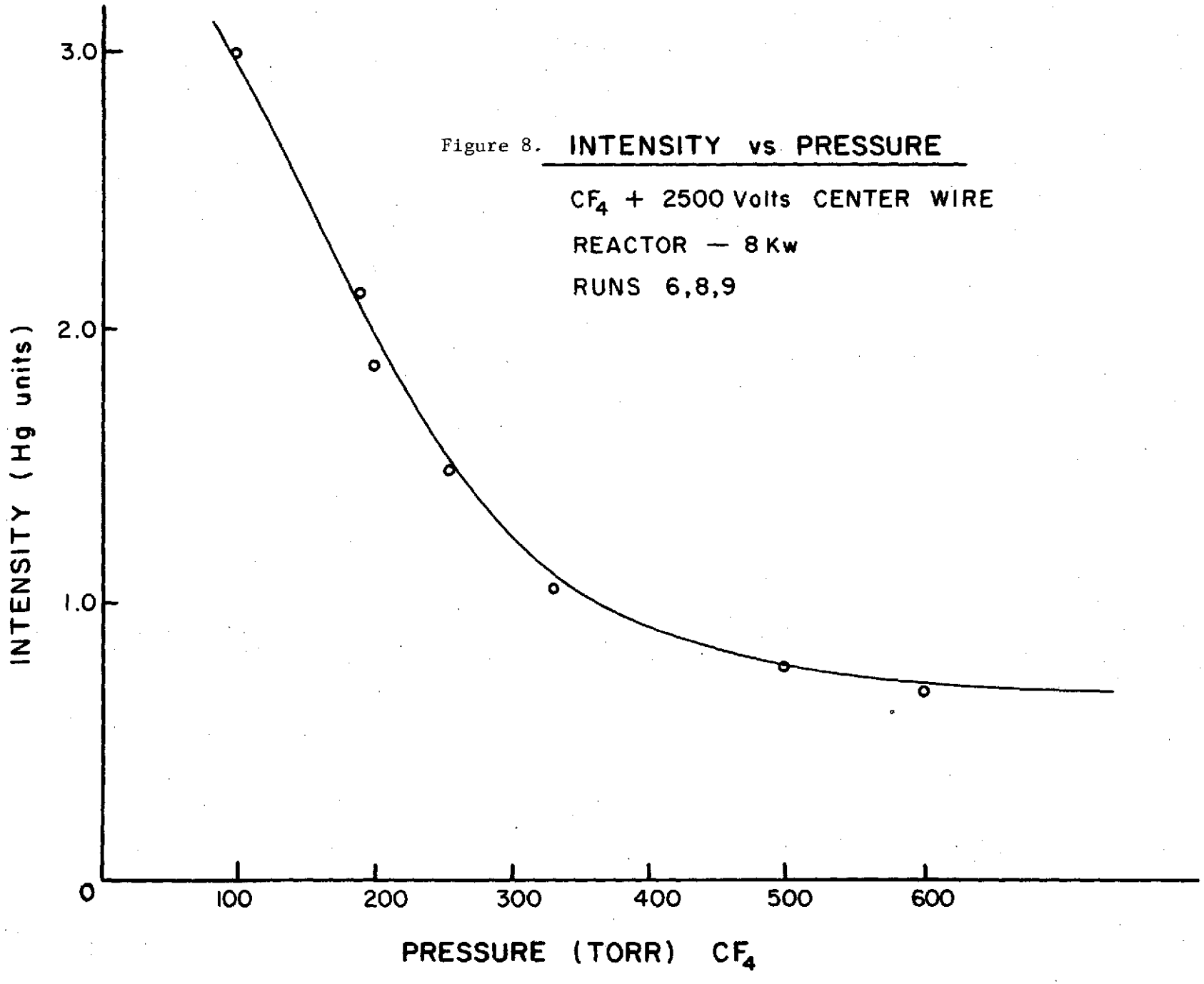
INTENSITY vs PRESSURE
CF4 + 2500 Volts CENTER WIRE
REACTOR — 8 Kw
RUNS 6,8,9
INTENSITY (Hg units)
3.0
2.0
1.0
0
100
200
300
400
500
600
PRESSURE (TORR) CF4

Figure 8.

Figure 9

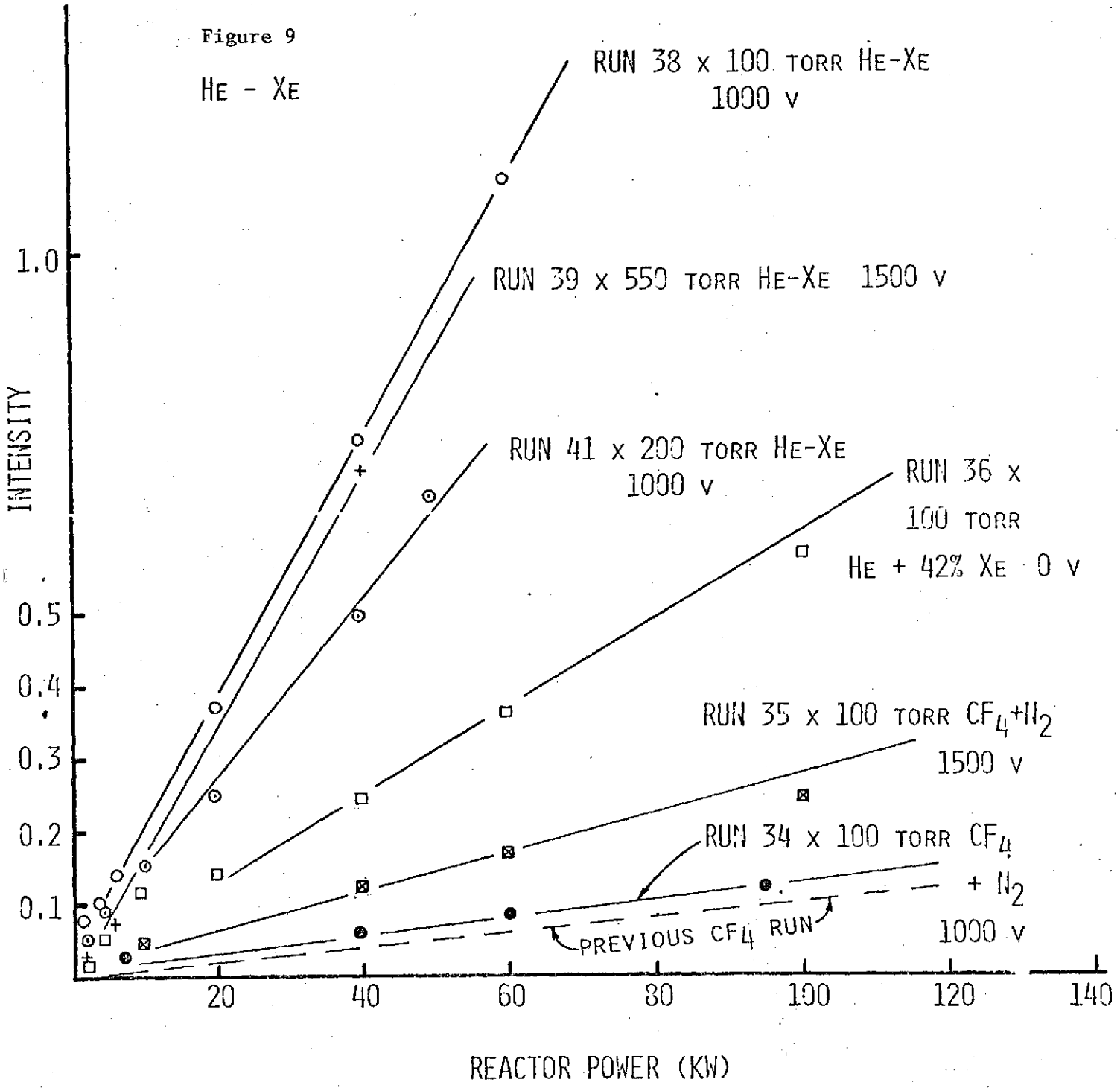
He - Xe
RUN 38 x 100 torr He-Xe
1000 v
RUN 39 x 550 torr He-Xe 1500 v
RUN 41 x 200 torr He-Xe
1000 v
RUN 36 x
100 torr
He + 42% Xe 0 v
RUN 35 x 100 torr CF_4+N_2
1500 v
RUN 34 x 100 torr CF_4
+ N_2
1000 v
PREVIOUS CF_4 RUN
INTENSITY
1.0
0.5
0.4
0.3
0.2
0.1
20
40
60
80
100
120
140
REACTOR POWER (KW)

Figure 10

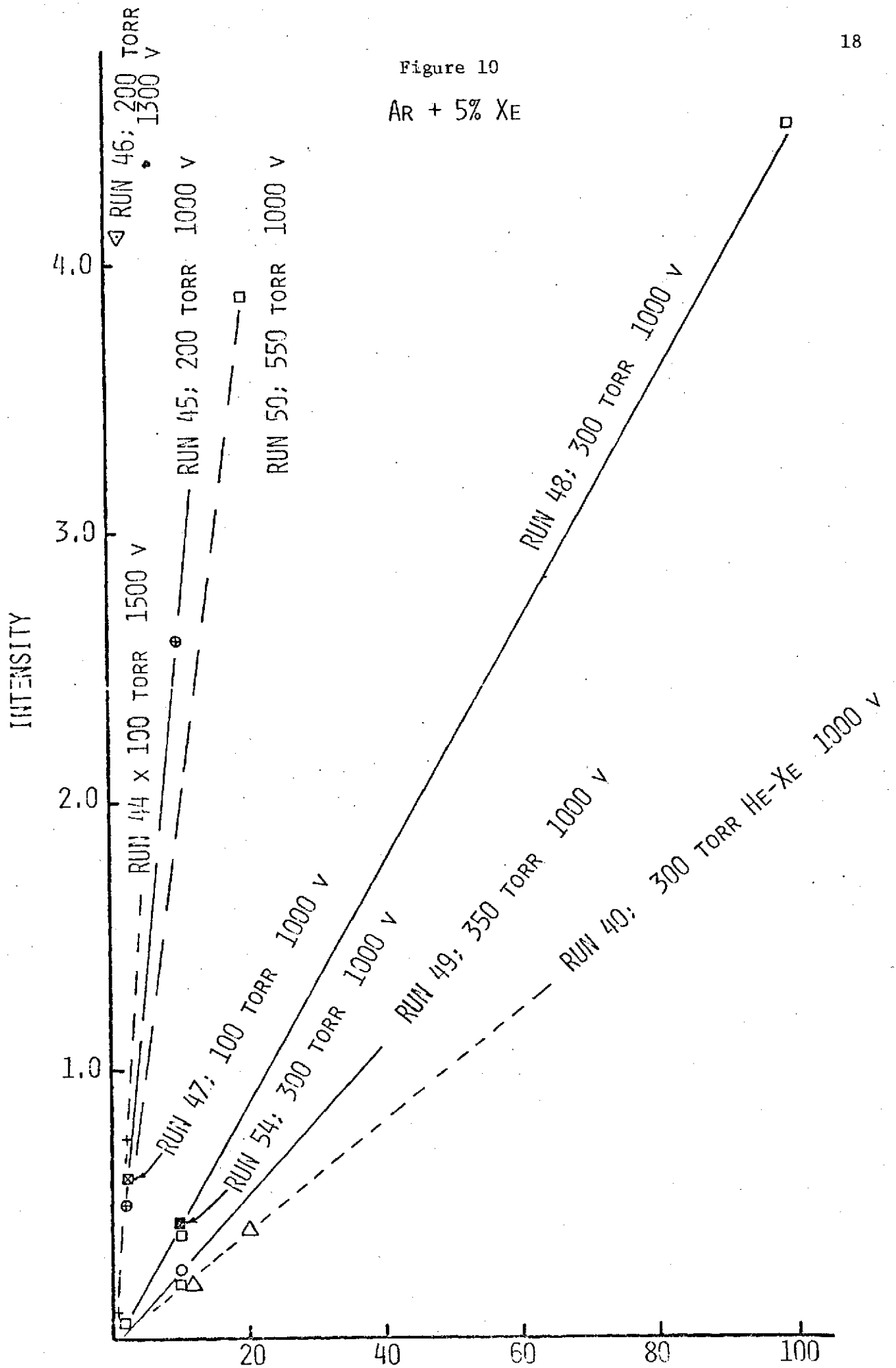
AR + 5% XE
INTENSITY
4.0
3.0
2.0
1.0
20
40
60
80
100
RUN 46; 200 TORR 1300 V
RUN 45; 200 TORR 1000 V
RUN 50; 550 TORR 1000 V
RUN 48; 300 TORR 1000 V
RUN 44 x 100 TORR 1500 V
RUN 47; 100 TORR 1000 V
RUN 54; 300 TORR 1000 V
RUN 49; 350 TORR 1000 V
RUN 40; 300 TORR HE-XE 1000 V

He-Xe, Ar-Xe.--In line with efforts to improve the signal to noise problem, other gases mixtures were tried that were very encouraging. Similar experiments as those with CF_4 were tried with a mixture of 50% He-50% Xe and Ar and 5% Xe. The results of these experiments are shown in Figures 9 and 10. For the He-Xe mixture, an increase in light intensity by more than a factor of 10 was observed over CF_4. For the case of Ar + 5% Xe mixture, a factor of 4 to 5 increase in light intensity was observed over the He-Xe mixture. These initial results indicated that for the several gas mixtures studied, the total light output was linear with reactor power up to 100 kW. To date, the Ar + 5% Xe mixture has shown the highest light output.

Description of the University of Florida Experiments

The design of the experiment for insertion into the University of Florida Training Reactor was primarily based on the experiences with the LASL experiments. Of primary interest is the high noise level produced by gammas on the photomultiplier detector. Also of importance is the requirement for high system and gas purity. Other factors are: low expected light output, possible radiation damage to the in-pile parts of the system, possibleheat dissipation problems from fissionable material, and UFTR safety requirements. The present experiment is shown schematically in Figure 11.

The heart of the system is the multi-purpose capsule for the irradiation of gases (MCFIG) which is a high quality vacuum tight system containing the gases under study and a cylindrical or plane foil coated with 93% enriched UO_2 along the inside wall of the capsule. The MCFIG was inserted into the center core region of the UFTR via the horizontal port and subjected to a flux of approximately 1.8×10^{12} $n/cm^2 sec$. Light emission from 1600 Å to 3 microns can be observed through a sapphire window mounted at one end of the MCFIG.

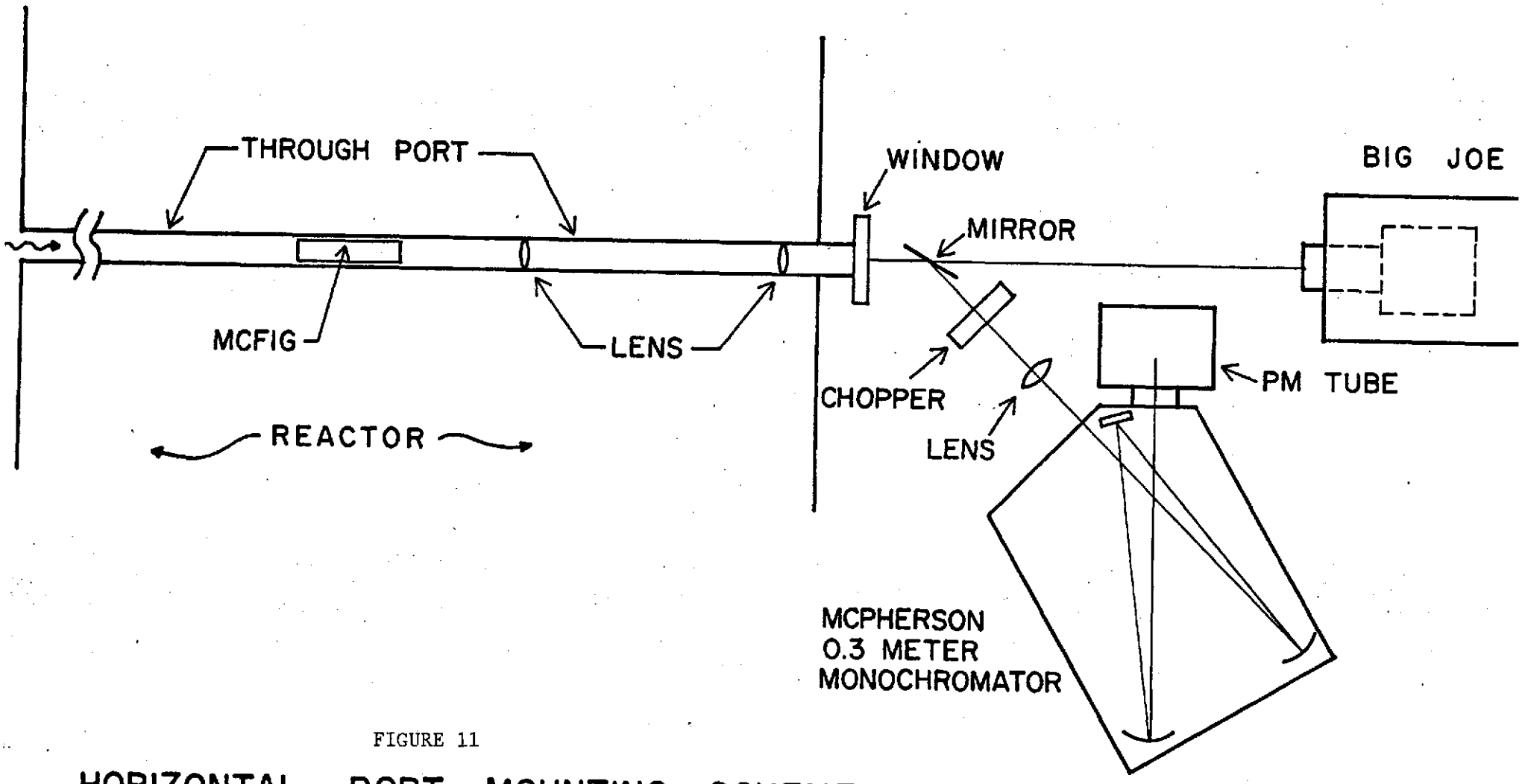

FIGURE 11

HORIZONTAL PORT MOUNTING SCHEME

Future capsules may be designed with LiF windows and spectral studies could then be made into the vacuum ultraviolet as low as 1150 Å. For most studies a lens assembly will be inserted in the test tube to bring the maximum amount of light on the spectrograph slit. For minimum radiation damage to the optics, S1 UV grade quartz lens will be used, which limits the observable spectral region from 1800 Å to 2.5 microns. For light studies to shorter wavelengths it will be necessary to remove all optics and evacuate the light path from the MCFIG to the detector, including the spectrograph to less than 10^{-4} mm of Mercury to prevent light absorption by atoms in the light path. The spectrum was observed either photographically or with a scanning monochromator fitted with a PM tube. The PM tube will be shielded to reduce gamma noise problems. The PM tube output will be recorded by an instrumentation system and the output on an X-Y plotter or magnetic tape. For analysis, the photographic or magnetic tape data will be reduced by the UF Computerized Spectrum Analysis System. This system has been described in detail elsewhere.

MCFIG Design.--The gas capsules (MCFIG) were designed for increased safety over previous gas irradiation studies and the necessity for gas purity, as most gas contamination is due to its container. Presently, there are two designs, a one-window and a two-wondow version. The one-window system shown in Figure 12 will be made of stainless steel and will essentially be considered expendable, although reuse is desirable. The two-window system shown in Figure 13 will be made of Zircalloy-4 and will be used for studies where low activation or frequent handling is desired. A thermocouple port is provided in both versions so that the capsule temperature can be monitored to provide an indication of the kinetic pressure inside and also insure that the MCFIG does not become overheated. Cylindrical or planar enriched UO_2 coatings of 1 or 3 microns thickness will be fitted inside each capsule. Each MCFIG will be

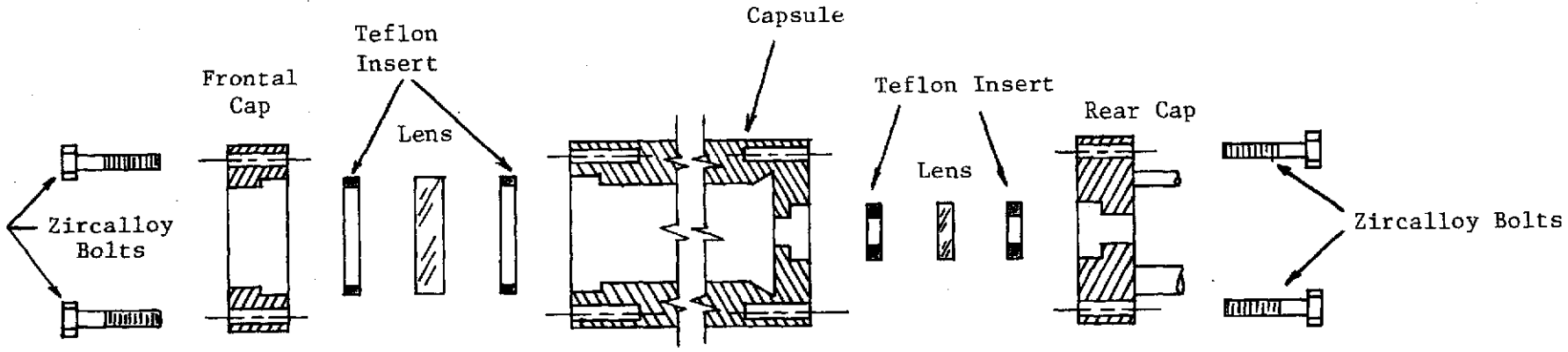

Figure 13. Zircaloy MCFIG.

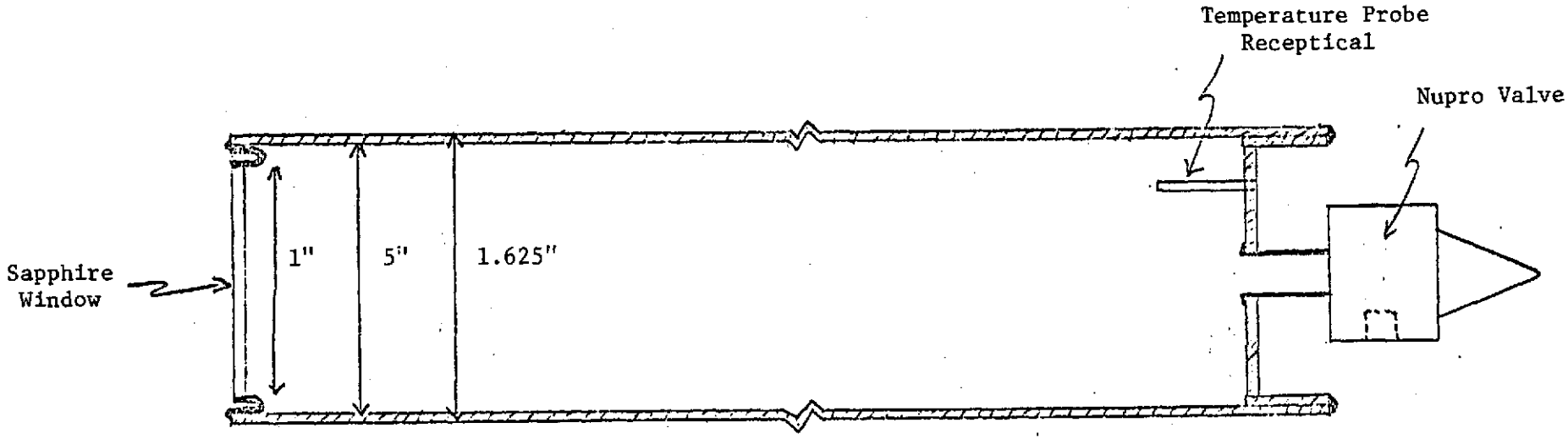

Figure 12. Stainless Steel MCFIG with One Window.

evacuated to a high vacuum and filled with research grade gases at various pressures.

Instrumentation System.--Data acquisition for this type experiment is difficult due to the low expected light levels, gamma noise and activation problems. To attack the first problem, it is necessary to use the appropriate optics. A schematic showing the basic optical setup to be employed in the experiment appears in Figure 14. Because of uncertainties about the amount of light that will be observed, two optical arrangements at least will be tried and the optimum one used.

Three instrumentation systems are planned for use in these studies. The simplest is the use of photographic film but use will be limited due to long exposure times. The other two systems are for use with the scanning monochromator and PM tube with the function of combating the gamma noise problems. One is the use of a simple RC low pass filter on the PM output to integrate the high frequency gamma noise. A schematic of the last concept is shown in Figure 15. A digital PDP 8/e computer will be the central controller and processor for this system. The chopped signal from the PM tube will be passed through a band pass filter and amplifier system which should reduce the high and low frequency gamma noise.

The drive unit on the scanning monochromator will be a stepping motor operated by the computer. Each step of the motor will correspond to approximately 0.25 Å. At each step the computer will take digital samples when the chop wheel is open and when it is closed. The difference between the open and closed samples will be an average optical signal at each 0.25 Å step. This signal will be stored, and the computer will tell the stepping motor to proceed to the next data point. This stored signal will at some later time be fed into an interface unit into the IBM 1800 and use made of the University

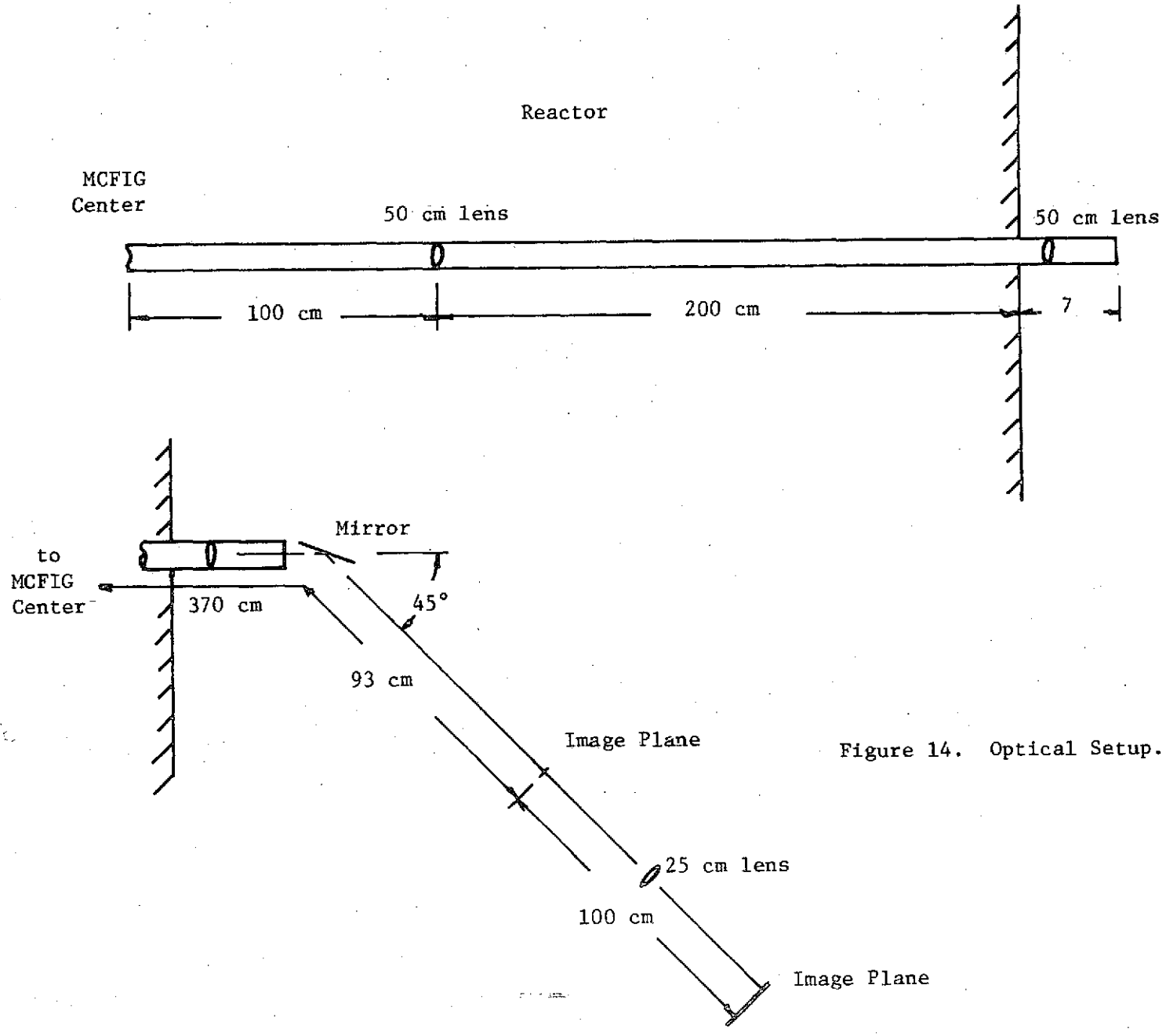

Figure 14. Optical Setup.

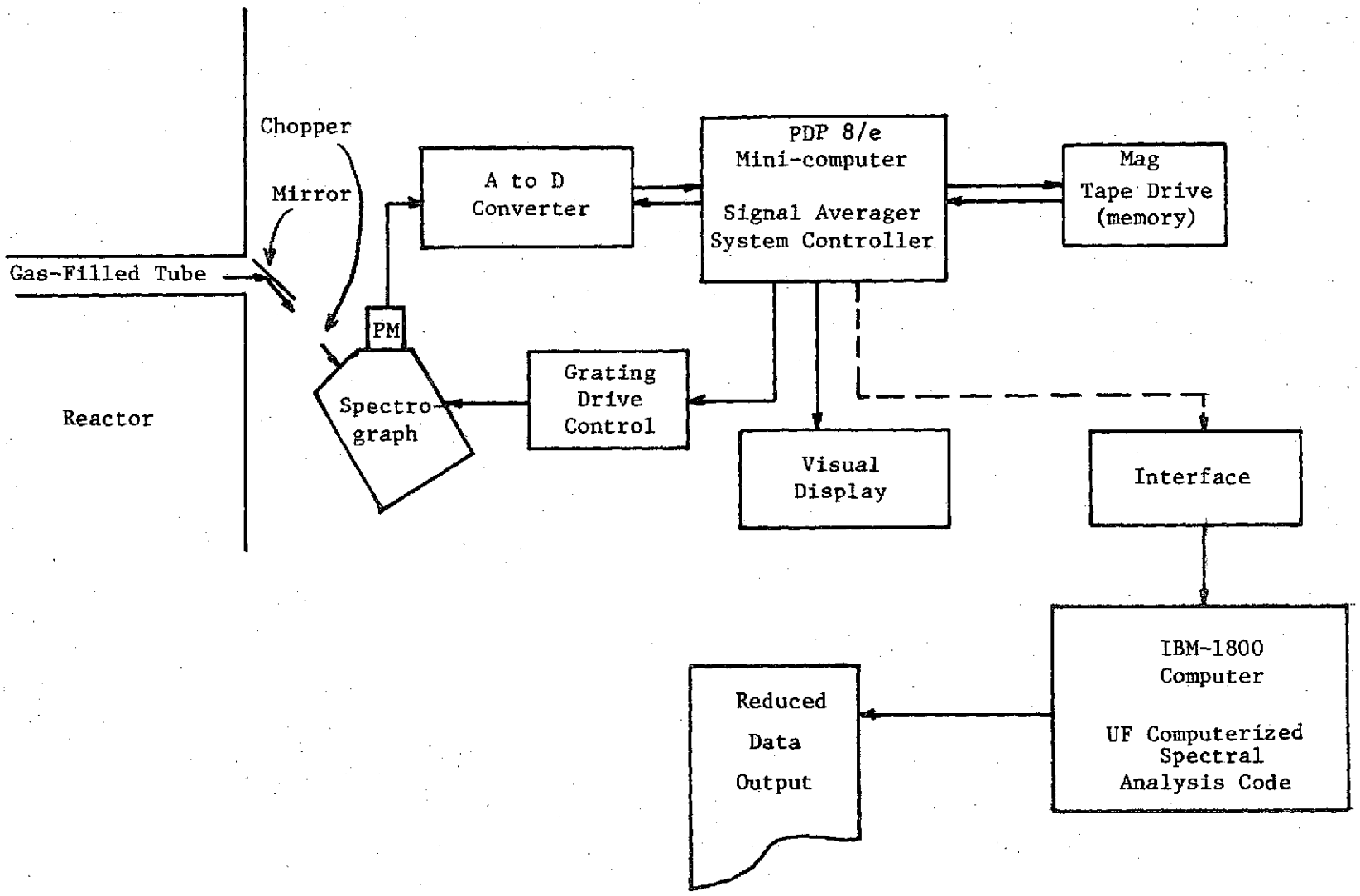

Figure 15. Instrumentation System

of Florida Computerized Spectrum Analysis System [1]. This system offers the advantages of greater system flexibility, improved signal to noise ratio, greatly increased wavelength and signal accuracy and permanent data storage, but has the disadvantage of increased complexity which requires time and patience to conquer.

Experimental Results.--The experimental efforts at the University of Florida are in their infancy. This report has indicated our development and subsequent improvement of an experimental system to perform this type of research. Preliminary indications are that our spectral resolution and signal to noise is significantly better than previous researchers. This past year has also seen a significant improvement of our data and data analysis systems. At present, a MCFIG containing one atmosphere (760 torr) of ultra-pure argon is under investigation with a planar source of fission fragments. The present experimental configuration enables us to perform detailed studies of the spatial variation of the emission of the excitation due to fission fragments as they come out of the planar source. This information can provide a significant contribution to understanding the interaction processes of the fission fragments with the gas. The initial results have indicated a surprising and hoped for absence of impurity spectra and as a result, very high purity argon spectra never before observed under reactor conditions.

An argon spectrum from 1800 Å to 8300 Å is presented in Figure 16. Of particular interest are the continuum emissions centered at 2350 Å, 3300 Å, and 4200Å. Also of interest is the presence of the strong Argon I emission in the region from 6900 Å to 8200 Å. The laser lines of the argon ion were also observed with significant emission. An experimental investigation is underway to determine if a population inversion exists in these Ar II lines.

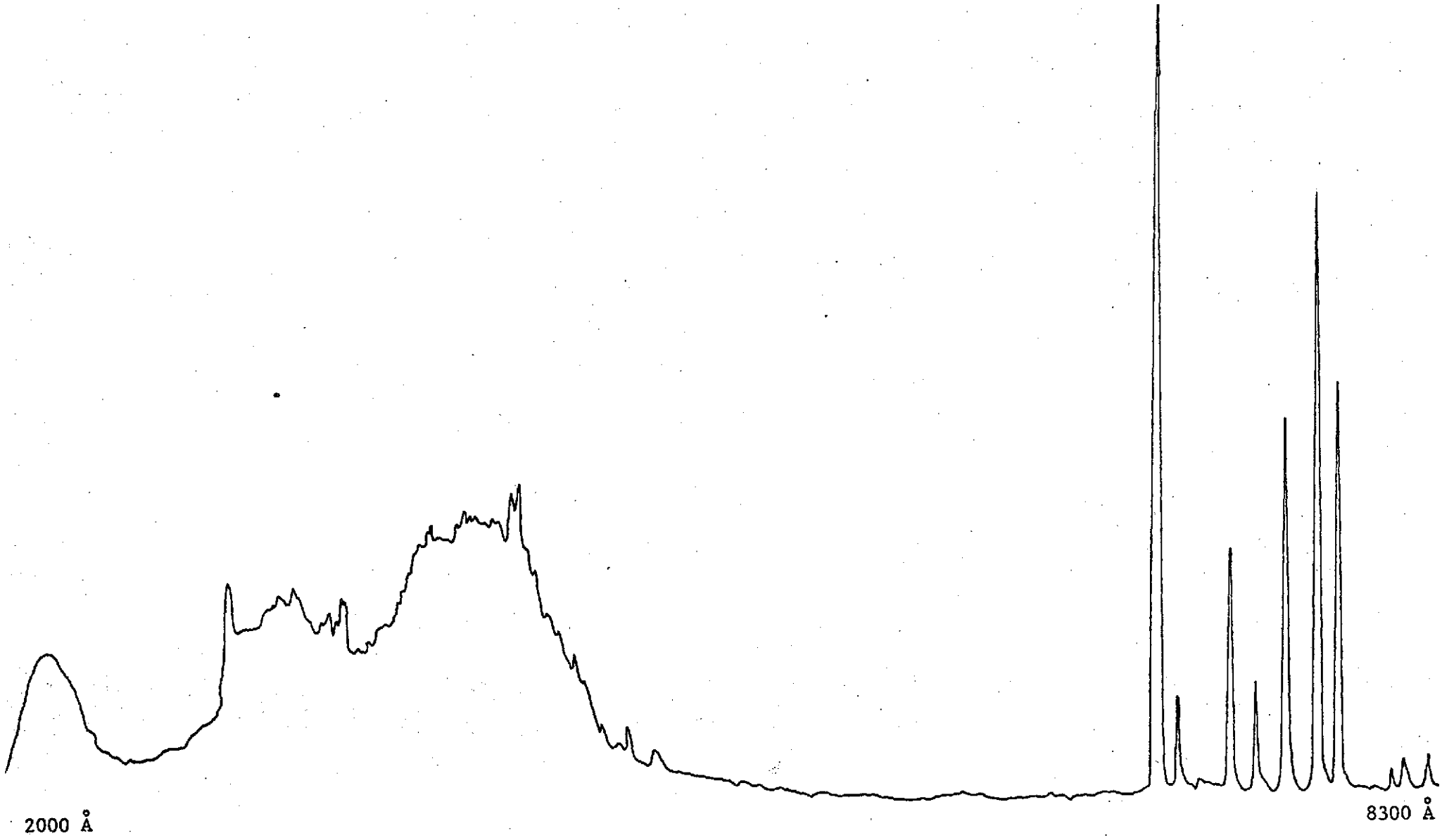

Figure 16. Argon Spectrum 760 Torr

POPULATION INVERSIONS IN FISSION FRAGMENT EXCITED HELIUM

by

G.R. Shipman

ABSTRACT

A theoretical analysis of fission fragment excited helium has been accomplished to explain the population inversion between the 4^2P and 4^1D states. The inversion shows a pressure dependence which has been observed in experimental studies. This study shows that direct nuclear pumping of helium is possible.

POPULATION INVERSIONS IN FISSION FRAGMENT EXCITED HELIUM

Discussion

The data gathered from previous fission fragment excitation experiments has been under analysis for the last two years. The most immediate result has been the identification of two population inversions in helium. These inversions are shown in Figure 1. At low pressures where direct fission fragment excitation is the dominant effect, the inversions are seen to be small whereas at higher pressures where the secondaries are responsible for the bulk of the excitation, the inversions are large. This indicates that electrons rather than fission fragments are pumping the inversion. These inversions occur because the electron excitation cross section for the P states is significantly larger than that of the D states, while the radiative decay rate is smaller (see Figure 2). The rapid increase in the inversion of the n = 4 states with pressure is a result of the 4^1p state population increasing at a much faster rate than that of the 4^1d. Since the ^1p states are connected to the ground state by an allowed dipole transition while the ^1D states are not, it is likely that the inversion is caused by direct excitation from the ground level. The inversion is not caused by the high energy tail of a quasi-Maxwellian electron swarm. This can be seen by comparing the population ratio for the fission fragment excited case with the ratios of the same states obtained from two common laboratory discharge lamps. The inversion appears to be due to fast electrons created in fission fragment collisions with neutral helium atoms. That these inversions have been made to lase with an

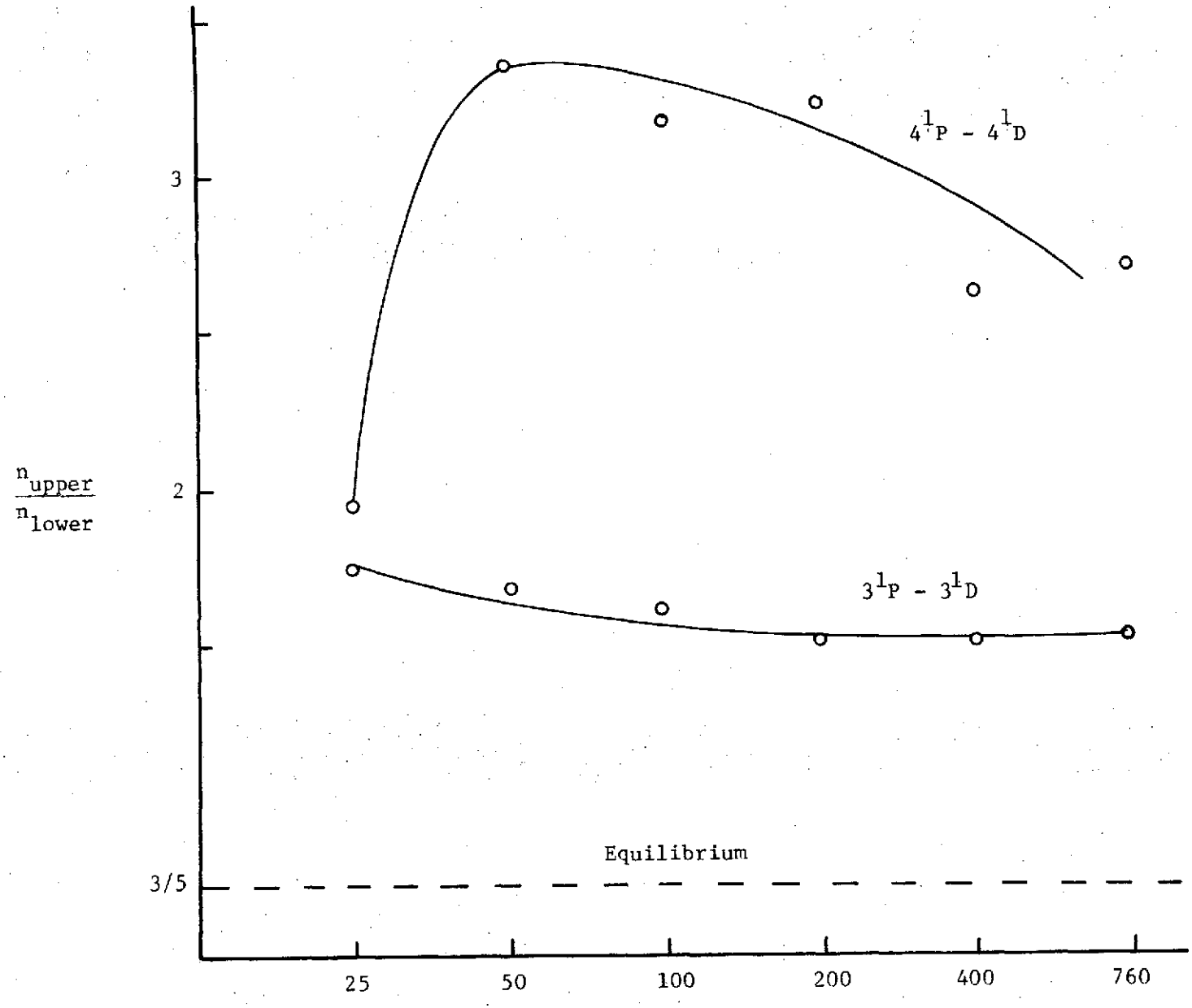

Figure 1. Population Inversions of He.

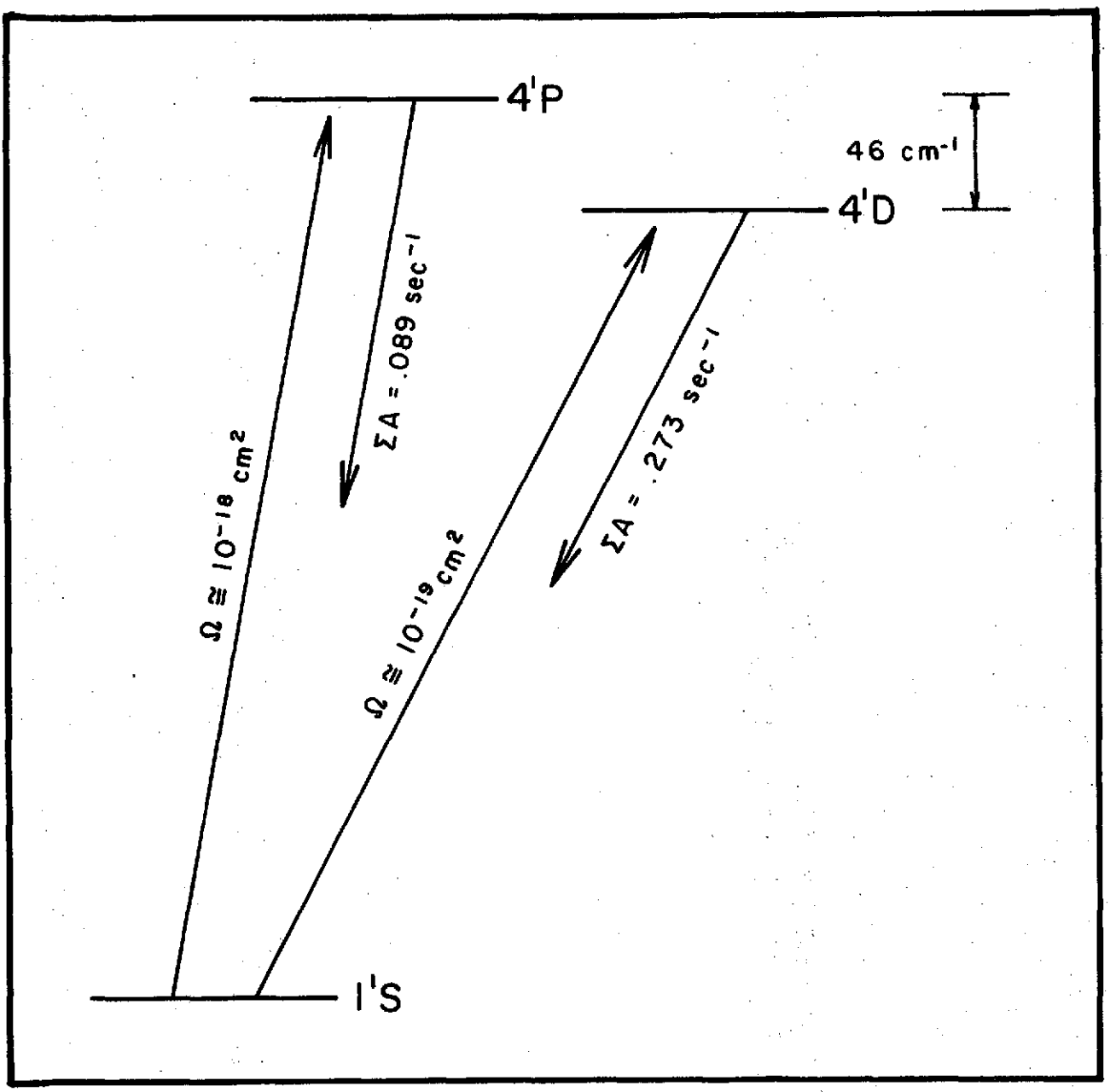

Figure 2. Excitation and De-excitation Cross-sections of 4'P and 4'D States

electron beam [1] tends to support this conclusion. The decrease in the inversion with pressure is probably due to equiliberating collisions between helium atoms. It is to be noted that the inversion persists to pressures which are quite high compared to electrically pumped atomic lasers.

One of the chief differences between an electrically excited gas and a fission fragment excited gas is in the shape of the electron distribution function. In the energy region where the electrons have sufficient energy to cause excitation and ionization of the noble gases (above 10 eV) the distribution function for the electrical case is monotonically decreasing. On the other hand, the slowing-down distribution produced in fission fragment excitation, the number of electrons with a certain energy increases up to a maximum in the 100s of eV range; the particular energy of the maximum depends upon the energy spectrum of the primary particles, the ionization cross section of the target gas, and the energy distribution of the secondaries.

In an attempt to observe this difference, the ratios of the relative state populations of some argon I to argon II lines were plotted against pressure. These ratios are shown in Figure 3. The results are rather puzzling. While there is a great deal of scatter in the points, the general trend seems to indicate an increase in ArII excitation with pressure. If direct excitation from the ground state by electrons is the dominant mechanism for populating these states, the curves indicate an increase in the average electron energy. This is contrary to what one might expect since the increasing occurrence of electron-electron collisions at the higher pressures should tend to increase the thermalization rate of the swarm and hence lead to lower mean energies. It would be instructive to compare these curves with the electrical discharge, but this has not yet been done. A similar plot was made for the H alpha

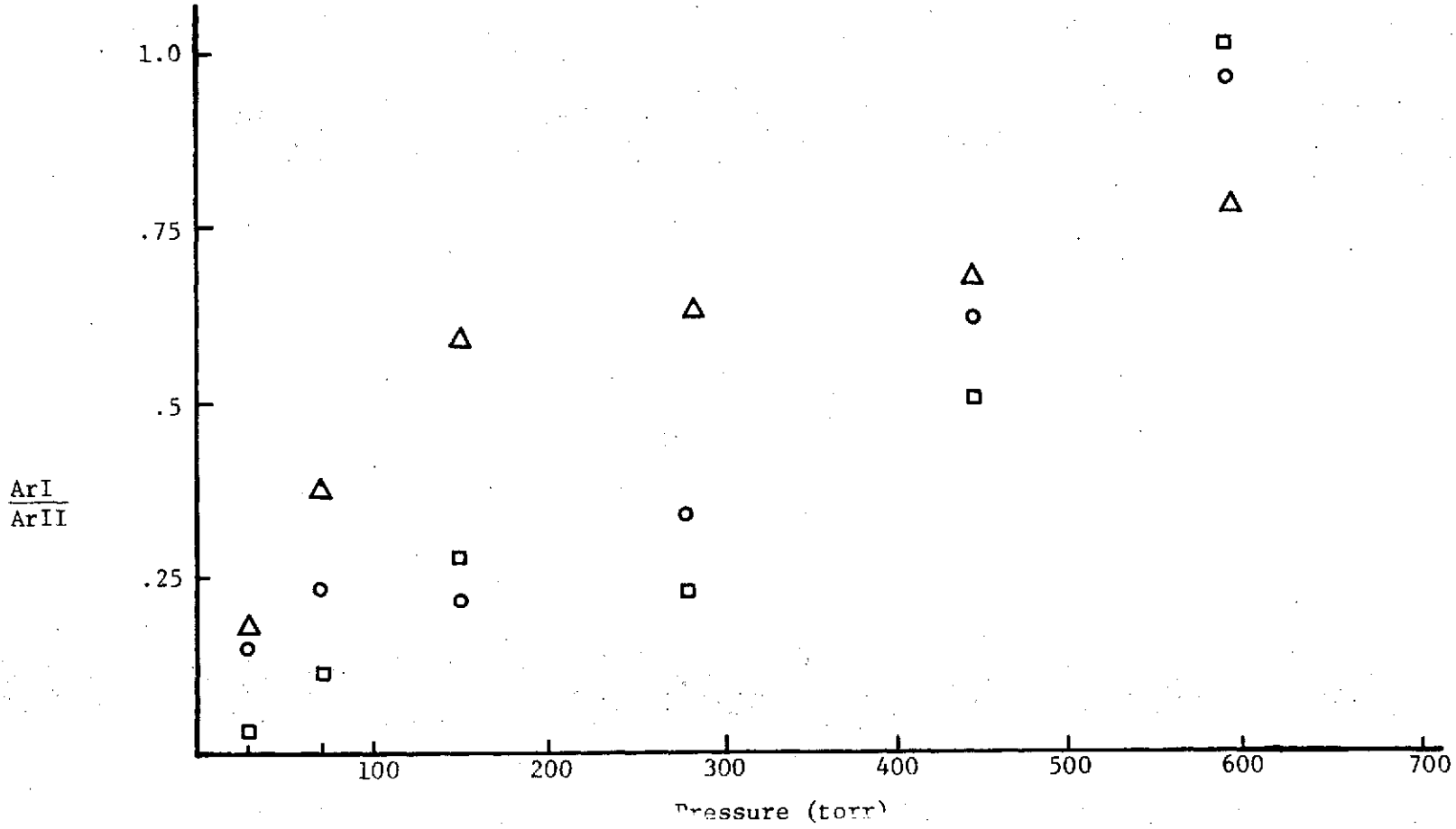

Figure 3. Population Ratios of ArI to ArII.

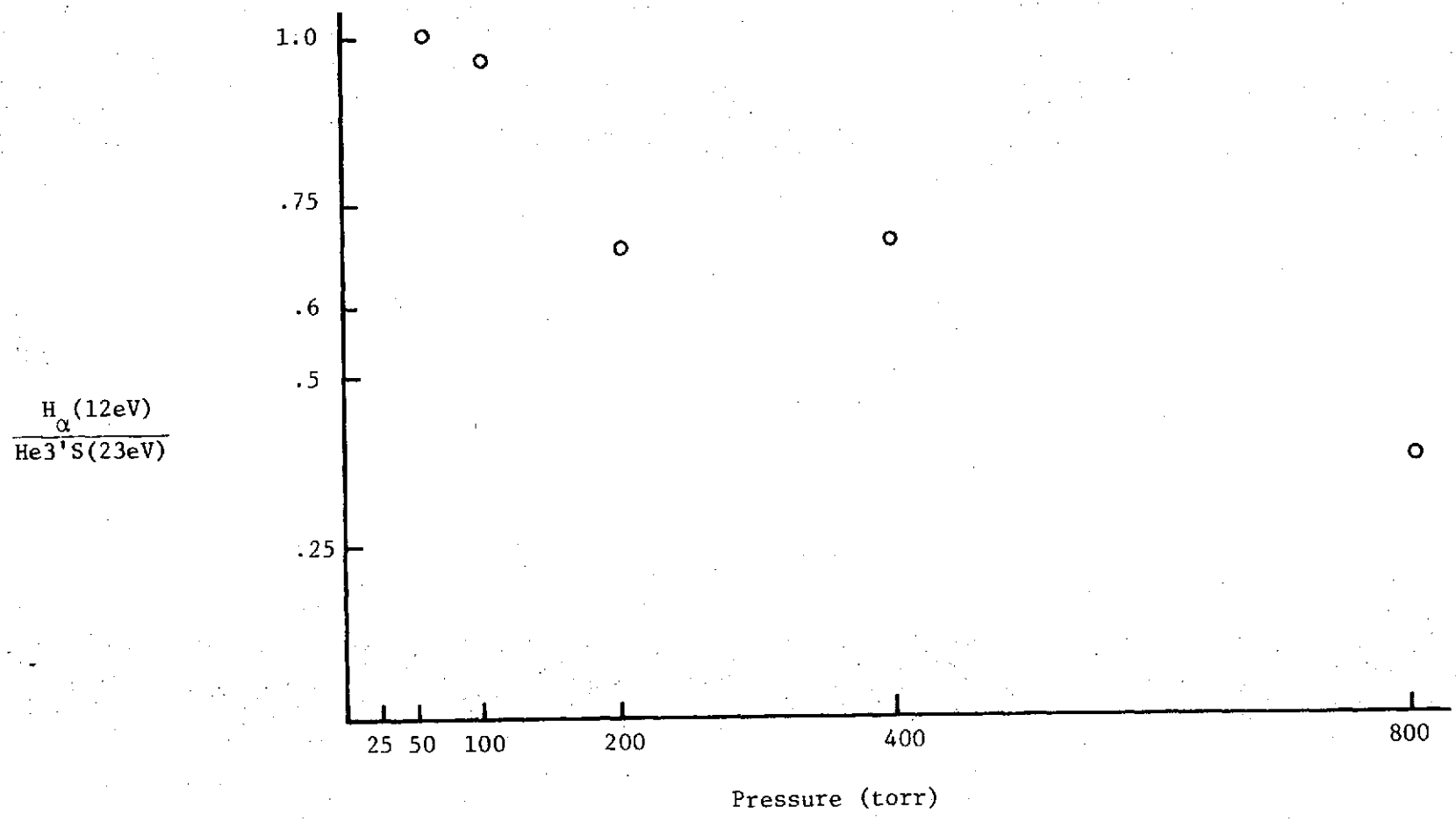

Figure 4. Ratio of H_α to 3'S State of He vs. Pressure.

hydrogen line at 12 eV and the 3^1S state of helium at 22 eV. Again the curve in Figure 4 shows the same pressure dependence. An explanation of these results has yet to be given.

A comparison has been made between the relative excited state population in helium as derived from our fission fragment data and the alpha particle helium excitation data obtained by Thiess and Miley [2]. Normalizing the two curves at one atmosphere to allow for differences in photon collection efficiency, the curves seen in Figure 5 are seen to be nearly identical, both showing the same pressure dependence. There exists a systematic divergence between the two curves as the pressure decreases. In all but one case, the fission fragments show more excitation at each pressure than do the alphas. Since the curves are normalized at one atmosphere, this difference is not due to the difference in energies of the two particles. In an attempt to find out what causes this divergence, experiments are currently underway using a Cf^{252} source which emits both fission fragments and alpha particles.

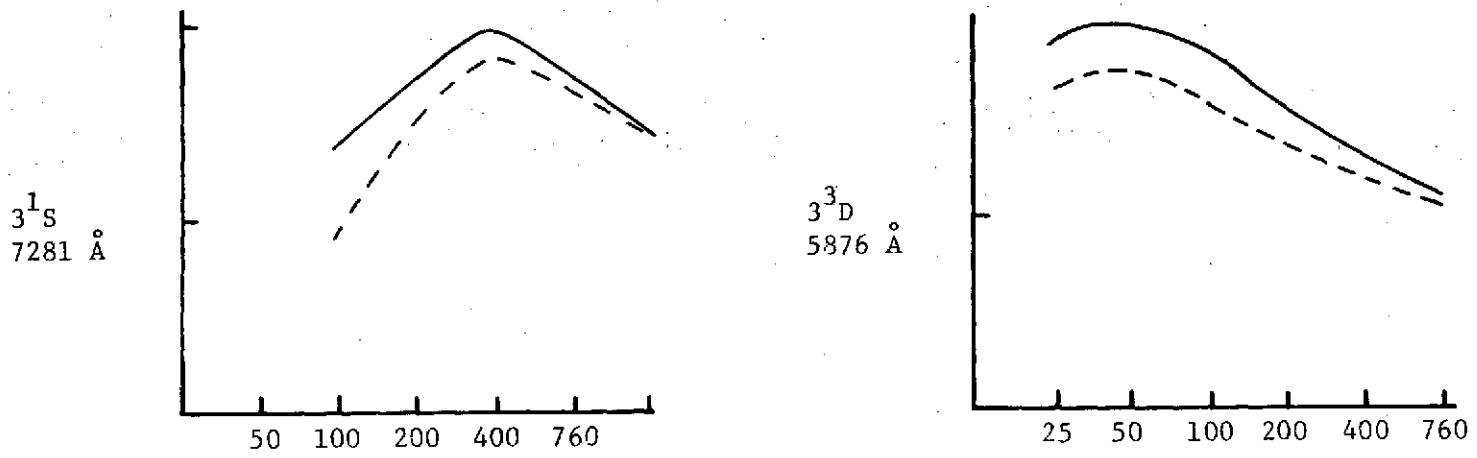

Figure 5. Normalized Relative State Populations in He due to Fission Fragments and Alphas vs. Pressure (torr).

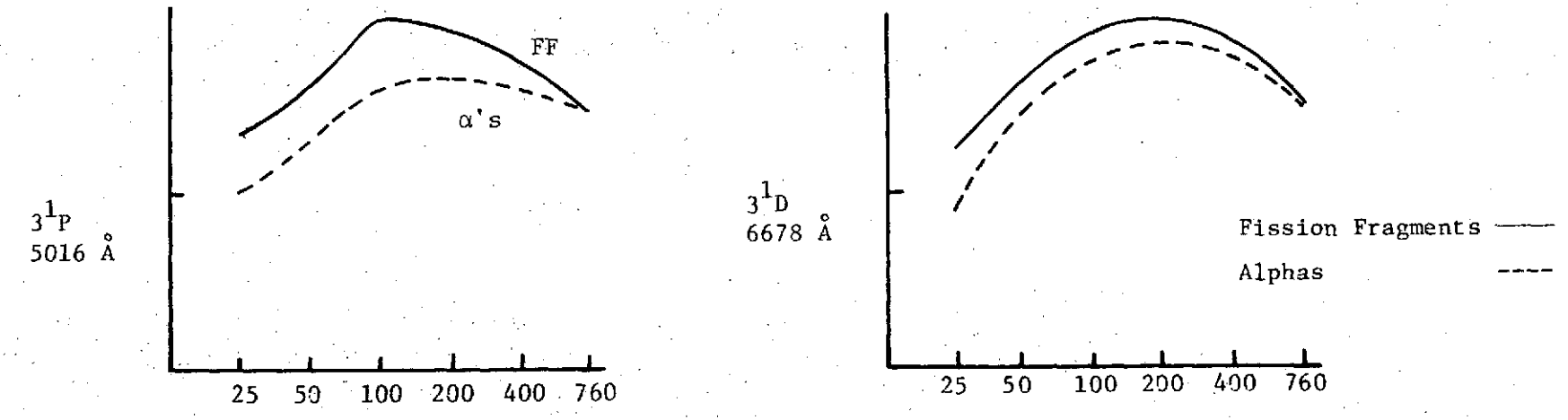

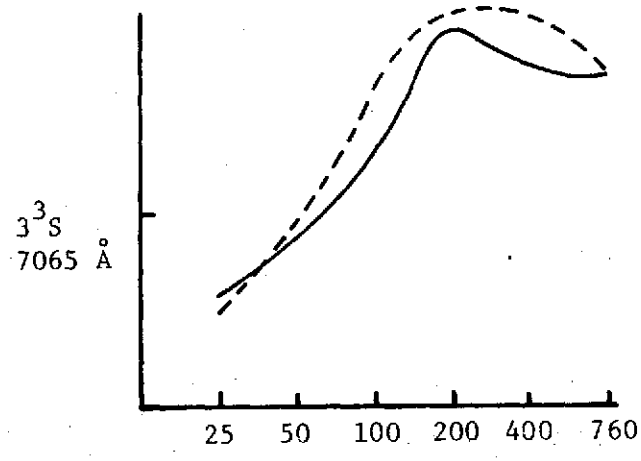

Figure 5 (continued)

References

1. CRC Laser Handbook, Chemical Rubber Company, Cleveland, Ohio, 1971.

2. Thiess, P. and G. Miley, private communication to be published.

DIRECT NUCLEAR PUMPING OF A HELIUM-XENON LASER*

by

James L. Fuller
H.H. Helmick

ABSTRACT

Experiments performed at the Godiva Facility of the Los Alamos Scientific Laboratory have demonstrated for the first time direct nuclear pumping of a laser.

*Cooperative effort between University of Florida and Los Alamos Scientific Laboratory.

DIRECT NUCLEAR PUMPING OF A HELIUM-XENON LASER

Introduction

Although attempts to achieve nuclear pumping of lasers date back to the early 1960s, demonstration of feasibility of nuclear pumping has not been accomplished prior to the experiments reported herein.

Nuclear pumping is understood as the direct excitation of a laser by fission fragments.

Practical implications of using an optical resonator include the benefit that power can be coupled out of the reactor system at useful energy levels, which otherwise would degrade to low quality heat.

A large body of work exists concerning excitation of crystals by γ-radiation, enhancement of electrical discharge lasers by nuclear reaction products and initiation of chemical lasers by γ-radiation[1] (performed in add-on experiments). A survey of this previous work can be found in References 2 and 3. In contrast to prior work, the present experiment uses solely fission fragment energy, which is deposited directly in the lasing gas.

Experiment

The laser device used consisted of two separate quartz sections, each of which had NaCl brewster windows. One section was an electrical discharge laser, used for optical alignment only. The other section contained a lining of ^{235}U

metal and was surrounded by a polyethylene sleeve. This sleeve which served as a neutron moderator had an annular thickness of 7.5 cm. The dimensions of the two sections were approximately the same, being 19 mm in diameter and 30 cm long. Both sections were on the same optical axis inside a common resonator housing a broadband flat reflector and a 4 meter radius spherical broadband reflector placed 118 cm apart.

A 1 mm hole in the spherical mirror was used to couple the laser output to the detection system. A cryogenically cooled gold doped germanium detector was located 18 meters from the laser and enclosed by heavy radiation shielding. The light path had four 90° bends, accomplished by first surface mirrors to protect against streaming of γ- and neutron radiation.

A remote control gas handling system was incorporated into the system to allow adjustment of gas pressures and mixing ratios in a high radiation environment.

The Godiva IV prompt burst reactor[4] was used to produce a pulsed fast neutron flux. A small portion of this flux entered the moderator surrounding the laser and was subsequently thermalized. This thermal neutron flux induced fissions in the ^{235}U metal lining of the laser tube. Fission fragments emerging from the surface of this lining enter the gas transferring their energy to it while being slowed down.

Results

Initial success was obtained by using a He-Xe 200:1 gas mixture at a total pressure of 200 Torr. Improved output was obtained with a ratio of 20:1 and subsequent work performed with this mixture.

Figure 1 shows the laser output versus time as well as reactor power versus time. As can be seen the laser output is delayed with respect to the fast neutron flux.

Since the lasing action is caused by fission fragments induced by slow neutrons, laser output lags the fast neutron pulse by the neutron thermalization time.

The light output exhibits a threshold for onset and termination of laser action. The rise and fall time of the output signal is linear with the fission rate in the ^{235}U metal lining.

A careful analysis of the shapes of the slow neutron pulse and the laser output pulse revealed that they coincide. For this reason the authors believe the observed laser signal should be considered as a CW output.

The wavelength was established to be near 3.5 μm by use of filters. It is therefore assumed that the Xe $5d[7/2]^0_3$ - $6p[5/2]_2$ 3.508 μm transition was produced, a laserline which can also be excited electrically to produce CW output. Preliminary calibration shows the observed light output power to be at least 10 mw.

Figure 2 is a plot of laser output versus fission fragment energy made available to the laser gas for two different gas mixtures.

It is apparent that over the range investigated so far, a linear relationship exists between energy input and laser output. It is also obvious that the laser output is very sensitive to gas mixture ratio. Further investigations are required to determine the optimum ratio. The threshold energies for the gas mixture and laser cavity used in this experiment can also be found in Figure 2.

From the apparent parallelity of the dashed lines in Figure 2, a possible conclusion is that the changes in gas mixtures mainly affects the threshold energies.

Confirmation that the signal was indeed produced by fission fragments only was obtained by covering the ^{235}U metal lining with an aluminum foil. No measurable laser output was obtained. The aluminum foil was consequently

removed and autoradiographed to ensure that fission fragments were imbedded in but did not penetrate through the foil.

In order to confirm that the observed light output was due to stimulated emission, the totally reflecting (flat) mirror was obscured and as a result the output signal disappeared. This also confirms that the signal output was not produced by γ-radiation interference with the detectors or air.

Discussion

The results presented here prove the feasibility of direct conversion of nuclear energy into laser light. The development of such direct conversion processes could have far-reaching significance in the areas of power transmission and communications over large distances.

With regard to the potential of this energy conversion process, it should be pointed out that the efficiency is not limited by the restrictions of the Carnot cycle or any other thermodynamic cycle, since temperature is not involved in the conversion mechanism. Another point of interest is the fact that a resonator is involved. Stimulated emission means that more energy is channeled into the energy band represented by the laser frequency. Without the use of a resonator (spontaneous emission only) a considerably smaller amount of energy would have been emitted in this energy band. The energy extracted by stimulated emission is at the expenses of the lower quality energy, i.e., heat into which the high quality kinetic energy of the fission fragment would have been degraded. Therefore, the resonator can be viewed as an "energy trap," which constitutes a concept for extraction of energy from a reactor system superior to a heat engine.

References

[1]P. B. Lyons, J.S. Clarke, D.S. Metzger, "Gamma-Initiated HF Laser," IQEC-8 Preview, Abstract 52, Laser Focus, p. 43, May 1974.

[2]K. Thom and R.T. Schneider, "Nuclear Pumped Gas Lasers," AIAA Journal, 10, 400-406 (1972).

[3]R.T. Schneider, "On the Feasibility of Nuclear Pumping of Gas Lasers," paper presented at the Third Workshop on Laser Interaction and Related Plasma Phenomena held at Rensselaer Polytechnic Institute, Troy, New York, August 13-17, 1973.

[4]T.F. Wimett, R.H. White, R.G. Wagner, "Godiva IV," In "Fast Burst Reactors," by R.L. Long, Paul D. O'Brien, Tech. Coord. Dec 1969, U.S. AEC Division of Technical Information, p. 95.

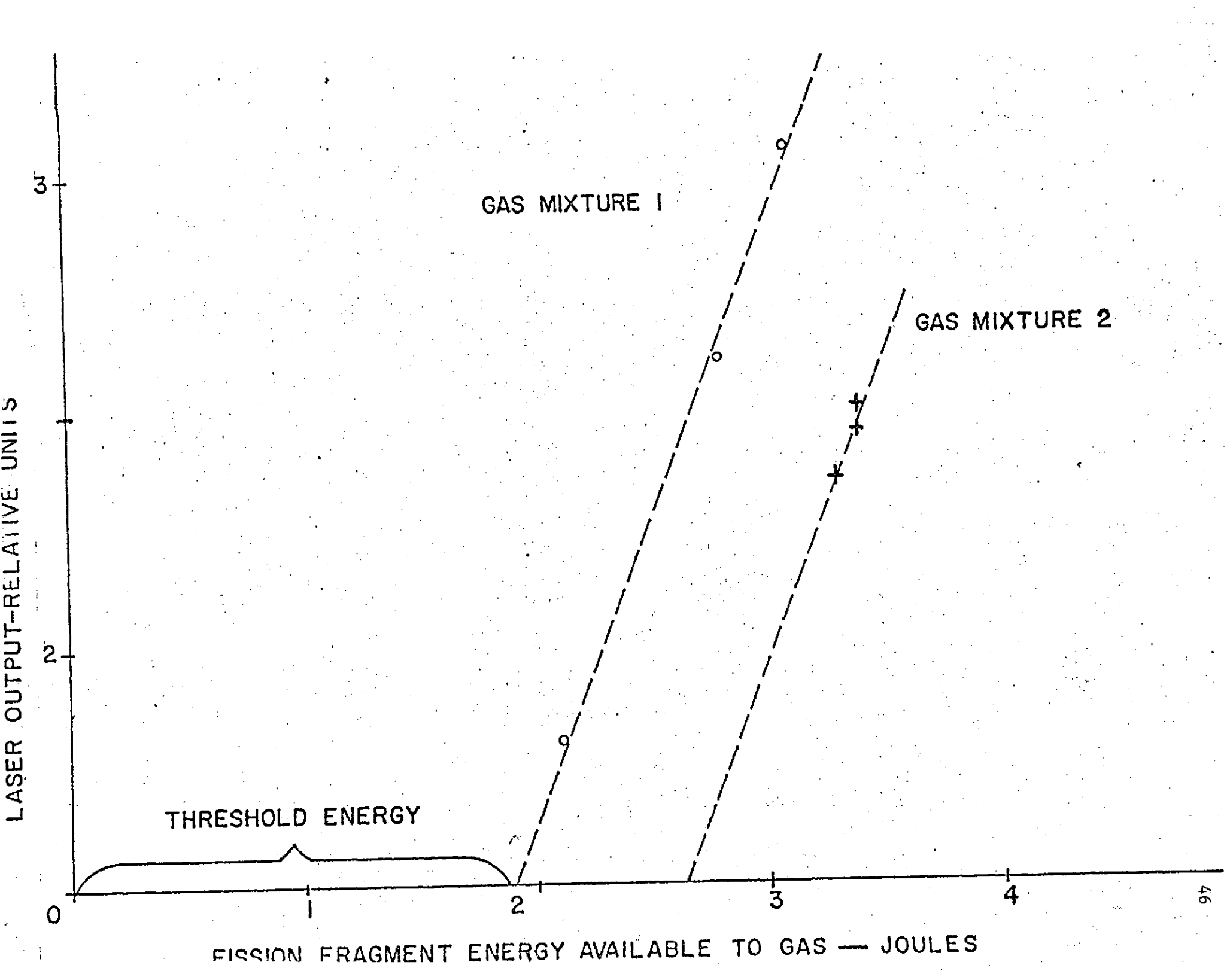
GAS MIXTURE 1
GAS MIXTURE 2
THRESHOLD ENERGY
LASER OUTPUT-RELATIVE UNITS
FISSION FRAGMENT ENERGY AVAILABLE TO GAS — JOULES
0
1
2
3
4
46

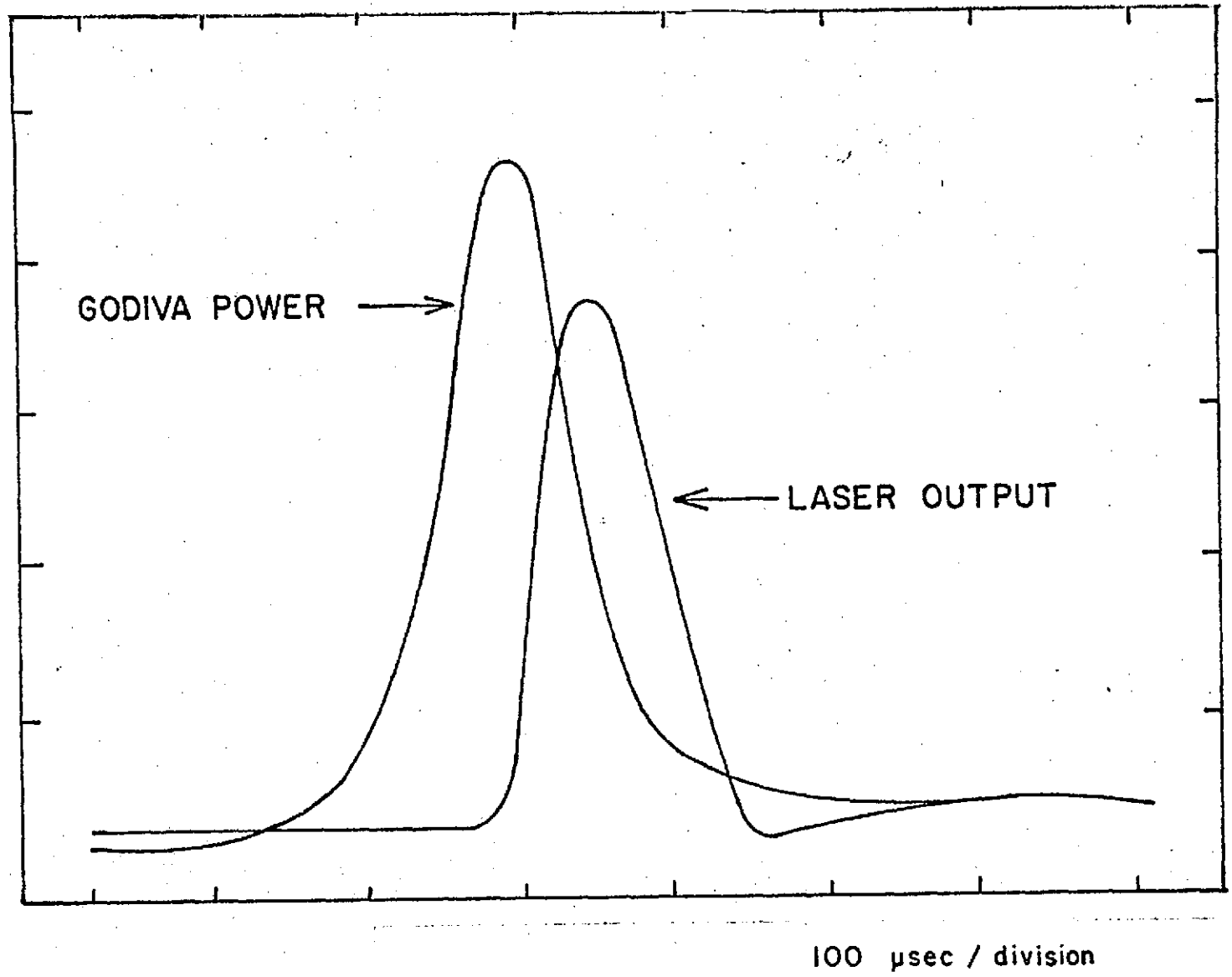
GODIVA POWER
LASER OUTPUT
100 μsec / division

NUCLEAR AUGMENTATION OF A CO_2 GAS LASER

by

J.F. Davis III

ABSTRACT

Experimental studies have shown that the output of a CO_2 laser is significantly increased by products of the nuclear reaction $He^3(n,p)T$. The experimental descriptions and results are presented in which the output from a CO_2-N_2-He^4 laser is compared with the output from a CO_2-N_2-He^3 laser exposed to the thermal neutron flux from a reactor of about 10^{11} neutrons/cm^2-sec.

NUCLEAR AUGMENTATION OF A CO_2 GAS LASER

Introduction

There are several important reasons for searching for more direct methods of transferring or pumping energy from isotope or reactor sources into lasers. New pumping techniques may be more efficient, and may offer unique characteristics. Simplified coupling could also offer weight reduction and improved realiability which may be of advantage in space applications. There are also many theoretical advantages in pumping lasers directly with energetic nuclear reaction products. The power densities attainable with nuclear reactions are very large compared to those of chemical or electrical processes; an advanced nuclear-powered laser could be quite compact but still immensely powerful.

Therefore, we undertook a study of the effects of nuclear radiation on CO_2 laser output. The basic idea of the experiment was to replace the natural helium normally present in a CO_2-N_2-He electrically pumped laser with Helium-3. The laser was then exposed to a thermal neutron flux from the University of Florida Training Reactor, which produced the $He^3(n,p)T$ 760 keV reaction inside the laser cavity. The laser output power was then compared to the case without Helium-3.

Experimental Description

Figure 1 shows the details of the electrical discharge tube used to study the effects of an external ionization source on the operation of a low pressure, continuous wave CO_2 laser. The laser was a conventional water-cooled,

LASER PARAMETERS

Optical Cavity		1 meter
Tube Diameter		3.8 cm
Cavity Volumn		1 liter
Operating Static Pressure		6-10 torr
Mixture $He:N_2:CO_2$		8:1:1
Neutron Flux	High Side	$10^{11} n/cm^2 sec$
	Low Side	$5 \times 10^9 n/cm^2 sec$
Nuclear Power Input		0.2 mwatts
Electrical Power Input		~70 watts

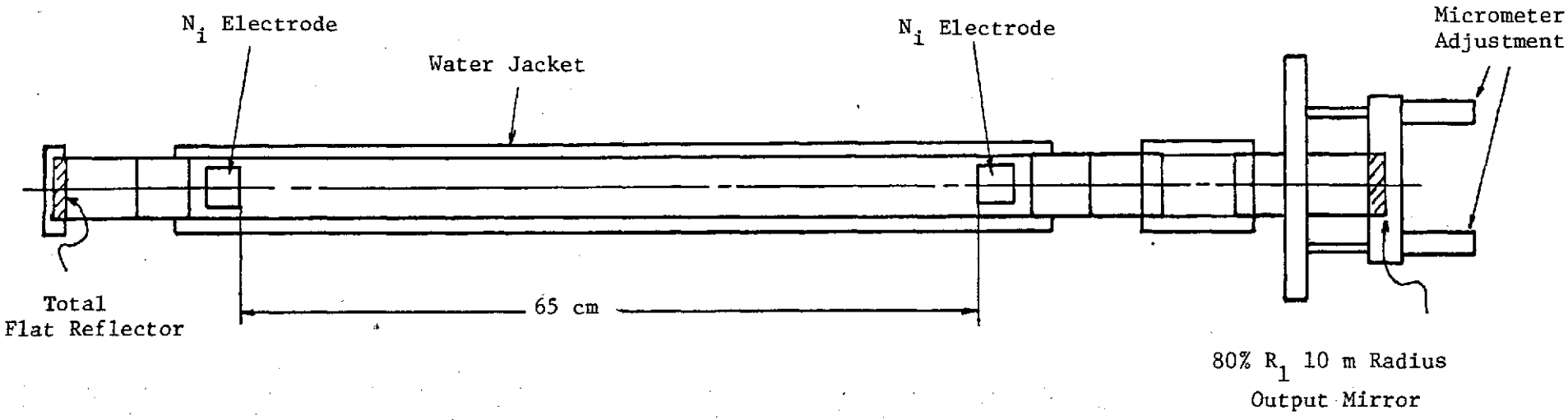

Figure 1. CO_2 Laser.

internal-mirror design, with a cavity length of 1 m and active discharge length of 65 cm. Tube diameter was 3.8 cm and the cavity volume was approximately 1 liter. Mirrors used were a 99% reflective flat and an 80% reflective germanium output coupler with a 10 m radius of curvature. The typical spot size was approximately 2 cm and the laser typically operated in the TEM_{04} mode. Maximum laser output outside the reactor was about 15 watts with flowing gas, with excitation provided by a DC power supply at (typically) 5 kV and 50 ma. Best performance without gas flow was about 2.4 watts at 3.6 kV and 30 ma.

The experimental procedure followed began with evacuating the system and premixing the gases (1:1:8 CO_2:N_2:He) for several minutes in a 1-liter flask to insure uniformity of gas mixtures. The laser could not be operated in the flowing gas mode with helium-3 due to the very high cost ($150 per liter at STP) of the gas. With the reactor at the desired power level, the gas mixture was released to the laser system and the DC glow discharge ignited. The laser output power characteristics were monitored versus input current and voltage.

Care was taken so that each data run was consistant and therefore any effects could be attributed to the Helium-3. In addition, only data of immediately successive runs were compared.

The nuclear power input to the laser via the Helium-3 reactions was approximately 160 μwatts, whereas the electrical power input varied between 40 to 100 watts. Nevertheless, Figure 2 shows that with Helium-3 there is a significant increase in laser power output. The lower curve is the power output versus current with natural Helium and the reactor off. The upper curve is with Helium-3 and with the neutron flux present. There was an enhancement of laser output over all ranges of current and above approximately 25 mA the enhancement effect seemed to be rather constant.

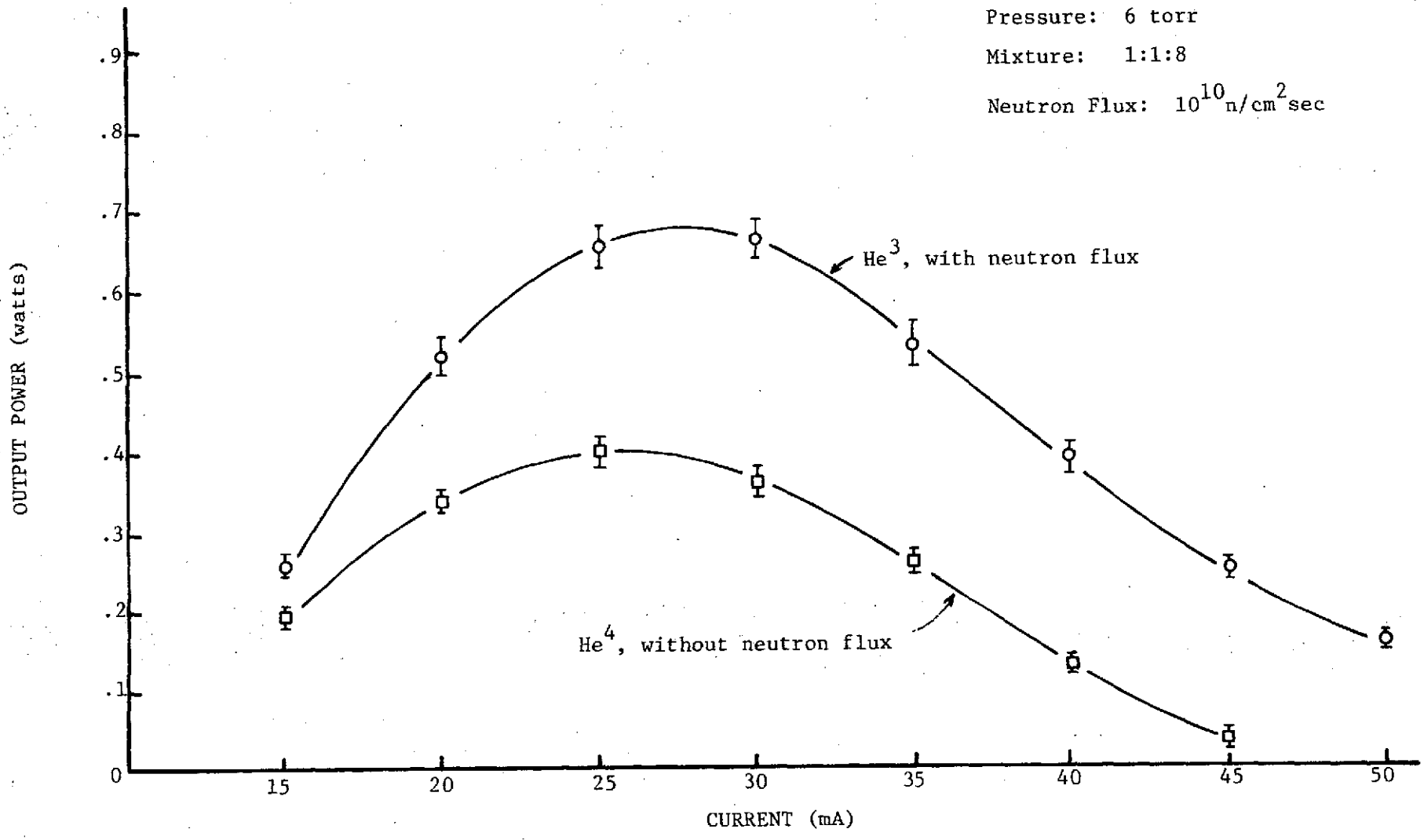

Figure 2. Enhancement of Laser Output due to Nuclear Reaction Products

Out next task then was to isolate the effects of the Helium-3 in the laser output. The laser was inserted into the reactor in such a way that one end of the laser was subjected to a much higher flux than the other. The flux was approximately 10^{11} n/cm^{2}sec on the high side and fell off to approximately 10^9 n/cm^{2}sec at the other end. Thus, we compared the laser output power with the addition of Helium-3 and first the anode then the cathode subjected to the higher neutron flux. Figure 3 shows the results of this experiment. With the reactor on, the lower curve is the output power versus current with the high flux on the anode and the upper curve is with the high flux on the cathode. Clearly, the effects of the Helium-3 on the laser output power is confined to the cathode region. Figure 4 shows the efficiency versus current for 4 consecutive data runs. The three lower curves coincide within experimental error. Two of the lower curves are with normal Helium and with switching the polarity of the electrodes. The third lower curve is with Helium-3 and the anode in the high neutron flux. The upper curve is with Helium-3 and the high flux on the cathode. Power output versus current for these 4 runs also show the same characteristics.

Figure 5 shows the I-V curves for four consecutive runs. The upper two curves are for Helium-3 with the neutron flux and the others for just natural Helium. Both are for the case when the electrode on the high flux side of the laser is the anode. These two curves fall within our experimental error. The lower two curves are for natural Helium and Helium-3 with the neutron flux, both for the case when the cathode is nearest the reactor.

The shape of these curves can be explained by the fact that as the current is increased the ionization rate in the positive column of the glow discharge increases very rapidly. However, the ambipolar loss of charged particles to the walls changes relatively slowly as the current increases. This implies

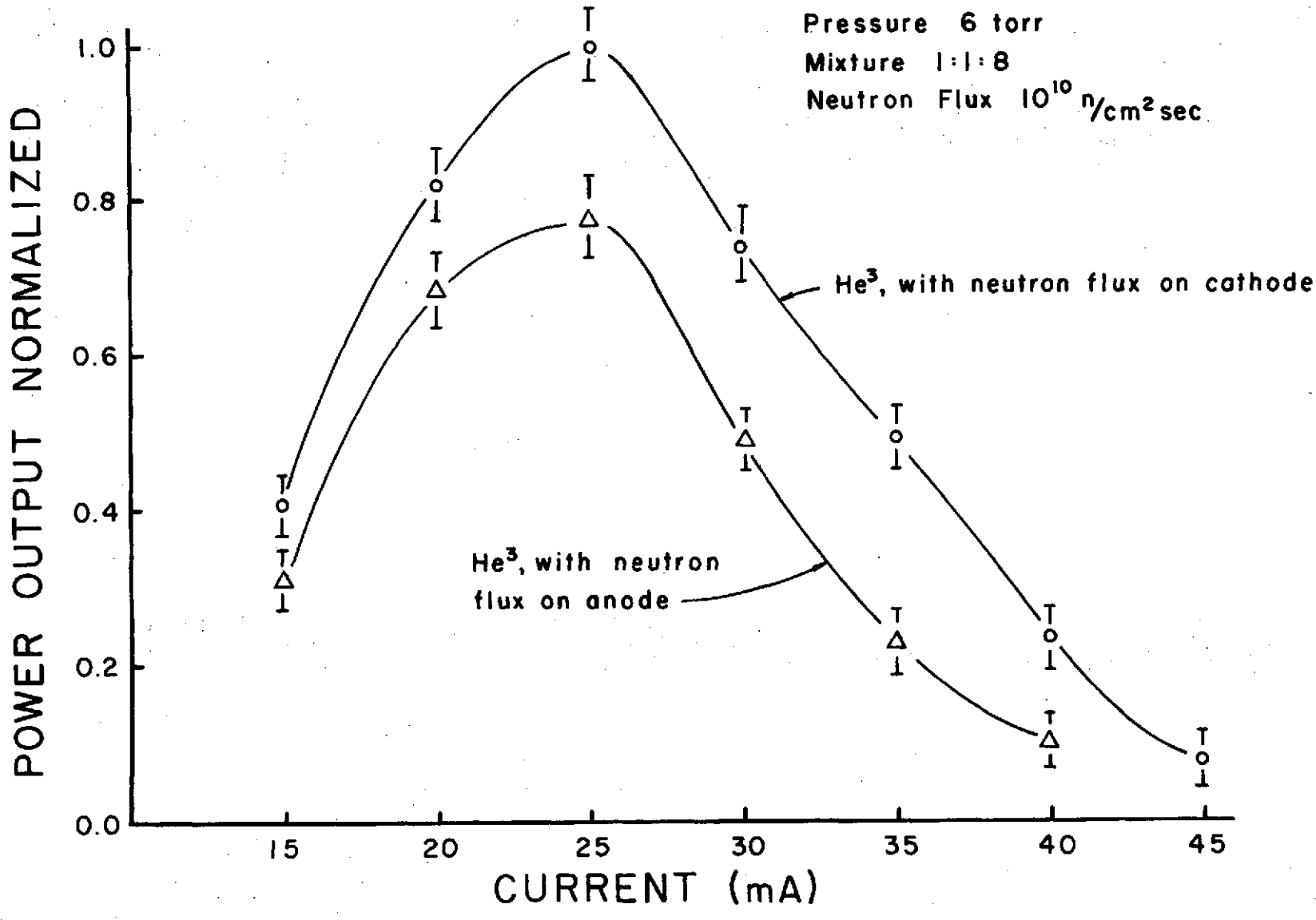
Pressure 6 torr
Mixture 1:1:8
Neutron Flux 10^{10} n/cm²sec
He³, with neutron flux on cathode
He³, with neutron flux on anode
POWER OUTPUT NORMALIZED
1.0
0.8
0.6
0.4
0.2
0.0
15
20
25
30
35
40
45
CURRENT (mA)

Figure 3

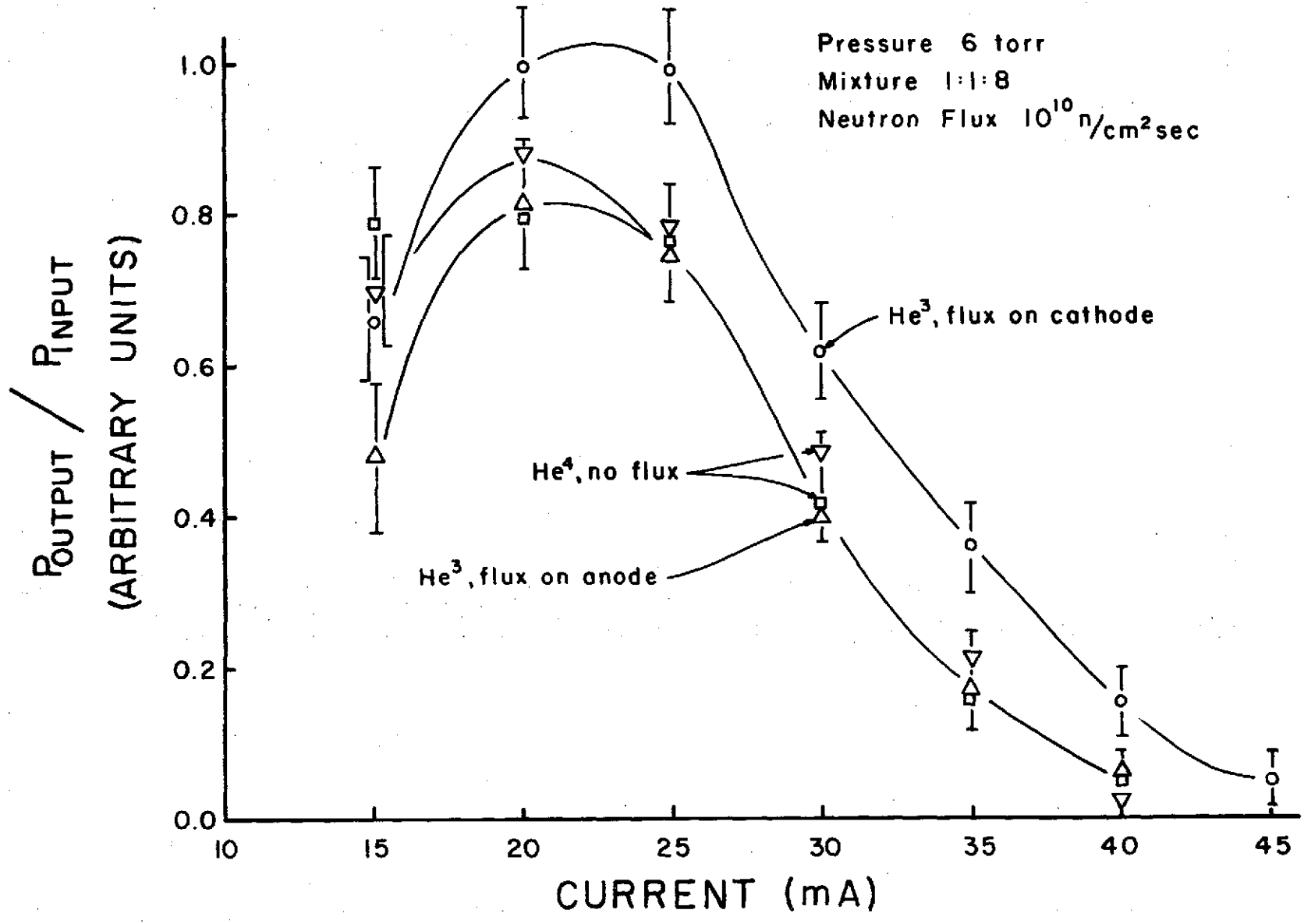
Pressure 6 torr
Mixture 1:1:8
Neutron Flux 10^{10} n/cm²sec
P_{OUTPUT} / P_{INPUT} (ARBITRARY UNITS)
1.0
0.8
0.6
0.4
0.2
0.0
He^3, flux on cathode
He^4, no flux
He^3, flux on anode
10
15
20
25
30
35
40
45
CURRENT (mA)

Figure 4

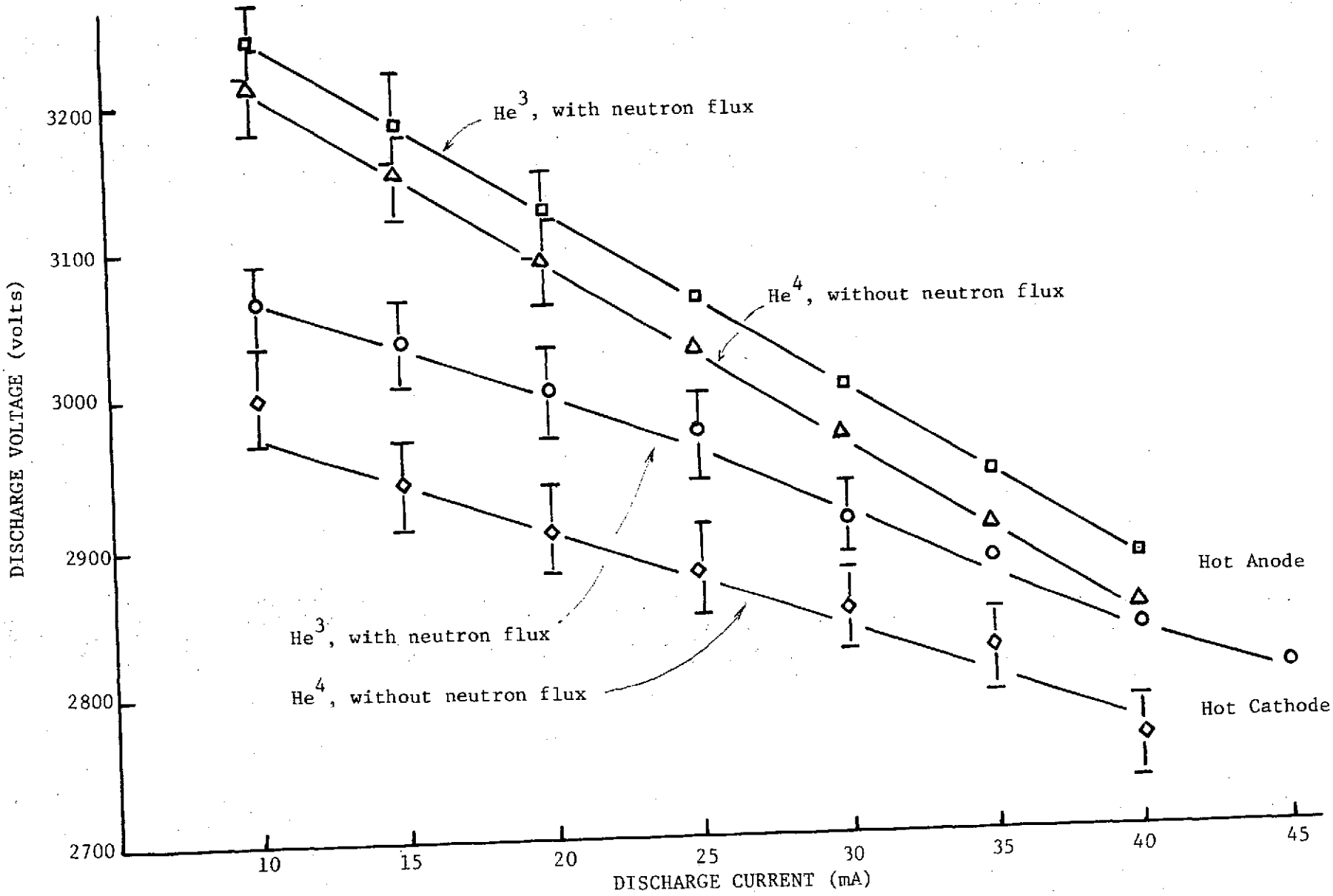

Figure 5. I-V Characteristics of CO_2 Laser

MEASUREMENTS ON A REPETITIVELY PULSED HIGH POWER CO_2 LASER

by

James L. Fuller

ABSTRACT

Described are the details of a high-power longitudinally pulsed CO_2 laser. Studies of pulse-rate, voltage and output power are performed. An attempt to augment power output using a radioactive cathode was attempted and results inconclusive.

MEASUREMENTS ON A REPETITIVELY PULSED HIGH POWER CO_2 LASER

Introduction

To investigate properly the possibility of modifying a conventional laser device for nuclear pumping experiments, the basics of operation of the laser must first be understood. For this reason, an axially pulsed, high power CO_2 laser was constructed and studied. The construction and system details follow in the next section. Following this, experimental results are presented and analyzed.

Having made this study, enhancement of the CO_2 laser output via nuclear reaction product preionization was attempted. The reasoning behind this experiment and the results of the attempt are given in the final section of this report.

System Design, Construction and Other Practical Considerations

This section will be divided into two parts. The first will deal with the electrical power supply used as a pumping device for the laser. The second section will deal with the discharge tube-resonator, with some details of the measurement optics and gas-handling system.

Power Supply.--Figure 1 pictures the overall power supply assembly showing several of its major components. It can be described as a high voltage pulse modulation system that has the capability of producing high voltage, high current pulses on a repetitive basis. The system was originally designed and used as a Klystron test facility by the Sperry Electronic Tube Division in Gainesville, Florida. When the need for such a facility was terminated, Sperry donated the power supply to the Department of Nuclear Engineering

that a lower voltage is needed to balance the diffusion losses with the ionization rate. Hence, a lower voltage accompanies a higher discharge current resulting in the negative slope characteristic of the I-V curves.

Looking again at the bottom two curves, the enhancement effect was seen only when the neutron flux was on the cathode region. What can be inferred from these curves is that at the same values of voltage we have a higher current with the Helium-3.

Discussion

To explain the results of the experiment is a difficult task due to the large number of interdependent variables such as gas temperature, current and the degree of dissociation. However, a few general conclusions can be drawn on the basis of this data.

First, it can be concluded that the effect is not due to direct nuclear pumping since the nuclear power input is very small. Secondly, the E/N ratio with and without Helium-3 changes only slightly and will not have an appreciable affect on the laser output.

It is known that the enhancement is due to some effect or effects in the cathode region. More directly, the enhancement can be due to one of several possibilities:

1. Lower gas temperature at the same values of current thereby reducing the population of the lower laser level.
2. A shift in the electron energy distribution such that the upper laser level (or the N_2 level) is more efficiently populated.
3. A change in the degree of dissociation.
4. An increase in the number of secondary electrons due to bombardment of the cathode by nuclear reaction products.

More likely the enhancement is due to a combination of these processes. It is well known that the dissociation of CO_2 and N_2 producing CO, O and N,

subsequently leads to the formation of large quantities of NO, NO_2, O_2 and NO_2. These molecules accumulate to such densities that the dominant positive and negative ions are directly related to the minority species. The introduction of the Helium-3 may then change the density of these negative ions in the vicinity of the cathode thus causing an enhancement effect.

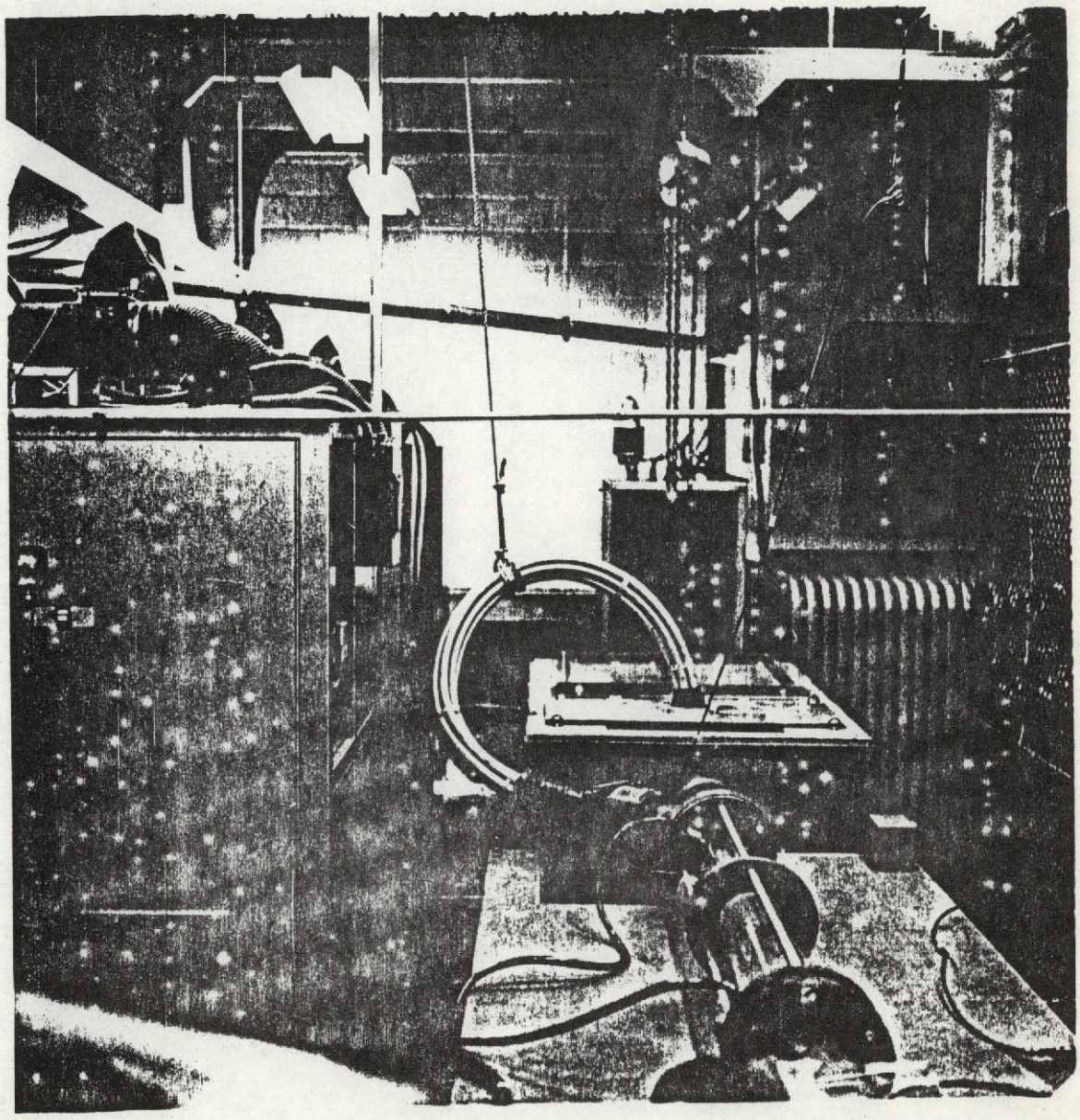

Figure 1. Overall view of the 100 MW pulsed power supply.

Sciences at the University of Florida. A detailed description of the major components of the power supply has been given previously by R. DeYoung [1].

The power supply is capable of producing pulses in the megawatt region on a repetitive basis and the pulse repetition rate and output voltage can be easily and continuously varied by the system's operator. Some of the specifications associated with this devide are:

Output voltage, peak: 300 KV maximum, continuously variable

Output current, peak: 300 amps maximum

Pulsed power output: Nearly 100 megawatts maximum instantaneous

Output voltage pulse full width: 5 microseconds

Repetition rate: 2 to 380 Hz, continuously variable

Output Impedance: On the order of 1000 ohms

A block diagram of the system is presented in Figure 2 and can be used in clarifying its operation. The power supply is fed by 440 volts a.c., 3 phase, 60 cycle @ 300 amps per phase maximum from its own transformer bank outside the laboratory. This power goes directly into a large circuit breaker unit that can be manually or automatically closed and opened. It affords both overcurrent and under-voltage protection and is automatically opened if any one of the many interlocks throughout the system is tripped. The system's electronics are powered by a separately fused 110 volt a.c. line. From the circuit breaker unit, the voltage is fed into a large motor driven, variable a.c. transformer, an inductrol. The inductrol output ultimately controls the peak voltage output of the power supply and is continuously variable from 0 to 910 volts by means of a switch at the system's control deck.

A picture of the control deck is found in Figure 3. The center section houses the electronics for controlling the output voltage and repetition rate of the power supply. The right-hand section houses electronics used to monitor

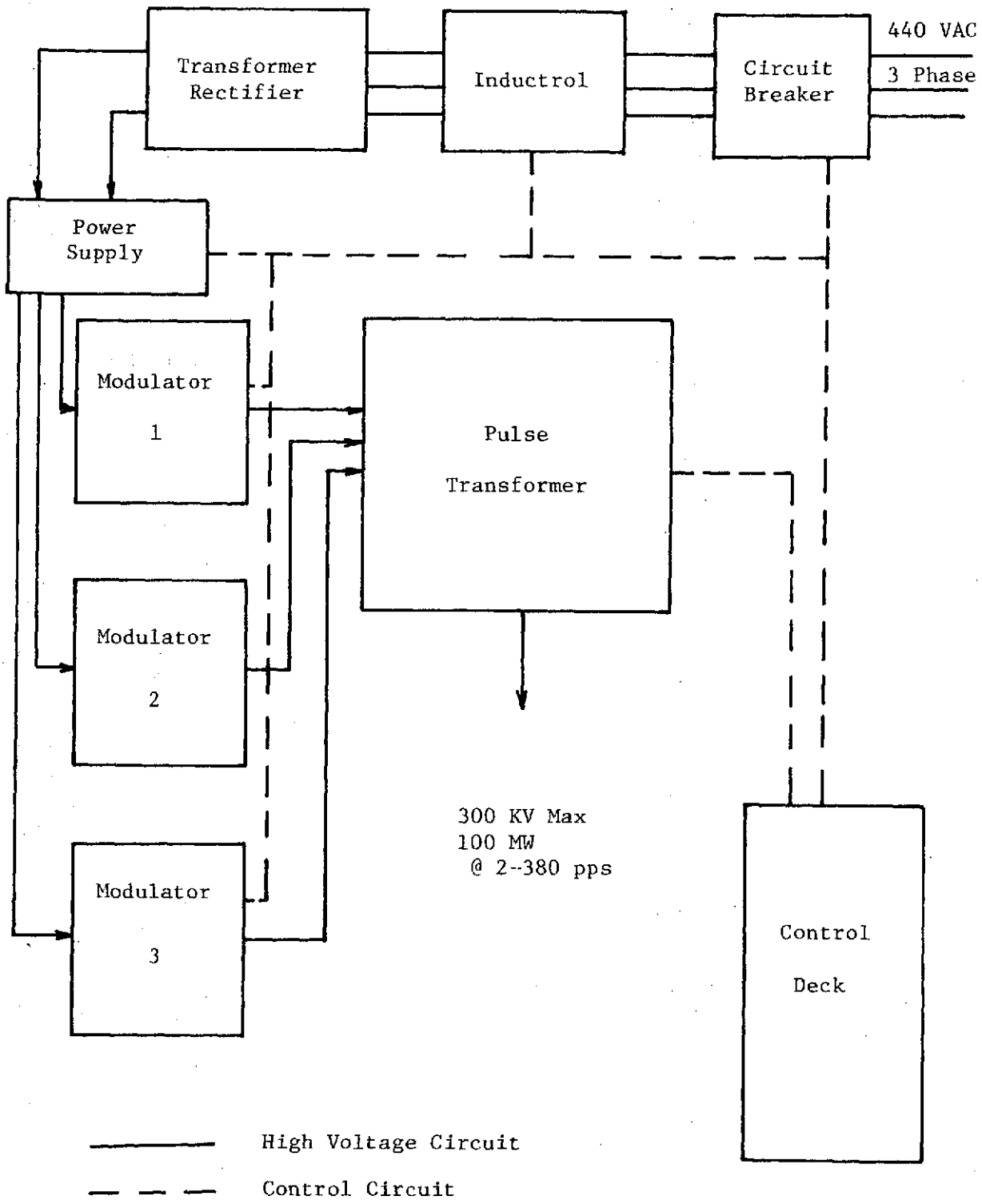

Figure 2. Power Supply Block Diagram

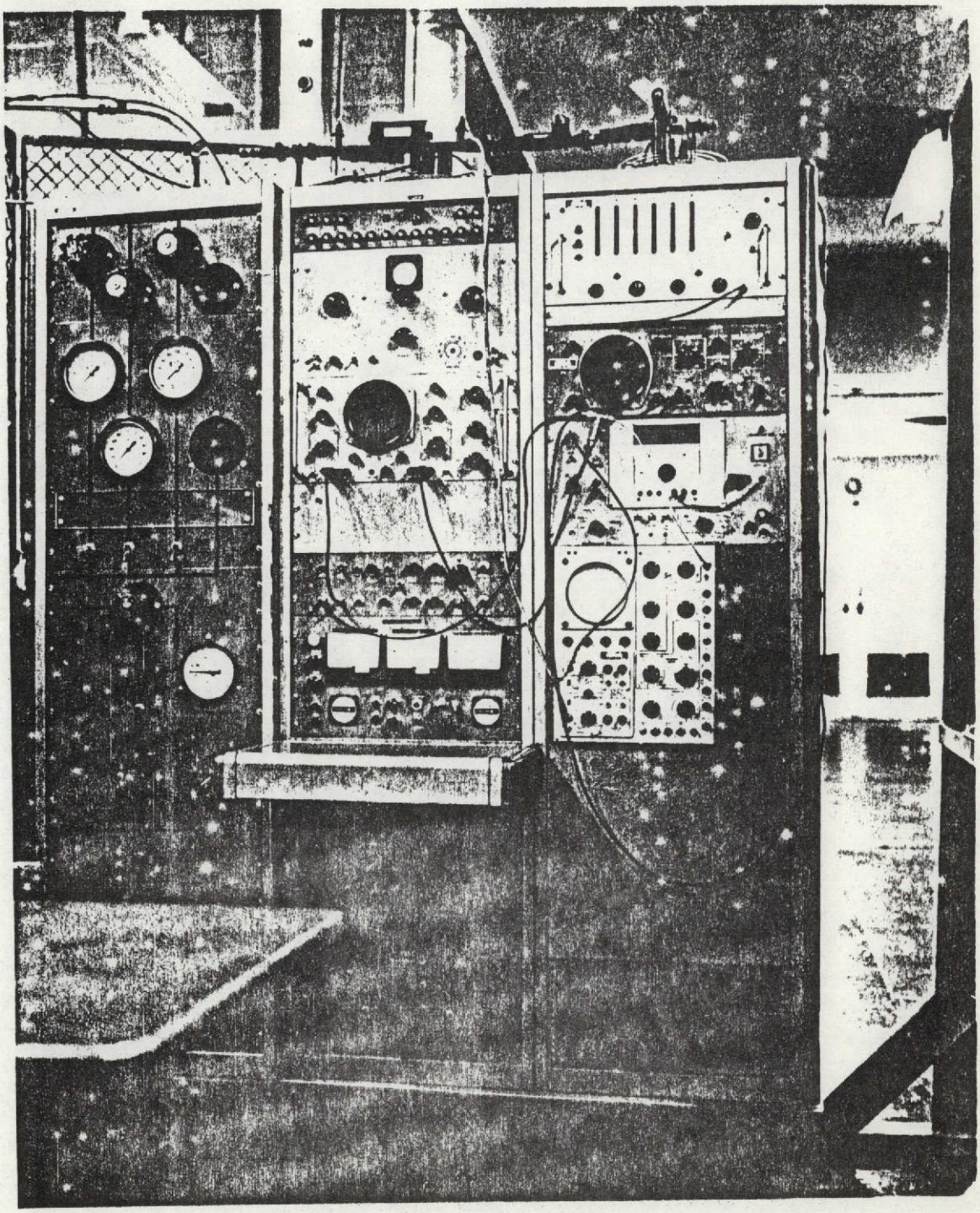

Figure 3. Power supply - Laser system control deck.

various important supply parameters. The left-hand section contains the gas handling system controls for the laser discharge tube. The control deck is a self-contained unit isolated from the dangerous areas of the experiment by a heavy gauge wire partition. The only entrance into the laser/power supply area is through an interlocked door in the partition. Opening the door while the system is in operation will immediately cause the main circuit breaker to open, shutting the high voltage, and therefore the laser, off.

From the inductrol the voltage is fed into a large transformer-rectifier unit. The transformer steps up the inductrol output substantially--up to 30 KV, 3 phase, from 910 volts in. From here, the voltage is fed into the rectifier housing (located on top of the transformer) which contains 12 air-cooled RCA 857B mercury vapor diodes.

High voltage direct current leaves the transformer-rectifier unit and is fed into a small power supply. This serves as a filtering unit for the d.c. input and as a component in a transmission line charging network. This artificial transmission line is subdivided into three parallel, identical units. The use of only a single unit in place of the three to obtain the same power output would not be feasible due to the power limitations of the pulse modulator circuitry. The operation of each system is identical to the other two. A view of the interior of one of the modulators is shown in Figure 4, followed by a schematic diagram in Figure 5. The left-hand side of the unit houses the capacitor bank-inductor assembly that acts as a transmission line. The right-hand side houses the rest of the electronics including the hydrogen thyratron (switch).

A complete analysis of the modulator circuitry has been reported by DeYoung [1]. Summarizing its operation here, an initially open circuit artificial transmission line is charged to a substantial voltage, the maximum associated stored energy being 55 Joules per modulator or 165 Joules for the

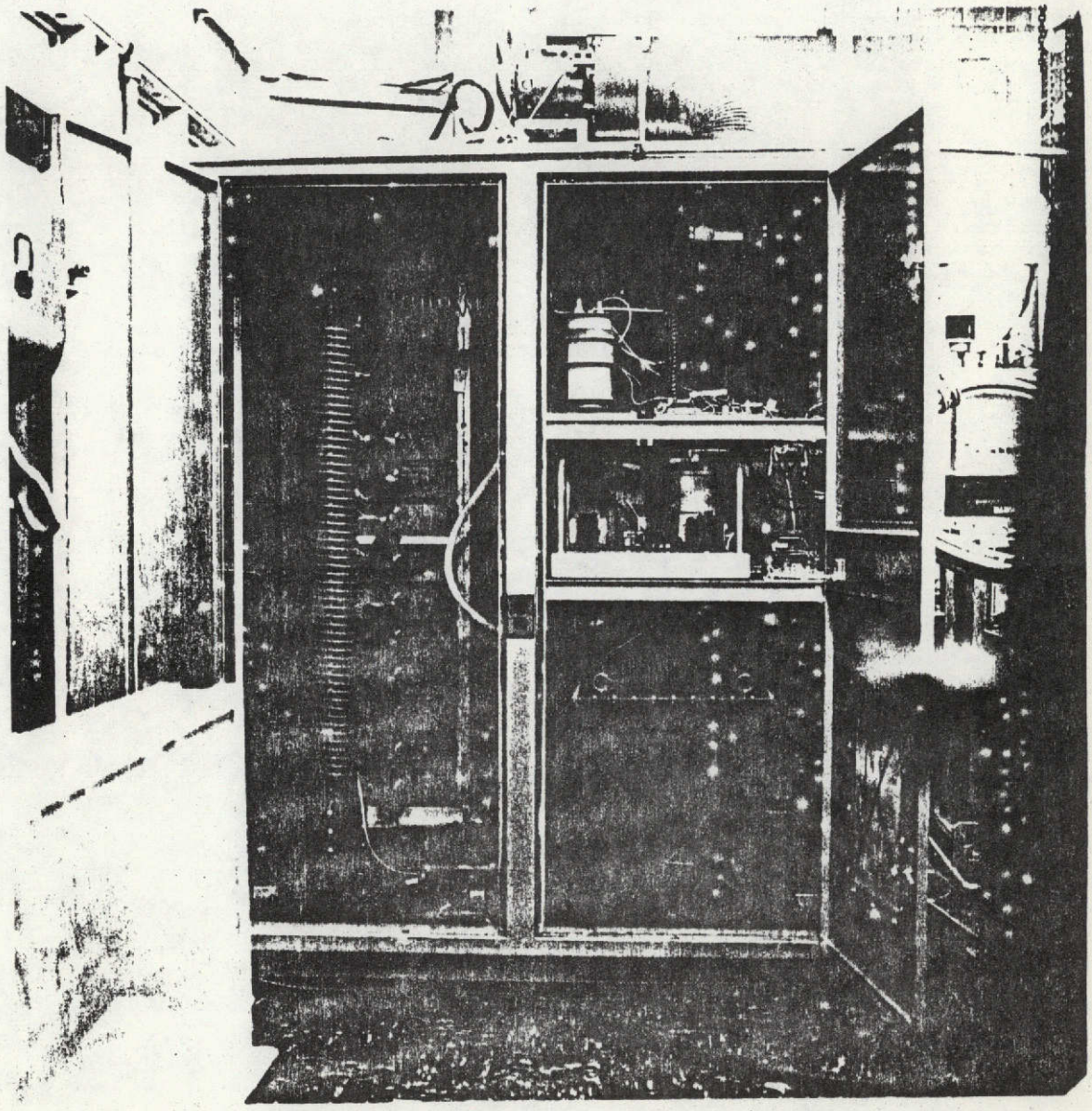

Figure 4. Pulse modulator interior view.

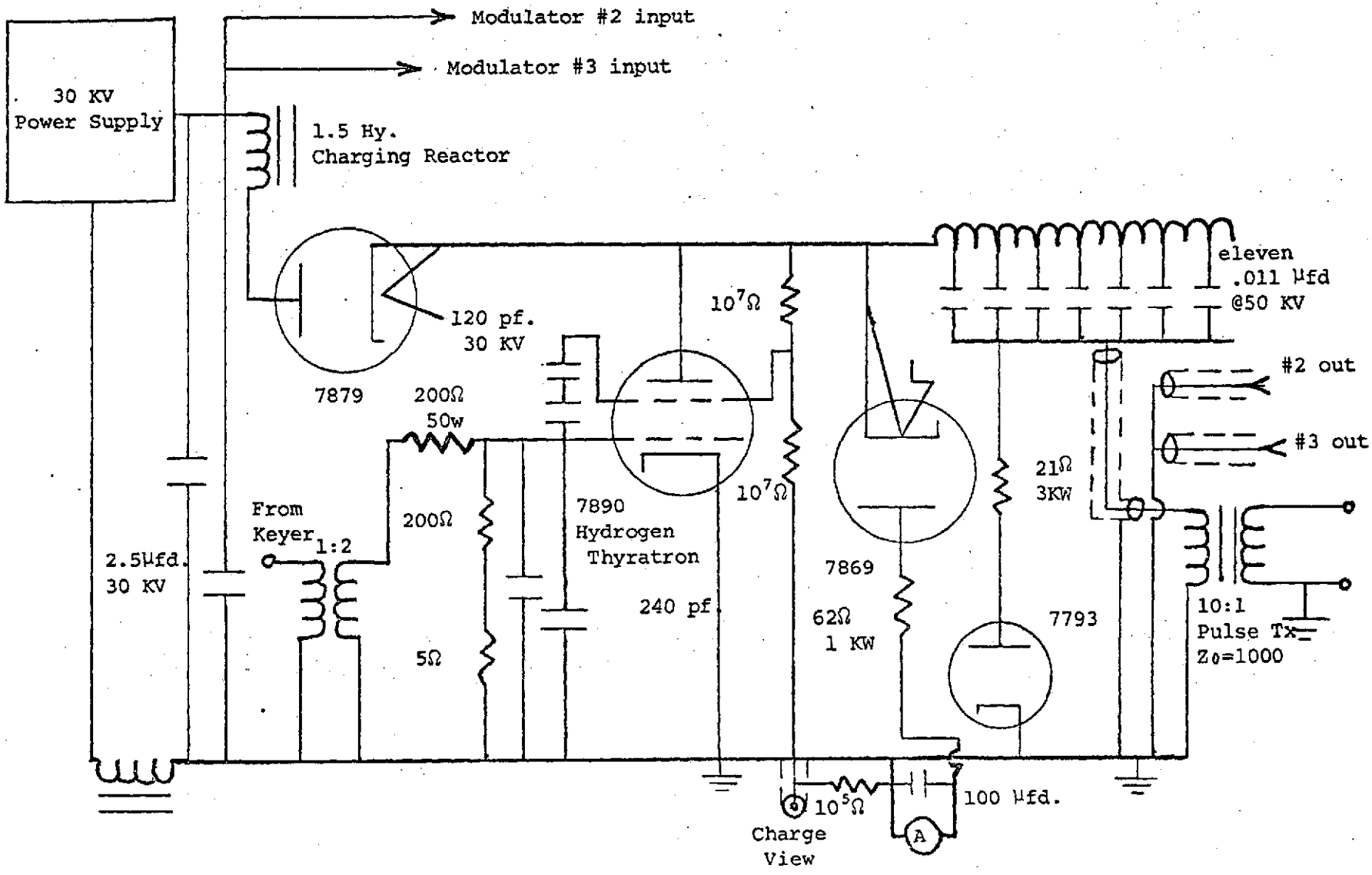

Figure 5. Pulse modulator schematic diagram.

entire system. This transmission line is composed of eleven, .011 microfarad capacitors tapped on to a copper coil 6 inches in diameter and 5 feet long. The transmission line, a 1.5 henry charging reactor and two 2.5 microfarad capacitors form a resonant circuit whose resonant frequency is the charging frequency. When the transmission line is fully charged, a trigger pulse is applied to a GE 7890 hydrogen thyrathon, causing the thyratron to become a low resistance path to ground and the transmission line goes on to discharge through a large pulse transformer. The discharge repetition rate is variable and is predetermined by the operator at the control deck. All three modulators, being in parallel, feed into the pulse transformer, which in turn steps their output voltage up ten times, to 300 KV maximum. The power supply output can be monitored at the control deck using a capacitor voltage divider and a pulse current coil to monitor the peak output voltage and peak current, respectively. The output of the pulse transformer is coupled to the discharge tube by shielded high voltage cables which can be easily recognized in Figure 1.

To conclude, one should be reminded of the more unique features associated with the power supply, to be used as a laser pumping device. They are:

(1) the system's high voltage, high power capability being 300 KV at 100 megawatts,

(2) the easily varied repetition rate of 2 to 380 pulses per second, and

(3) output voltage pulse full-width of 5 microseconds.

Feature (1) places the supply in a class just below several other systems in operation at various laboratories throughout the country. McKnight, Dezenberg and others at the Army's Redstone Arsenal have used Marx generator systems capable of up to 700 KV at comparable or greater powers [2]. They are in the process of building a 2 megavolt supply, while Alan Hill of the Air Force Weapons Laboratory has been using a megavolt supply for some time [3,4]. Hill's

megavolt supply is similar to the pulse modulation system and could be expected to have similar features. However, almost all other pulsed laser research is being carried out using the Marx generator devices which are somewhat lacking with respect to features (2) and (3). The output repetition rate of the Marx systems is not as easily varied as with a pulse modulation device. Maximum repetition rates are typically less than 50 Hz. Also, the time constants associated with high voltage, high energy Marx systems are inherently longer than that associated with the pulse modulation system. McKnight, Dezenbert et al., reported output voltage pulse widths in the range of 40 to 80 microseconds for their 700 KV Marx system. This is a factor of 8 to 16 greater than the 5 microsecond width for the device described in this chapter. The importance in the difference lies with the experimentally observed phenomenon that at pressures of interest (less than 100 torr) the glow-to-arc transition time is on the order of 35 microseconds [2,3]. At excitation times less than 35 microseconds it is expected that arcing will be less of a problem.

Laser Assembly.--Though laser systems can be categorized by their basic configuration (for example: TEA, axially pulsed, etc.), very few systems used in laser research are constructed identically. Each investigator designs a system in accordance with his specific needs. The needs associated with this project called for a laser configuration that

(1) would be especially resistant to thermal (heating) effects,

(2) would be versatile enough to be used for nuclear pumping experiments as well as more conventional laser experiments.

With these items in mind, among others of somewhat lesser importance, the system pictured in Figure 6 was designed and constructed. It can be described as an axially pulsed system built in a modular form having epoxy endsections with a cylindrical quartz cavity and plexiglass water-jacket sealed between them. The overall length of the system is 2.5 meters, with the quartz cavity

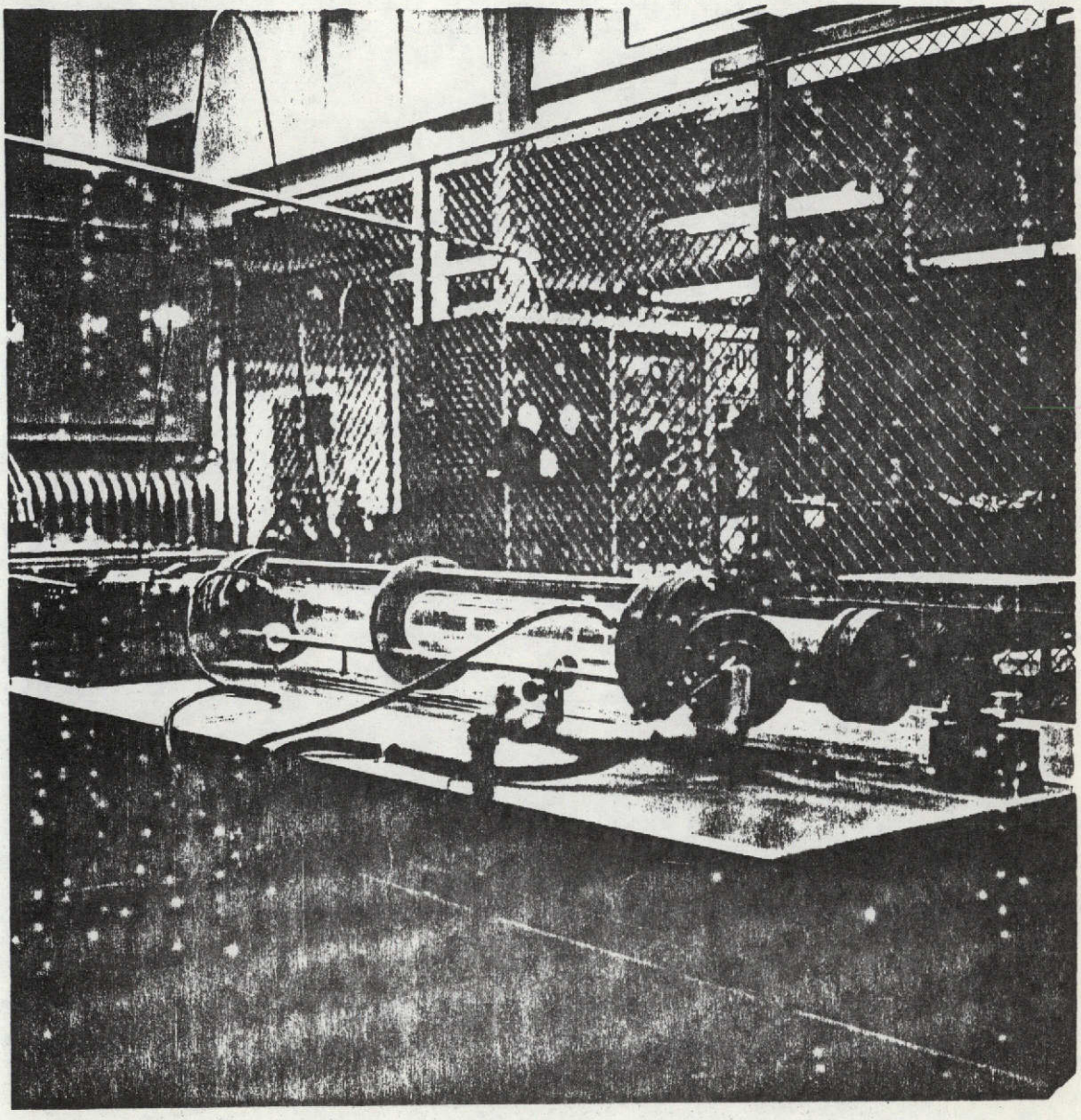

Figure 6. Assembled laser.

being 77 mm in diameter and 1.6 meters long. The complete unit is supported on its bench by adjustable aluminum mounts as pictured.

In constructing the laser as a modular unit, the second criterion above could more easily be met. Nuclear pumping experiments, planned as a future program of study, might very well require the use of various interchangeable cavities. These cavities could be coated with different substances, depending on the particular experiment. For maximum energy deposition in the plasma by any nuclear reactions at the wall of the cavity, one would also design the system using relatively large diameter cavities, and is why the inside diameter of the unit pictured is 77 mm. Yet, the system could easily be adapted to "conventional" (non-nuclear) experiments by using an uncoated cavity. Large diameters are not considered too detrimental to conventional operation. It is true that smaller diameter systems would be characterized by higher flow-through velocities, which is advantageous from a gas cooling and impurity depletion standpoint. However, large diameter systems are characteristically more efficient than their smaller diameter counterparts and are the only systems suitable for nuclear pumping experiments [2]. The modular design would facilitate any required increase (or decrease) in the overall length of the laser.

Nuclear pumping experiments might also require the use of various types of electrodes. There are two reasons for this. It is hoped this axially pulsed system can be operated at relatively high pressures (up to 1 atmosphere), again to maximize nuclear reaction energy deposition in the positive column. Preliminary studies by DeYoung showed that a basic pin-cathode configuration worked well for this application [1]. However, these studies were not conclusive and it is felt additional configurations might be investigated. The second reason one might want to use various electrodes is that the possibility exists that a neutron activated, radioactive, cathode material might allow for

the more efficient operation of a laser through some sort of pre-ionization mechanism. It will be necessary to activate cathods in a nuclear reactor, keep them in a shielded location when not in use, as well as to try various materials. All this is more easily facilitated if the cathode can be easily removed and replaced in the laser. Then to meet this design criterion, the high-voltage cable-cathode-laser endsection shown in Figure 7 was built. The actual unit, separated from the laser endsection, is pictured in Figure 8 showing the stainless-steel, 6-pin cathode used. Each pin is connected to the pulse transformer secondary through a ballast resistor to assure an equal current flow through each stainless-steel rod.

In designing an axially pulsed system (the TEA concept would not be particularly suitable for coated cavity experiments and is not of primary interest with respect to conventional pumping experiments at this time) to be used in conjunction with the 100 MW pulsed power supply, it was felt that thermal degradations of the laser construction materials could become a significant problem. Criterion (1) alludes to this. After all, time averaged input powers up to 200 KW might be possible. The use of a quartz cavity midsection would help to overcome the problem somewhat; the flanged endsections needed to be made from heat resistant material also. What's more, the material used would have to be an electrical insulator. The endsections could not be made of glass due to this material's characteristically poor mechanical properties. The possibilities were reduced to (a) nylon, teflon type materials, (b) acrylics, (c)polyesters and (d) epoxy materials. Elimination is accomplished by noting that the acrylics are generally characterized by low deformation temperatures, on the order of 200°F. The polyesters are extremely difficult, impossible in some respects, to machine. Teflon and nylon materials are very expensive and cannot be bonded to each other or to other materials without using sophisticated techniques. Epoxy was the only alternative.

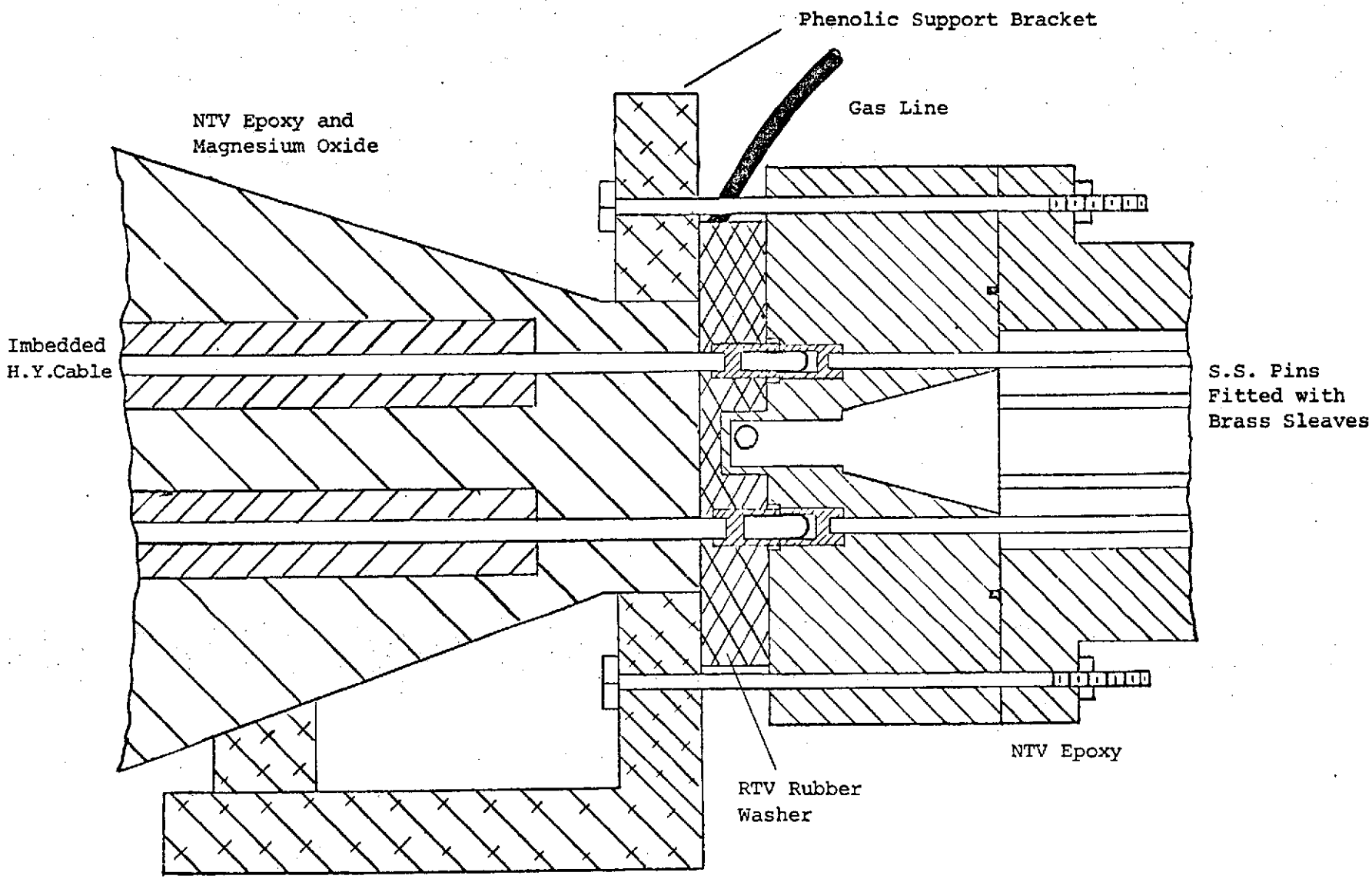

Figure 7. High voltage cable-cathode-laser coupling (apprx. 1/2 size).

The epoxy materials are generally characterized as having outstanding electrical insulating properties, deformation temperatures in the 350° to 450° range, very good mechanical properties (being especially easy to machine) and are relatively inexpensive, especially if one casts the basic solid shapes needed himself. This construction technique was utilized for this work. The specific epoxy used was a 1-to-1 combination of NTV hardner and HV resin base, oven-cured for 15 minutes at 200°F.

Views of the two endsections are found in Figures 1, 6, and 8. Features common to both include flanged optics attachments and off-axis, flanged electrode attachments. Both electrodes had to be placed off-axis, of course, so they would not interfere with the optical path. To couple the electrode attachments into the cavity, a 45-degree configuration was used as an alternative to a 90-degree configuration. Both electrodes are recessed back into the 45-degree pieces. The cathode has already been discussed and is the more important of the two electrodes. The anode in this system is attached directly to ground and whose shape or configuration would not be expected to have any noticeable effect with respect to the electric field pattern within the cavity for the separation distances used. This would hold true only if the configuration of substantial surface area is employed. For this reason, a stainless-steel, hollow-cylinder anode, six inches long was installed.

The quartz cavity seal is accomplished as shown in Figure 9. Bolting the large end-flanges together compresses two O-rings, sealing the quartz tube to the interior of the epoxy endsections. The water-jacket is also pressure sealed using recessed rubber gaskets mounted in the large endflanges.

A hemispherical resonator configuration employing a large radius mirror is used in conjunction with this system. The flat mirror is a 51 mm diameter coated silicon substrate that is 100 percent reflective at 10.6 microns. It is

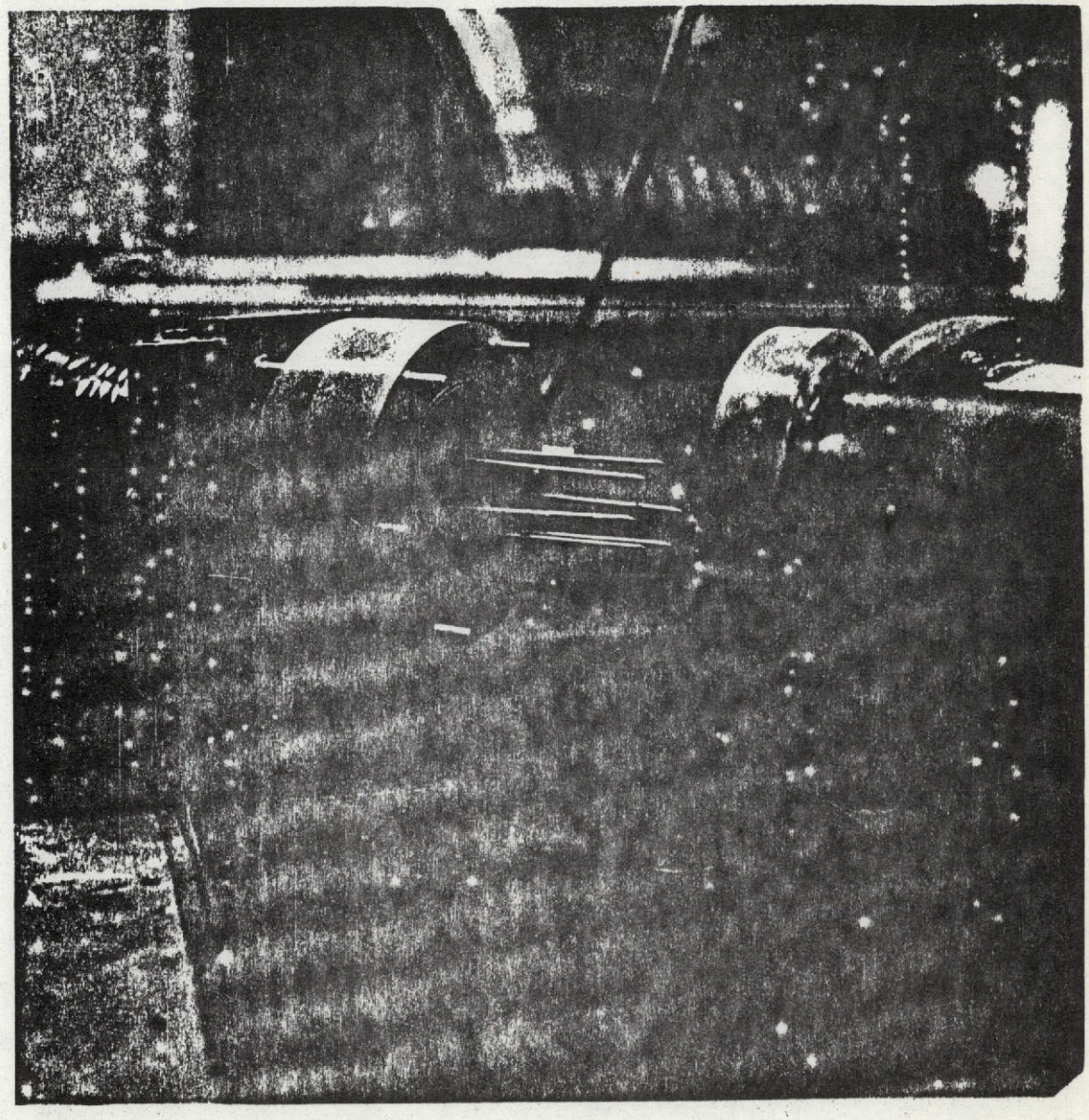

Figure 8. Stainless steel, six-pin cathode.

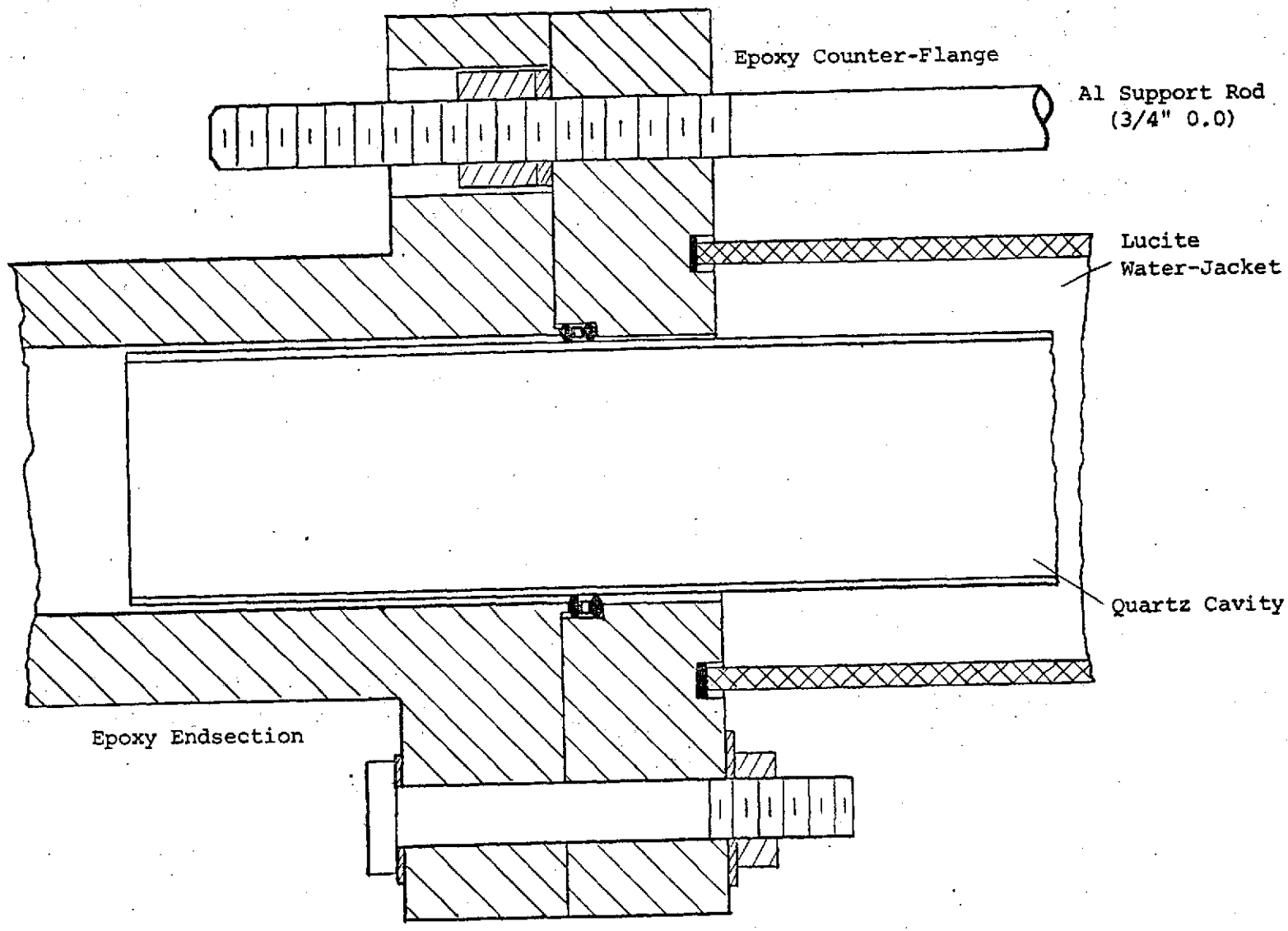

Figure 9. Cavity/Water-Jacket seal to epoxy endsection (apprx. 1/2 size).

mounted in a non-adjustable manner, being recessed into an epoxy flange perpendicular to the cavity axis at the cathode end of the laser. Mounted in an adjustable carrier exterior to the anode end is an 80 percent reflective, 10 meter radius of curvature spherical mirror also 51 mm in diameter. It is made using a germanium substrate and is anti-reflective coated on the output side. Light is coupled from the plasma to the exterior mirror through a NaCl Brewster window (as can be seen in Figure 6). From the index of refraction of salt at 10.6 microns, Brewster's angle is found to be 56 degrees, requiring a 34 ± 1 degree mounting angle of the polished salt flat to the optical axis of the resonator. Due to size limitations on commercially available polished salt flats, he Brewster window is the limiting aperature of the system. Maximum beam diameter was limited to 34 mm. Indeed, one of the more important planned, future modifications of the system is to install 76 mm mirrors and a salt flat to take complete advantage of the plasma media, to increase the system efficiency.

A large radius, hemispherical resonator configuration was chosen for practical reasons. The fact that a small TEM_{oo} spot size (on the order 4 mm) is characteristic of the particular configuration used is overshadowed by other factors; it is usually very difficult to obtain lowest order mode operation of long, large diameter lasers anyway. When the laser described in this work was operating, high order mode structured unfocused beams of 34 mm diameter were seen. The complicated spatial distribution of the field was not particularly important as the beam was focused during the taking of the data. A hemispherical resonator, on the other hand, is very easy to keep in alignment, particularly because with the flat mirror having been installed perpendicular to the laser cavity axis, all further alignment adjustments are made using only the spherical mirror. As final alignment adjustments to obtain the best

beam quality had to be made while the laser was in operation (at low power), placing the flat at the cathode, high-voltage input, end of the laser allowed the experimenter to align the laser in relative safety.

To complete the description of the optics employed in conjunction with the laser, it is necessary to describe the measurement apparatus used to monitor the beam structure and intensity. This arrangement is pictured in Figure 10. To intermittently check the beam structure, the thermal image plate was used in conjunction with an ultra-violet light. To obtain quantitative information concerning the beam's magnitude and structure with time, the laser light was focused by a germanium, concave-convex lens 51 mm in diameter having a 50 mm focal length. The lense focused the light on to the 1 mm x 1 mm active surface of a Barnes T-301 pyroelectric detector. The degree to which the output infrared light energy is focused is known as a function of the lens-to-detector distance. The pyroelectric detector, operated in the current mode, would allow for the oscilliscope display of laser pulse rise times as fast as 150 nanoseconds, and has a responsivity of 1.5 microamps per watt. The output of this detector was fed through a short length of coaxial cable to a current preamplifier. Calibration of the detector-preamplifier as a unit will be discussed in conjunction with the data, in the next section. The output of the preamplifier was fed through an amplifier into a Tektronix 555 dual-beam oscilliscope. The lower beam was used to display the current pulse as measured at the anode of the laser using a Pearson Electronics Model 1025 pulse current coil (20 nanosecond response time). Both cables were terminated into their characteristic impedance at the input of the oscilliscope. A typical set of data is shown in Figure 13.

The characteristics of the laser light output monitored using the pyroelectric detector were studied as a function of pumping voltage, voltage

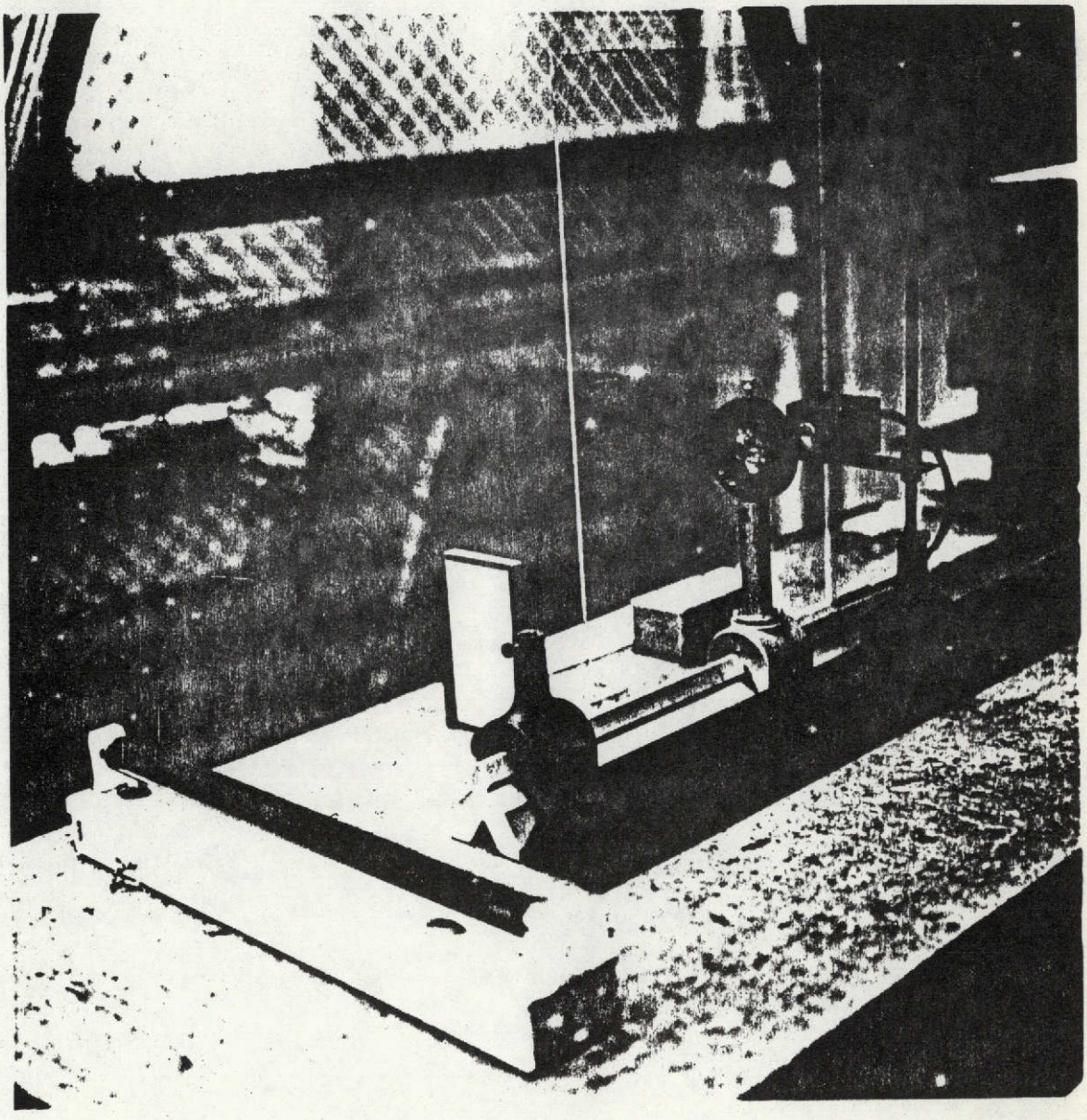

Figure 10. Measurement optics showing pyroelectric detector.

PRECEDING PAGE BLANK NOT FILMED

pulse repetition rate, gas mixture and pressure. Particulars relating to the power supply, specifically in relation to the former two parameters, have already been given. It remains to present details associated with the latter two parameters, that is, information concerning the gas-handling system. A schematic diagram of this system is given in Figure 11 which is fairly self-explanatory. The gas mixtures used contained CO_2, N_2, and helium. The system as constructed could be easily adapted to use additional constituent gases, however.

The mixes were statically premixed in the large chamber shown in Figure 11. This chamber actually consisted of three high-pressure cylinders. The vacuum pump used to maintain the flow provided a constant flow rate above 1 torr of 283 liters/minute. This corresponded to a 2-second volumetric dwell time of the constituent gas. The pressure in the laser cavity was controlled using a regulator and a special regulating valve, as shown in the schematic diagram. The pressure was monitored using a vacuum gauge running to the anode endsection of the laser. Pressure drops across the laser were assumed negligible.

As noted in Figure 11, gas flow was in the direction from cathode to anode. Flow direction can be an important consideration. In a longitudinal discharge gas stream, the working voltage decreases appreciably when the gas flows from the cathode, and increases somewhat when the flow is toward the cathode. No explanation is offered concerning this phenomenon. However, D. Smith of UARL has pointed out another factor that makes it important to flow the gas from cathode to anode in CO_2 laser systems [6]. This directional dependence is caused by an axial variation of I_s, the saturation intensity of the laser medium. This effect is especially noticeable when the dwell time of the gas in the discharge tube is on the order of seconds--as in the system used for this work. Transit times of this order are commensurate with times required

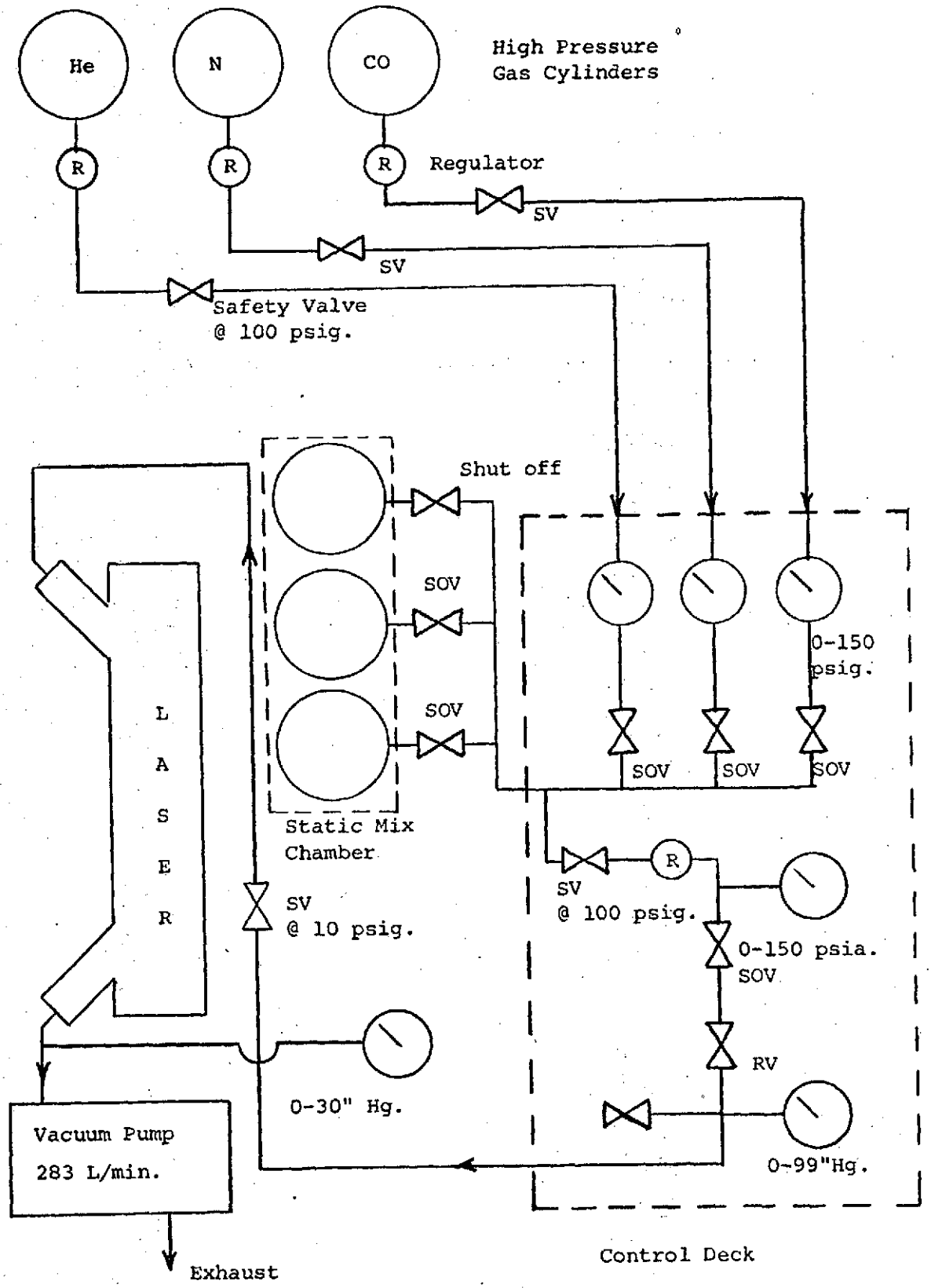

Figure 11. Schematic diagram of gas handling system.

for substantial CO formation in the discharge. Having left all that concerning gas discharge physics for the next chapter, let it suffice to say that the presence of CO in a CO_2 laser discharge can adversely affect the inversion. Then the flow direction is seen to become important through the possible introduction of axial gradients in the laser medium composition. Smith noticed better CO_2 laser performance when the gas flow was from cathode to anode. In the system constructed by this author, the cathode pins are circumferential about a nozzle from which the gas flows from a high pressure line. The gas leaves the system flowing through the anode pipe. The vacuum pump and ground are attached to the exterior protruding section of the anode pipe as can be seen in Figure 6.

With this, the discussion of the practical aspects associated with the laser system can be concluded. Certain problems encountered in the operation of the laser (while the data was being taken) will be discussed in the next section.

Preliminary Laser Performance Data and Analysis

Experimental Method.--A brief description and photograph of the measurement optics and instrumentation has already been given. Yet, before any actual data is presented, certain details of the detector-preamplifier calibration procedure, actual measurement procedure and data reduction calculations should be presented.

As it was important to know the variation with time of the laser output, the Barnes T-301 detector had to be used in conjunction with the current preamplifier (i.e., had to be operated in the current mode). More elaborate and expensive pyroelectric detectors are housed with their own preamplifier and a factory-determined calibration factor for the unit in volts/watt per detector area (typically 1 mm x 1 mm) is specified by the manufacturer. With units such as this it is fairly easy to obtain accurate, absolute determinations of the

magnitude of the laser output intensity variations with time. However, the Barnes unit is not housed with a preamplifier. The user must supply his own and experimentally determine the responsivity of volts/watt if more than just relative intensity variations are wanted. The actual analysis of measurements made while operating the laser will now be given.

It would seem only to be a calculation problem if the current preamplifier gain could be specified in mvolts/μamp, whereby a conversion to mvolts/watt could easily be obtained knowing the detector responsivity in μamp/watt. Yet, the current preamplifier gain factor varies with the type of detector connected to the preamp input. The particular preamplifier used, a RIDL Model 31-17, was factory calibrated in conjunction with a silicon semiconductor detector used in nuclear radiation detection.

Using the measurement electronics described in the last chapter, the Barnes-RIDL unit responsivity, R_{dp}, can be found knowing

$$R_{dp} = \frac{V(\text{volts}) \times 10^2 \left(\frac{\text{mm}}{\text{cm}}\right)^2}{I_p \left(\frac{\text{watts}}{\text{cm}^2}\right)} \times \frac{F}{G}, \qquad (1)$$

where the active area of the Barnes T-301 is 1 mm^2 and where

V = linear amplifier peak output voltage,

I_p = laser output peak intensity, measured using some other detector,

F = "focusing factor" of germanium lense, being the ratio of the focused beam area to the unfocused area (focused area always geater than 1 mm^2), and

G = voltage signal gain due to linear amplifier.

Thus R_{dp} can be found in units of volts/watt per square millimeter.

In determining I_p for the above, a Coherent Radiation Model 201 power meter was used. This device was designed for use with cw laser systems. However, at pulse rates greater than approximately 10 Hz, it essentially acts as an integrator (due to the fairly long recovery times of the thermopile active element). Measuring the average laser output power P_a, the peak intensity can be determined from

$$I_p = \frac{P_a(\text{watts})}{w(\frac{\text{pulses}}{\text{sec}}) \times t_h(\frac{\text{sec}}{\text{pulse}}) \times A_t(\text{cm}^2)} ,$$

where

w = laser pulse repetition rate (assumed equal to power supply pulse rate),

t_h = full-width at half-maximum of laser pulse (measured using pyroelectric detector), and

A_t = Model 201 thermopile cross section area (2.84 cm^2).

Several experimental determinations of the parameters needed in equations (1) and (2) yielded an average value of R_{dp} = 2.8 mvolts/watt per square millimeter for the Barnes-RIDL unit employed.

This experimentally determined value of R_{dp}, however, should only be used to estimate the absolute laser power. The error associated with this responsivity factor could be substantial. Uncertainties in the measured parameters of equations (1) and (2) were found to cause a possible error of 16 percent. Secondly, account must be made for the use of a cw device in determining I_p. Some cooling of the thermopile active element should be expected to take place between pulses. The time between pulses was on the order of 10 milliseconds during the calibration experiments. Estimation of the amount of cooling was not possible as no data concerning the recovery time of the thermopile was available.

Regardless of whether R_{dp} was known accurately or not, relative variations in the laser output as a function of the four independently varied parameters

still could accurately be determined. The data will be reported in relative units, then. Estimations, when made, of the total power output of the laser will be given ignoring any uncertainties associated with R_{dp}. For future experiments, as a system improvement, a pre-calibrated pyroelectric detector-preamp unit should be obtained now that the problems associated with using such devices are better understood.

The relative laser output power variations were determined from

$$P_p = \frac{[(V_m \pm \sigma_n)\text{volts}]F_m}{[(V_N \pm \sigma_N)\text{volts}]F_N} \times \frac{(G_N \pm \sigma G_N)}{(G_m \pm \sigma_G)}, \qquad (3)$$

where

V_m = measured peak output voltage of linear amplifier (Barnes-RIDL unit at input),

σ_m = percent error associated with measuring V_m found from ±1 mm oscilliscope grid reading accuracy,

F_m = focusing factor associated with V_m determination,

G_m = linear amplifier gain factor,

G = percentage error associated with G_m, found from ±1 mm oscilliscope reading accuracy during gain setting calibration of amplifier, and

V_N, etc. = normalization parameters and uncertainties.

The data was normalized with respect to laser output using the 1:2:4 mixture at 0.2" Hg, at 35 KV/m and 51 pulses per second.

The uncertainty associated with the discharge current peak amplitude was controlled by the same ±1 mm oscilliscope grid reading accuracy as well as the ±1 percent accuracy of the pulsed current coil used. The calculated uncertainties associated with measuring pulse-widths and time differences were attributed to oscilloscope reading inaccuracies. A reporduction of a typical data set is shown in Figure 13. Figure 12 is a reproduction of the power supply output voltage waveform into a low pressure plasma load.

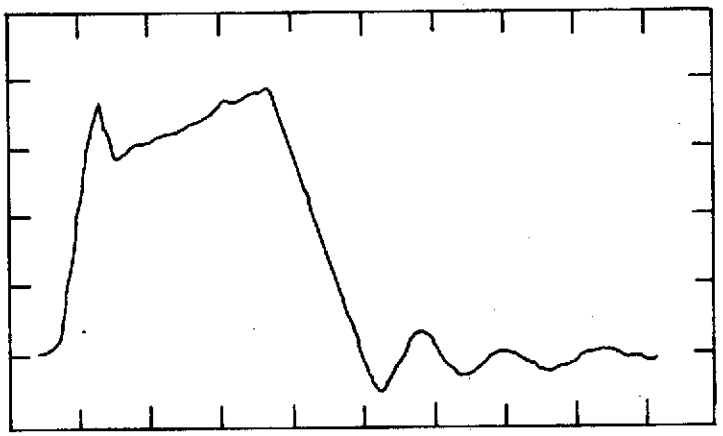

Figure 12. Typical power supply output voltage pulse (low pressure plasma load). Abscissa scale @ 1 μsec/cm.

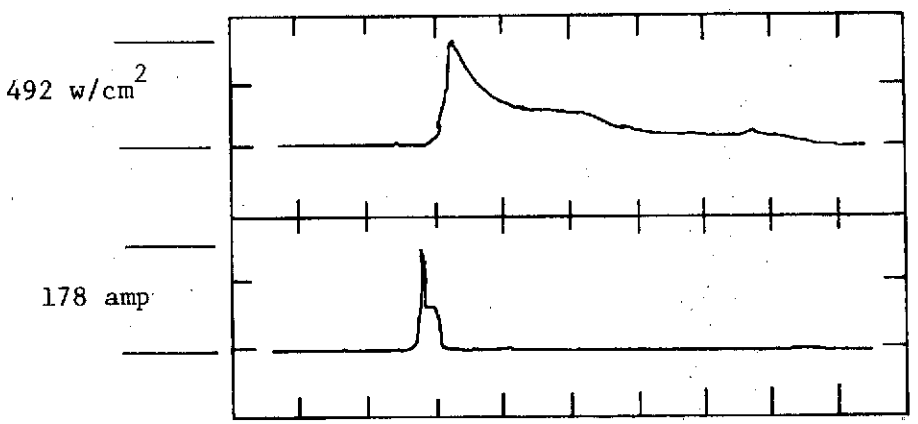

Figure 13. Typical data set. Abscissa scale at 10 μsec/cm, ordinate scales both @ 2 volts/cm.

One is reminded of the four independent parameters:

1. Gas mixture
2. Gas pressure
3. Power supply output voltage amplitude
4. Power supply voltage pulse repetition rate.

The discharge tube laser operation was monitored as a function of these parameters. The systematical method used to make the measurements was to first select the appropriate mixture and then vary the latter three parameters. Three different mixes were investigated. A mix having been selected, one of the three different predetermined operating pressures was chosen. At this operating pressure, then, the output voltage was selected starting with 10 KV with investigations every 10 KV up to 80 KV being made. The output voltage having been selected, the laser operation was monitored at various pulse rates. As mentioned in the last section, the pulse repetition rate could be easily and continuously varied from 2 to 380 Hz. To facilitate a systematic investigation of the laser output as a function of pulse rate, the sequence of 2, 5, 10, 25, 50, 100, 150, 200, 250, 300, 350 Hz was used. This sequence having been completed, the laser output was "tuned" for its optimum value and data was taken at this repetition rate also.

Gas mixtures of CO_2:N_2:He of 1:2:4, 1:2:8, 1:4:4 were used. These mixes were chosen for various reasons including the fact that Dezenberg et al., obtained results that showed, using a laser system similar to the one described in this work, the optimum CO_2:N_2 ratio is between 1:4 and 1:2 where the optimum CO_2:N_2:He ratio is 1:4:4 [2].

As mentioned previously, three pressures of operation were investigated. They were 0.2, 0.6, 1.0 inches of mercury. An upper limit on the discharge pressure was set by the upper limit on the voltage potential needed to initiate the discharge. Conceptual plans for this experiment envisioned the use of

pressures up to one atmosphere (shown to be feasible through DeYoung's experiment [1]). However, at pressures above 1.0" Hg and voltages above 80 KV, electrical breakdown into the laser water-jacket occurred through the double O-ring seal. Another improvement, then, that should be made before future experiments are begun is to modify the cavity-to-endsection seal, making it more resistant to breakdown, or remove the water-jacket altogether and use forced air cooling as Hill did when encountering similar problems [4]. Nonetheless, much interesting data was obtained at the lower pressures and voltages used.

As the four independent parameters were varied, several dependent parameters were monitored. These were:

1. Discharge current pulse amplitude
2. Discharge current pulse time variation (e.g., pulse width, rise time),
3. Laser output pulse amplitude,
4. Laser output pulse time variation,
5. Current pulse to laser pulse time delay,
6. Optimum pulse rate, and
7. General plasma characteristics.

In monitoring the general plasma characteristics, such items as the homogeneity of the plasma, pulse rate at which plasma constrictions (arcs) occurred were noted.

In this experiment, the power supply output voltage amplitude was specified knowing the transmission line charging voltage and the 10:1 step-up factor of the pulse transformer. The unmodulated direct current charging voltage was read from an appropriate panel meter at the control deck. Ten times this value was taken as the power supply output pulse (assumed square) amplitude. The oft-used E/N parameter is usually specified in the literature knowing only

the charging voltage, electrode separation and total gas pressure. No account of the always varying plasma complex impedance or reflections is made [3]. This convention will be used in the following presentation for both E and E/N.

Experimental Results.--Measurements made with the CO_2 laser described in the last section led to the results presented in Tables 1 through 9. The symbolic representation of the parameters is:

E = applied field strength,

I_d = peak discharge current measured at anode,

P_p = laser output peak power in relative units,

t_f = laser pulse full-width (at baseline),

w = pulse repetition rate,

t_h = laser pulse full-width at half-maximum, and

t_d = time (delay) between end of current pulse and beginning of laser pulse.

A relative power of 1.0 is estimated to correspond to 62.6 KW.

In the tables, specifications of an "incomplete discharge" mean that visually no positive column was seen and no lasing was detected. The term "unstable discharge" refers to the condition where at low repetition rates no positive column was formed, but as the pulse rates were increased an arc was generated, no lasing having been detected at the transition point. The notation "no lasing detected" refers to the condition where a positive column was formed but no measureable amount of lasing occurred. Transitions from a lasing condition to a non-lasing condition which was immediately followed by the formation of a very bright, highly constructed discharge have been noted by the notation "arcing began."

By referring back to the repetition rate sequence and output voltage sequence, one is better able to interpret the data tables. If, at a certain electric field strength (having completely gone through the pulse rate sequence)

Table 1

Data Measured with 1:2:4 Mix at 0.2 inches Hg.

E (KV/m) \ W (Hz)	I_d (amps)	P_p (r.u.)	t_f (μsec.)	t_h (μsec.)	t_d (μsec.)
5 \ -	----------Incomplete Discharge----------				
10 \ -	----------No Lasing Detected----------				
15 \ 51	62±3	.075±.006	28±2	12±2	42±2
15 \ 42	42±2	.063±.005	42±2	20±2	30±2
15 \ 120	----------Arcing Began----------				
20 \ 50	71±3	.14±.01	38±2	12±2	22±2
20 \ 37	71±3	.23±.02	32±1	15±1	5±1
20 \ 100	----------Arcing Began----------				
25 \ 51	105±5	.29±.03	32±1	5±1	6±1
25 \ 62	98±5	.80±.07	8±1	4±1	1±1
25 \ 82	----------Arcing Began----------				
30 \ 51	133±5	.71±.07	13±1	4±1	0±1
30 \ 59	----------Arcing Began----------				
35 \ 25	147±6	.11±.01	40±1	18±1	7±1

Table 1 Continued

W (Hz) / E (KV/m)	I_d (amps)	P_p (r.u.)	t_f (μsec)	t_h (μsec)	t_d (μsec)
51 / 35	142±5	1.00±.06	18±1	4±1	-1±1
55 / 35	----------Arcing Began----------				
25 / 40	178±6	.57±.04	54±1	5±1	0±1
39 / 40	160±6	1.9±.2	18±1	4±1	-1±1
45 / 40	----------Arcing Began----------				

Table 2

Data Measured with 1:2:4 Mix at 0.6 inches Hz.

E (KV/m) \ W (Hz)	I_d (amps)	P_p (μsec)	t_f (μsec)	t_h (μsec)	t_d (μsec)
- / 5	----------Incomplete Discharge----------				
- / 10	----------Incomplete Discharge----------				
- / 15	----------Unstable Discharge----------				
45 / 20	18±1	.0010±.0001	20± 2	4 ±2	36 ±2
75 / 20	----------Arcing Began----------				
24 / 25	58± 3	.0030±.0002	26± 2	20± 2	18± 2
51 / 25	71± 3	.0010±.0001	26± 2	4± 2	30± 2
53 / 25	----------Arcing Began----------				
25 / 30	93±3	.45±.04	26±1	8±1	5±1
48 / 30	----------Arcing Began----------				
23 / 35	107±5	.36±.03	24±1	10±1	1±1
40 / 35	----------Arcing Began----------				
25 / 40	133±5	.43±.03	30±1	13±1	4±1
30 / 40	----------Arcing Began----------				

Table 3

Data Measured with 1:2:4 Mix at 0.1 inches Hg.

W (Hz) / E (KV/m)	I_d (amps)	P_p (r.u.)	t_f (μsec)	t_h (μsec)	t_d (μsec)
- / 5	----------Incomplete Discharge----------				
- / 10	----------Incomplete Discharge----------				
- / 15	----------Incomplete Discharge----------				
- / 20	----------Unstable Discharge----------				
- / 25	----------Unstable Discharge----------				
25 / 30	36±4	.46±.03	18±2	5±2	18±2
30 / 30	----------Arcing Began----------				
- / 35	----------High Voltage Breakdown----------				
- / 40	----------High Voltage Breakdown----------				

Table 4

Data Measured with 1:4:4 Mix at 0.2 inches Hz.

W (Hz) / E (KV/m)	I_d (amps)	P_p (r.u.)	t_f (μsec)	t_h (μsec)	t_d (μsec)
- / 5	----------Incomplete Discharge----------				
150 / 10	18±2	----Sporadic Lasing----			28±2
158 / 10	20±2	.083±.007	44±2	15±2	40±2
165 / 10	----------Arcing Began----------				
53 / 15	36±3	.037±.003	20±2	4±2	63±1
101 / 15	53±4	----Sporadic Lasing----			72±2
74 / 15	49±4	.075±.006	64±2	4±2	29±2
110 / 15	----------Arcing Began----------				
51 / 20	62±3	----Sporadic Lasing----			30±2
80 / 20	----------Arcing Began----------				
54 / 25	107±4	.14±.01	16±1	4±1	4±1
70 / 25	----------Arcing Began----------				
51 / 30	124±5	.17±.01	13±1	5±1	3±1
60 / 30	----------Arcing Began----------				

Table 4 Continued

W (Hz) / E KV/m	I_d (amps)	P_p (r.u.)	t_f (μsec)	t_h (μsec)	t_d (μsec)
25 / 30	144±5	------Sporadic Lasing------			12±2
49 / 35	142±5	.26±.02	28±1	6±1	1±1
60 / 35	----------Arcing Began----------				
25 / 40	171±6	.11±.01	27±2	16±2	15±2
47 / 40	169±6	.28±.02	48±1	10±1	3±1
50 / 40	----------Arcing Began----------				

Table 5

Data Measured with 1:4:4 Mix at 0.6 inches Hg.

E (KV/m) \ w (Hz)	I_d (amps)	P_p (r.u.)	t_f (μsec)	t_h (μsec)	t_d (μsec)
5	----------	---Incomplete Discharge---			----------
10	----------	---Incomplete Discharge---			----------
15	----------	---Unstable Discharge---			----------
20	----------	---Unstable Discharge---			----------
25	40±4	.17±.01	20±2	8±2	18±2
25	----------	---Arcing Began---			----------
30	107±5	.34±.02	25±2	7±2	16±2
30	----------	---Arcing Began---			----------
35	----------	---High Voltage Breakdown---			----------
40	----------	---High Voltage Breakdown---			----------

Table 6

Data Measured with 1:4:4 Mix at 1.0 inches Hz.

W (Hz) / E (KV/m)	I_d (amps)	P_p (r.u.)	t_f (μsec)	t_h (μsec)	t_d (μsec)
5	----------	----Incomplete Discharge----			----------
10	----------	----Incomplete Discharge----			----------
15	----------	----Incomplete Discharge----			----------
20	----------	----Incomplete Discharge----			----------
25	----------	----High Voltage Breakdown----			----------
30	----------	----High Voltage Breakdown----			----------
35	----------	----High Voltage Breakdown----			----------
40	----------	----High Voltage Breakdown----			----------

Table 7

Data Measured with 1:2:8 Mix at 0.2 inches Hg.

W (Hz) / E (KV/m)	I_d (amps)	P_p (r.u.)	t_f (μsec)	t_h (μsec)	t_d (μsec)
- / 5	----------Incomplete Discharge----------				
150 / 10	27±2	.029±.003	28±2	4±2	59±2
197 / 10	36±2	.050±.004	40±2	6±2	56±2
230 / 10	----------Arcing Began----------				
98 / 15	53±3	---Sporadic Lasing----------			76±2
149 / 15	62±3	.034±.003	38±2	10±2	53±2
133 / 15	62±3	-----Sporadic Lasing----------			48±2
250 / 15	----------Arcing Began----------				
101 / 20	84±3	.061±.004	58±2	8±2	37±2
152 / 20	84±3	.010±.001	30±4	10±4	75±4
165 / 20	----------Arcing Began----------				
54 / 25	107±5	.016±.001	38±2	6±2	32±2
98 / 25	107±5	.020±.002	64±2	14±2	37±2
69 / 25	107±5	.023±.002	66±2	20±2	18±2

Table 7 Continued

W (Hz) / E (KV/m)	I_d (amps)	P_p (r.u.)	t_f (μsec)	t_h (μsec)	t_d (μsec)
112 / 25	----------Arcing Began----------				
50 / 30	124±5	.012±.001	52±2	16±2	11±2
104 / 30	124±5	.005±.001	49±2	10±2	26±2
69 / 30	124±5	.013±.001	54±2	34±2	10±2
110 / 30	----------Arcing Began----------				
26 / 35	124±5	.010±.001	44±2	22±2	17±2
50 / 35	133±5	.013±.001	40±2	28±2	8±2
66 / 35	142±5	.016±.001	50±2	27±2	6±2
110 / 35	----------Arcing Began----------				
25 / 40	156±6	------Sporadic Lasing--------			12±2
51 / 40	160±6	------Sporadic Lasing--------			7±2
105 / 40	----------Arcing Began----------				

Table 8

Data Measured with 1:2:8 Mix at 0.6 inches Hg.

W (Hz) / E (KV/m)	I_d (amps)	P_p (r.u.)	t_f (μsec)	t_h (μsec)	t_d (μsec)
- / 5	----------Incomplete Discharge----------				
- / 10	----------Incomplete Discharge----------				
- / 15	----------Incomplete Discharge----------				
- / 20	----------Unstable Discharge----------				
27 / 25	40±4	.008±.001	44±1	8±2	16±2
53 / 25	----------Arcing Began----------				
24 / 30	107±5	----------Sporadic Lasing----------			16±2
49 / 30	107±5	----------Sporadic Lasing----------			15±2
60 / 30	----------Arcing Began----------				
24 / 35	107±5	----------Sporadic Lasing----------			12±2
- / 40	----------High Voltage Breakdown----------				

Table 9

Data Measured with 1:2:8 Mix at 1.0 inches Hg.

W (Hz) / E (KV/m)	I_d (amps)	P_p (r.u.)	t_f (μsec)	t_h (μsec)	t_d (μsec)
5	----------	Incomplete Discharge			----------
10	----------	Incomplete Discharge			----------
15	----------	Incomplete Discharge			----------
20	----------	Incomplete Discharge			----------
25	----------	Unstable Discharge			----------
30	----------	Unstable Discharge			----------
35	----------	High Voltage Breakdown			----------
40	----------	High Voltage Breakdown			----------

no lasing was detected, the general plasma behavior was noted as explained above. If, however, lasing was detected, data was taken starting at the lowest sequence pulse rate for which output could be measured. Similar measurements were made at higher rates in the sequence until lasing action terminated. Termination invariably happened just before the formation of the arc. The arcing point having been found, laser output was tuned for optimum by adjusting the pulse rate and data was taken.

General Behavior.--At sufficient field strengths to maintain a homogeneous discharge, i.e., a discharge which seemed to fill the whole tube, the plasma could be caused to constrict and arc merely by increasing the pulse rate of the power supply. Constriction diameters ranged from about one-half of the discharge tube to 1 or 2 centimeters, at which point the arc usually formed. Visually, this is quite a dramatic effect.

Another general but related effect that cannot be explicitly deduced from the data tables was the continuous variation of laser output peak power with pulse rate. Lasing only occurred at intermediate pulse rates. When lasing did occur both t_d and thelight intensity (output power) varied dramatically with pulse rate. It was originally believed by the author that lasing would occur over a much larger pulse rate range than actually was seen. The "coarseness" of the pulse rate sequence given previously reflects this. Further experiments should perhaps be made over a smaller variation in the pulse rate so that the related effects can be better analyzed.

Other general observations can be made concerning the laser's operation as the four independent parameters were changed. The first being that there was always a delay between the time at which the current was maximum and the time at which the peak 10.6 micron output was seen. Secondly, the current pulse shape was fairly consistent (except for amplitude) over all the observations

made. It rose very fast, on the order of 1 μsec, and lasted only a short time, 2 to 4 μsec, being almost triangular in shape for nearly every case. The lowest pressure experiments did produce somewhat of a variation. The pulse still rose very fast to form an initial spike but was followed by a narrow plauteau and roughly one-half the amplitude of the initial spike. Yet the total width in these cases was still less than 5 μsec. A current pulse of this type can be seen in Figure 13. Laser pulses on the other hand, lasted anywhere from 8 to 64 μsec. The only general observation concerning the laser pulses that can be made is that they also were characterized by very fast rise times, 1 to 4 μsec, which terminated in the formation of the initial peak. This peak represented that point in time at which there was a maximum laser light output. Such a pulse is also pictured in Figure 13.

Mixture Dependence.--The more discernible effects of changing the partial pressure ratios on the laser's operational characteristics are illustrated graphically in Figures 14 and 15. It can be seen from Tables 1, 4 and 7 and Figure 14 that the optimum mixture at 0.2" Hg total pressure is 1:2:4, CO_2:N_2:He, with the helium-rich mix resulting in the poorest laser performance (as far as light output was concerned) below 40 KV/m. This observation is not a function of repetition rate. What's more, it would seem to be more a general result holding true for 0.6" and 1.0" hg, making comparisons among Tables 2, 3, 5, 6, 8 and 9. What numerical data that is available at these higher pressures follows the trend seen in Figure 14; the 1:2:4 mix produced the highest peak output intensity at any given electric field strength or pulse rate investigated. In general, it was much easier to generate laser action from the CO_2-rich mixture (1:2:4) at the higher pressures.

Another trend is illustrated in Figure 15. The delay times associated with the helium-rich mixture are considerably longer as compared with similar runs made with the 1:4, CO_2:He mixes at a total pressure of 0.2" Hg. Where comparisons are possible, the tabulated data does not produce any strong deviation

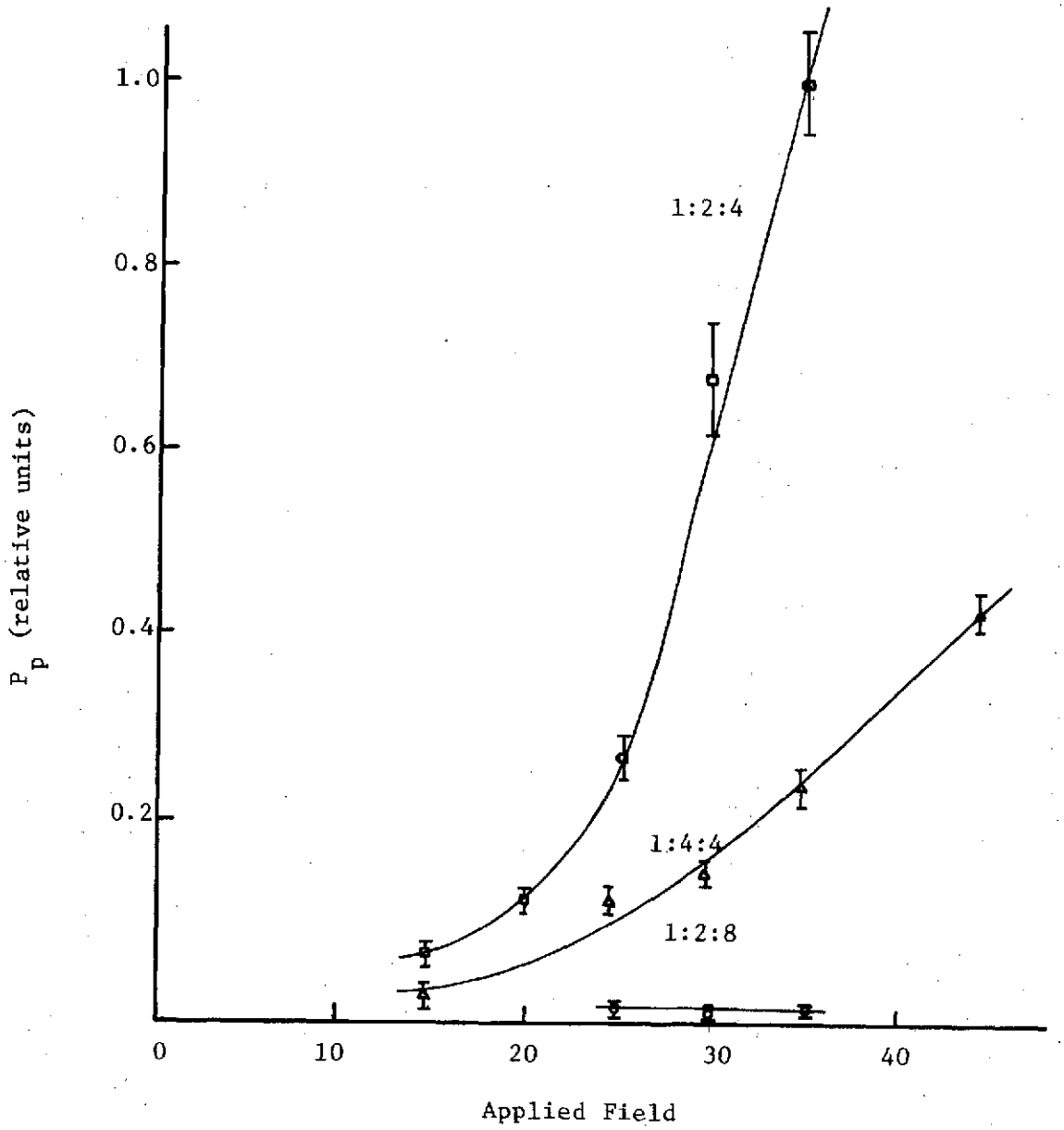

Figure 14. Laser output power as a function of applied field for different mixes at 0.2" Hg total pressure, approximately 50 pps.

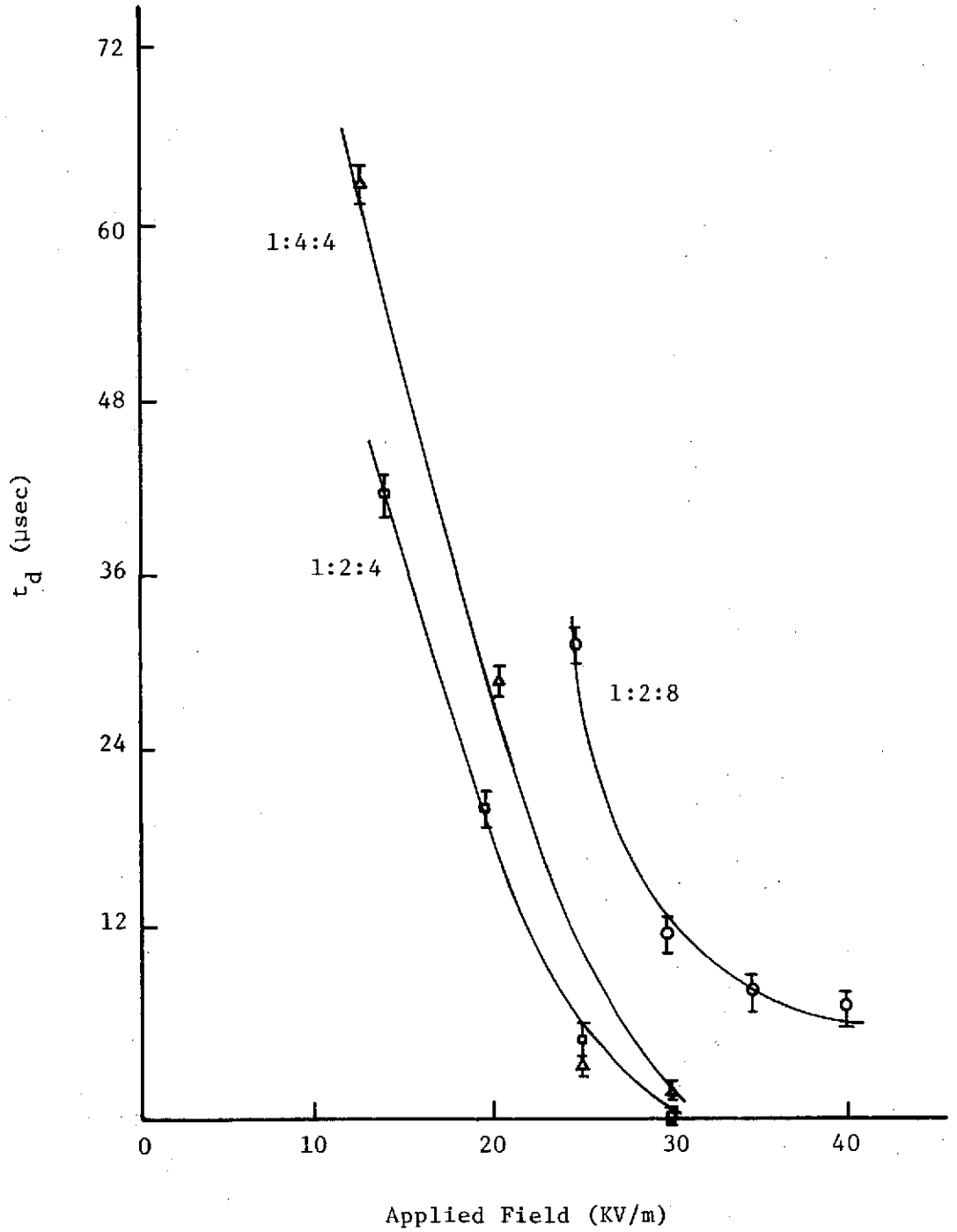

Figure 15. Time delay as a function of applied field for different mixes at 0.2" Hg total pressure, approximately 50 pps.

from the trend of higher pressures. However, at these higher total pressures the differences in t_d for each mix become much smaller, some being nearly equal. With respect to the laser pulse baseline full-width and full-width at half-maximum, no obvious trends are seen.

It was found that the discharge current peak amplitude varied somewhat with mixture also. The peak current amplitude was generally greater for the 1:2:4 mix at both 0.2" and 0.6" Hg overall gas pressure. Comparable amplitudes were generally less for the 1:2:8 mix. Except for a few cases where the amplitudes were nearly equal, no deviation from this trend was seen.

One final comparison can be made with respect to mixture operational dependencies. At low pressure the optimum pulse rate was generally higher for the 1:2:8 mix than for the other two mixes at comparable electric field strengths. The data is insufficient at 0.6" and 1.0" Hg for similar comparisons.

Pressure Dependence.--Due to the lack of higher total pressure data, it is difficult to deduce anything concerning the laser's gain characteristics with pressure. At the higher pressures under the applied field limits of the system (40 KV/m) it was difficult to generate any form of homogeneous discharge which made the generation of laser action also very difficult. Consequently, no trend was seen in the variation of the laser peak output power with pressure using what small amount of data that was available. The behavior of the various "time" parameters does seem to follow definite patterns, however. Trends were only deducible from Tables 1, 2 and 3, but in all comparable cases the time delay between current and laser pulses increased with pressure. On the other hand, the laser pulse full-width decreased as pressure was increased. In all cases but one, the full-width at half-maximum also decreased. Having substantially more data available, from all the tables it was seen that for fields greater than 25 KV/m, the optimum pulse rate decreased with increases in total mixture pressure. This result is not a function of the partial

pressure ratios. No trend below 30 KV/m was seen.

From the data tables, a trend in the variation of the optimum pulse rates (the pulse rates at which maximum power was attained for any given set of parameters) with the applied voltage can be seen. Generally, the optimum pulse rate values decreased as the electric field strength was increased. Out of the many comparisons made, there were only two exceptions to this trend, as can be seen in Table 1. This result, although independent of mixture or pressure, should not be applied to 1.0" total pressure operation due to insufficient data. Finally, where lasing did occur and was terminated by arcing, the pulse rate at which point the arc was initiated tended to decrease as the applied field strength was increased.

Pulse Rate Dependence.--General behavioral information concerning the variation with pulse rate of the plasma structure has already been given. The same sort of "tuning" effect occurred under lasing conditions and therefore, affected the laser's operational characteristics. Some of the laser pulse features changed dramatically with pulse shape. The invariable trend of the output peak power variance with pulse rate is depicted in Figure 16. In all cases where lasing occurred there was an associated optimum pulse rate. In most cases, changing the pulse rate caused a substantial variation in the output amplitude (a feature seen with Figure 16). Also, it was noticed that laser operation usually occurred over a relatively narrow pulse rate range and never over the entire 2 to 380 Hz. Lasing action never occurred at pulse rates greater than 250 Hz and usually cut off long before this rate was attained. Cutoff was accompanied, as has been mentioned, by the generation of an arc between the electrodes.

The discharge peak current amplitude also showed some variation with pulse rate in more than half of the comparable cases. This variation almost always

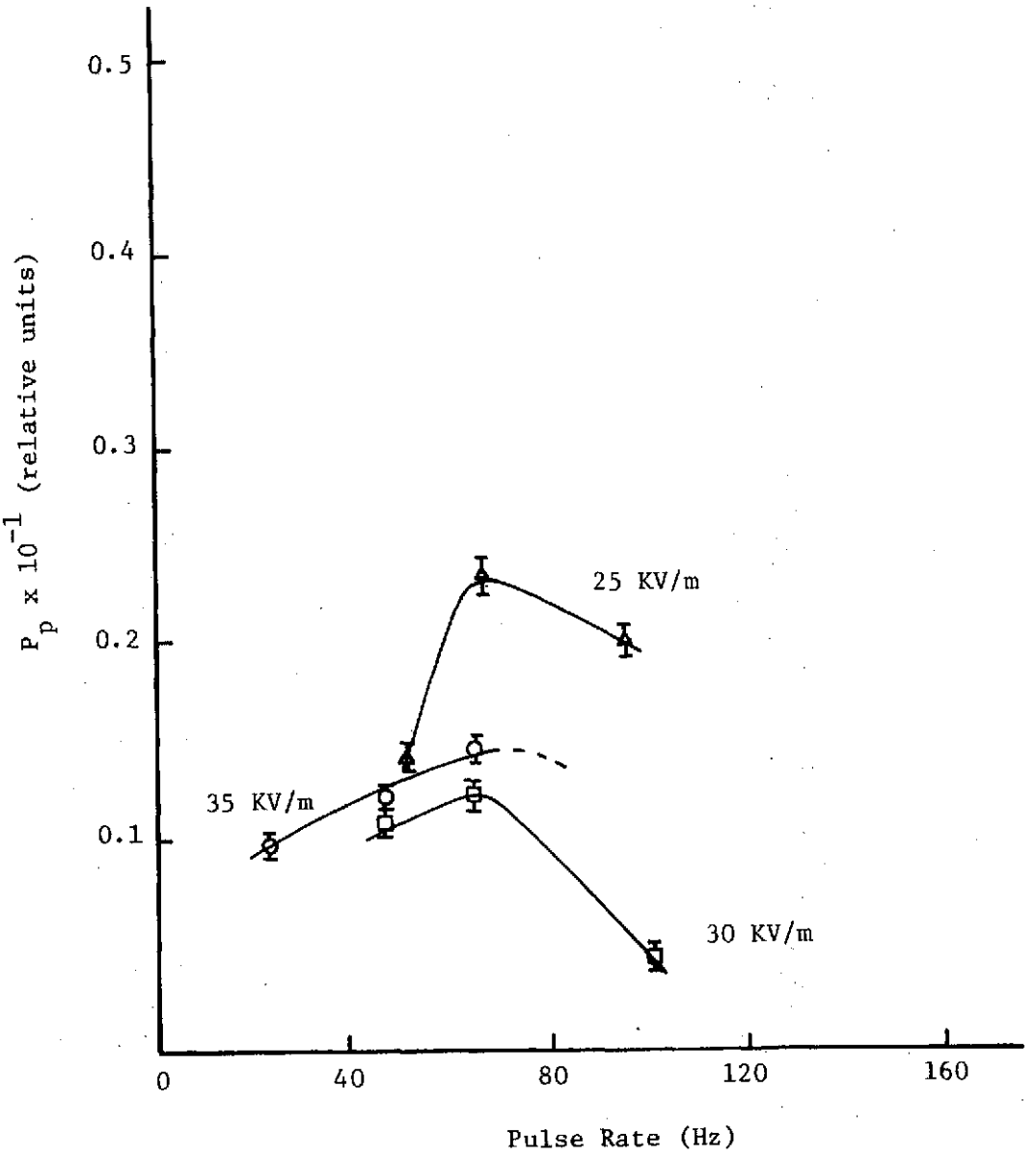

Figure 16. Laser output peak power as a function of pulse rate at various applied field strengths for 1:2:8 mix at 0.2" Hg.

resulted in an increase in the peak current amplitude as the pulse rate was increased; in only 1 of 15 determinations was the opposite true. No trend was seen with respect to the variation of discharge current with optimum pulse rate.

No trends could be deduced from the measurements made concerning any variation of the laser pulse full-width or full-width at half-maximum with pulse repetition rate. More data with respect to this analysis would be helpful. Yet, the current-to-laser pulse delay time did vary systematically with the pulse rate. This variation is illustrated in Figure 17 for the 1:2:8 mix at low pressure. This graph illustrates two effects. First, as with the output peak power, varying the pulse rate usually produced a dramatic change in t_d. Secondly, at the optimum pulse rate this delay time was found to be a minimum. This result is independent of mixture, pressure or applief field strength where comparisons could be made. Input energies were relatively low, being less than 10 joules per pulse. E/N values characteristic of the laser system were relatively large, estimated to be on the order of 10^{-14} to 2×10^{-13} Vcm^2. Finally, the optical axis radius was 1.1 centimeters smaller than the cavity cross section radius.

Discharge Instabilities.--The general discharge behavior, it is felt, is highly dependent on the amount of impurities generated in the cavity. The instabilities (discharge constrictions, arcs) seen as the pulse rate was increased, were attributed to the increasing buildup of impurities with increasing pulse rate. Convective removal of any impurities was relatively slow due to the 2 second gas dwell time reported. The fact that the threshold pulse rate for arc instability generation decreased as the applied field strength increased is consistent with the impurity hypothesis. The impurities most prevalent in a CO_2-N_2-He discharge come about through CO_2 and N_2 dissociation.

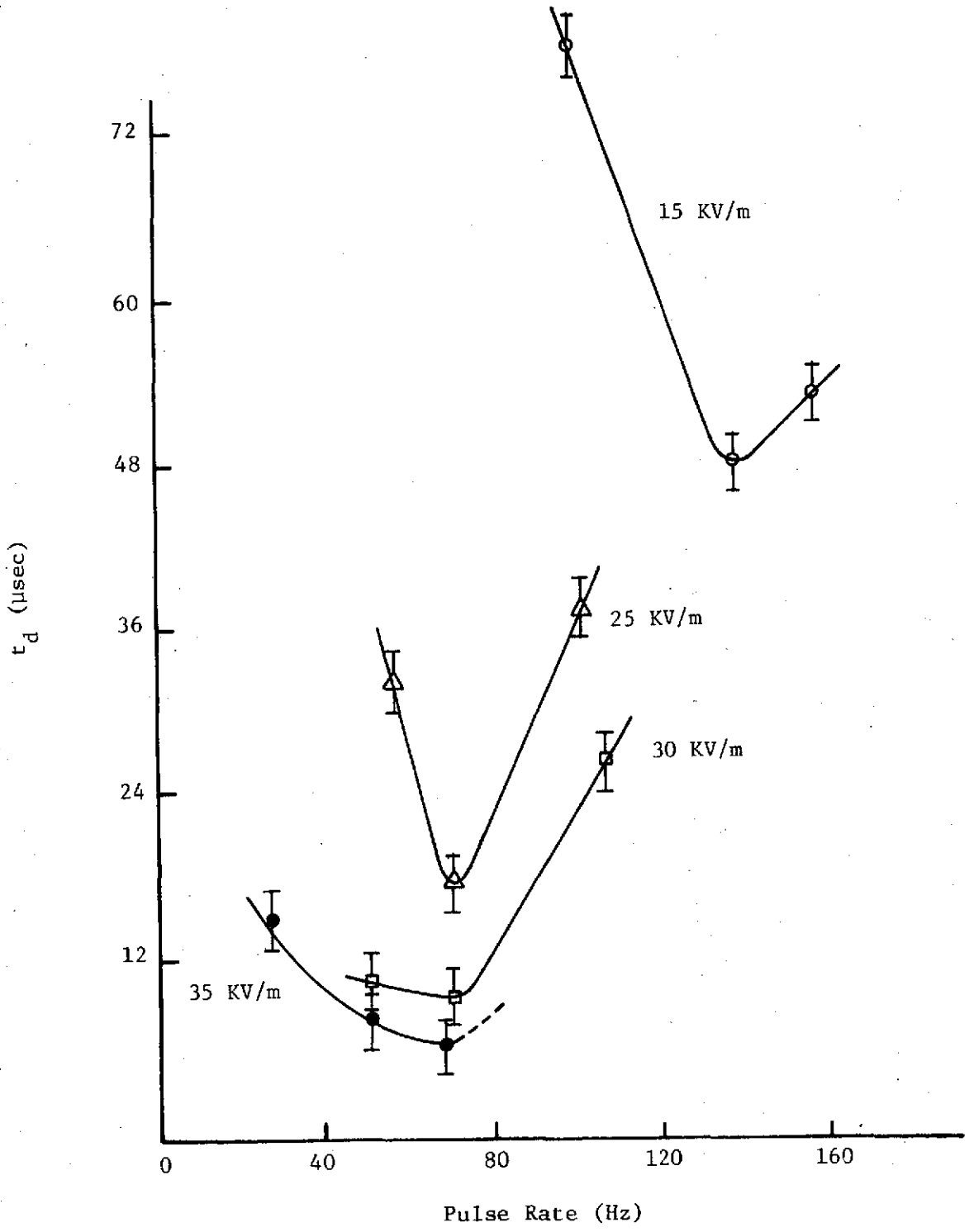

Figure 17. Time Delay as a Function of Pulse Rate at Various Applied Field Strengths for 1:2:8 Mix at 0.2" Hg.

The dissociation rate of CO_2 and N_2 would be expected to increase with the applied field strength.

At this time, not much is known about the effect of chemical processes on CO_2 laser discharge stability. The presence of both neutral molecular species and negative ion species has been related to discharge constrictions by others.

This completes the presentation of the experimental results. A substantial amount of information was obtained. Future work can be more specialized, say, in one or two specific areas. The experiments made in connection with this work, being somewhat superficial, are justified in that experience is needed in repetitively pulsed CO_2 laser operation before any detailed experiments can be effectively planned. With this in mind, the results can now be analyzed.

Results Analysis

The processes involved in the creation and destruction of the population inversion in a working CO_2 laser can be quite complex. Depending on the particular design of the laser system, however, certain processes are known to be more dominant than others. The results of a parametric study of the operation of a laser device are invaluable in the determination of these dominant mechanisms. A qualitative analysis of the data obtained should account for the various effects and trends observed.

The CO_2 laser studied in this work has already been described as a high power, repetitively pulsed unit. Several of its other characteristics are pertinent to this discussion. The gas flow velocities were relatively slow (1 meter/sec), allowing for 2 second dwell times. The discharge current pulses were short, always less than 5 microseconds. The negative ions are the

most suspect because of their subsequent generation from the neutral species as well as their perturbing effect on ionization kinetics, ionization stability, and on the electron energy distribution [7,8,9]. Working with continuous discharge devices, Wiegand found that fractional concentrations of NO_2 and N_2O as low as 10^{-6} could induce discharge constrictions [8]. Though seemingly small, it must be remembered that small amounts of impurity could nearly equal electron or positive ion concentrations in CO_2 systems. This is especially true for glow discharge devices where fractional ionization is relatively low ($<10^{-5}$).

The dissociation of CO_2 and N_2 producing CO, O and N can lead to the production of significant amounts of NO, N_2O, O_2 and NO_2. The more rapid negative ion production processes arise from CO_2 dissociation whereby O^- is first produced. The O^- is subsequently converted to other negative ion species through clustering reactions, charge exchange and rearrangement reactions. Significant amounts of CO_2^-, NO_2^-, O_2^-, NO_3^- and CO_4^- may then be generated [7]. Though these chemical processes might be expected to be more influential in continuous discharge devices, their effect on stability in repetitively pulsed systems could be expected to be significant also. The ionic reactions might continue taking place during the relatively long afterglow. Even if afterglow decay is complete before the next pulse arrives, the long-lived nature of some of the species could lead to a significant buildup in impurity concentrations over several repetitive pulses in slow-flow devices.

Discharge Current.--The dominant positive ion species in a CO_2-N_2-He pulsed discharge mix is CO_2^+ [10]. Thus, the electron density associated with a particular mix would be expected to be related to the fractional concentration of CO_2 used. This explains why higher currents were generally associated with the use of the 1:2:4, CO_2-rich mix as compared to the 1:4:4 or 1:2:8 mixes.

It also explains why it was usually easier to maintain a discharge using a 1:2:4 gas mixture. The fact that lower peak current amplitudes were seen using the 1:2:8 mix is expected using the above explanation, also.

It was observed that the discharge current increased or remained the same as the pulse rate was increased. If there was no residual ionization left between pulses, one would expect the current to remain constant as the pulse rate varied. However, in a slow-flow device such as the one investigated, any residual ionization would not appreciably be removed, convectively, between pulses. Recombination would be the dominant quenching mechanism. Residual ionization could retard electron diffusion through ambipolar processes. Also, it is likely that the afterglow decay times were of the order of the times between pulses. Then some residual electrons would be present near the cathode when the next pulse arrived. Even a small residual concentration of electrons would significantly effect the current amplitude through multiplication processes.

With increasing pressure, the average electron temperature would be expected to decrease. With this decrease, an associated decrease in electron density would be expected, the multiplication rate having decreased with temperature. This is consistent with the decrease in current peak amplitude observed as the discharge pressure was increased at constant pulse rate and applied field strength. Calculations of Nighan concerning the variation of the electron energy distribution as a function of E/N are also consistent with the observation and hypothesis [11].

The variation of current pulse shape with pressure is attributed to changes in the plasma impedance. As no measurements of V(t) as compared to $I_d(t)$ were made during the investigations, it is difficult to determine how the impedance changed. It is speculated that due to the capacitive reactive nature of the plasma, the current leads the applied potential somewhat. It is further

cross sections [13]. The excitation rate is also dependent on the electron density. Both of these factors account for the higher peak power amplitudes seen at the higher applied field strengths. On the other hand, no lasing was detected using less than 15 KV/m. It is felt that the electron densities were too low at these low field strengths, even at the lowest pressure of operation, to create appreciable inversion along the axis of the resonator.

To explain the variation of the peak power amplitude with pulse repetition rate, some additional ideas need to be formulated. The laser peak power increased with pulse rate until an optimum pulse rate was reached (corresponding to the highest value of P_p reached), after which the power began to decrease. Noting the behavior of the discharge current, it was deduced that the electron density increased with pulse rate. Then P_p would also be expected to increase. The fact that constriction diameters decreased as the pulse rate was increased, putting more plasma into the optical resonator region, may have affected the variations seen. However, Hill has reported the same sort of variance of P_p with pulse rate [4]. He did not attempt to explain the increases seen, only the decreases. The fact that both occurred during his experiments lessens the significance of the constructions.

S.S. Alimpev of Lebedev has observed decreases in P_p with increases in the pulse rate, just as reported by Hill and as seen in this work [19]. Hill, using 100 Joule input pulses into a 77 mm diameter x 2 meter long cavity, attributed attenuation to gas heating effects. His deduction is felt to be correct. However, no input energies greater than 10 joules per pulse were used in the work described herein. Stationary heating of the gas was small and thus could not a-count for the decreases in P_p reported. Instead, the formation of carbon monoxide from the dissociation of CO_2 is held responsible for the decreases in laser peak power with increasing pulse rate observed. The Soviets made the same deduction. $CO_2(010)$ bottleneck population buildup

with increasing pulse rate (increasing electron density) is not considered to be important. This is due to the relatively short lifetimes of these states (50 to 100 microseconds) as compared to the inter-pulse time (greater than 10 milliseconds).

The effects of carbon monoxide on the operation of a CO_2 laser are well known. CO is formed at the expense of CO_2. Also, the direct electronic excitation cross section of CO is high, so that these molecules constitute parasitic loss channels with respect to the excitation of the carbon dioxide. The combination of these two effects caused the decreases in P_p observed as the pulse rate was increased beyond the optimum pulse rate. Below the optimum pulse rate, CO formation and buildup occurred less rapidly and therefore was not the dominant process effecting laser output.

Time Delay.--There are several possible inversion mechanisms associated with CO_2-N_2-He discharges. With respect to the specific laser device studied, direct electronic excitation of the $CO_2(000)$ to $CO_2(001)$ was felt to be the dominant process. Other possibilities invlude selective excitation, cascading of $CO_2(00v_3)$, $v_3>1$, as well as recombination excitation of CO_2 to beneficial vibrational energy states.

In high E/N systems, the latter two mechanisms become increasingly important. However, at low pressures, CO_2 asymmetric stretch vibrational level lifetimes are relatively long, being on the order of 10^2 to 10^3 microseconds. Then the time delay associated with the dominance of cascade and/or recombination mechanisms would be of the same order of magnitude or greater. Since no time delays greater than 75 microseconds were observed, these processes did not create the inversion. It is of interest to note that direct electronic excitation of CO_2 has been put forth as the dominant inversion production mechanism when delay times of up to 300 microseconds were seen [17].

The metastable nature of $N_2(v=1)$ explains its long-lived characteristic.

speculated that decreases in the pressure cause the complex discharge impedance to change in such a manner as to allow for decreases in the time lag between the current and voltage pulses.

Laser Peak Power.--It is felt that the primary inversion mechanism taking place in the laser system studied was the direct electronic excitation of both $CO_2(001)$ and $CO_2(100)$, the upper and lower laser levels, and the subsequent more rapid decay of the $CO_2(100)$. This hypothesis explains the peak power variations observed as well as the time delay behavior as a function of the independent parameters. The time delay will be discussed in the next section.

In pulsed discharge CO_2 lasers using short excitation pulses (10 microseconds), a single excitation per molecule per pulse is most probable. The reason for this is that decaying $CO_2(100)$ molecules will become bottlenecked in $CO_2(010)$, which is characterized by lifetimes of between 50 and 100 microseconds (depending on the foreign particle additives used) [12].

The E/N values characteristic of the laser used in this work were estimated to be on the order of 10^{-14} to 2×10^{-13} V-cm^2. It is felt that a relatively small fraction of the total CO_2 molecular concentration was excited to lower vibrational levels of the electronic ground state. There are several reasons for this deduction. First, high discharge currents were observed and CO_2 is the primary electron donor in these high E/N laser devices. What's more, the fractional power transfer to the electronic state excitation of CO_2 is relatively large at E/N values (one to two order of magnitudes less than used) [7]. Lastly, based on the results of others, it is felt a significant amount of CO_2 dissociated, CO_2 having a dissociation energy of only 2.8 eV [7,8]. The hypothesis above is consistent with the observation of typically low efficiencies for high E/N, CO_2 laser devices.

The relative populations of the upper and lower laser levels are still very important. It is known that the electronic excitation cross section of

CO_2 to its (001) level is greater than that to its (100) level [12,13]. Gain via stimulated emission could be expected to occur when the population difference can be obtained before the current pulse has ended. However, if only a small fraction of the initially available CO_2 is being excited to the (001) and (100) levels threshold might not be reached until sometime after the end of the current pulse. This time would be characteristic of the time it took for a sufficient number of $CO_2(100)$ to decay to $CO_2(010)$. The lower laser lifetime has been experimentally determined to be approximately 10 to 100 times shorter than that of the upper level. Lifetimes on the order of milliseconds are reported for $CO_2(001)$ at low pressure excluding stimulated emission [14,15].

Other investigators support the direct electronic excitation hypothesis presented [16,17,18]. Other inversion mechanisms can be essentially ruled out by noting the variation of the time delay as a function of the independent parameters. More will be said about this in the next section. However, the ideas presented thus far can be used to explain the parametric variation of the laser peak power observed while experimenting with the laser device described.

The fact that the 1:2:4, CO_2-rich mix gave the highest laser output is to be expected. CO_2 (000) concentrations would be expected to be greater. Also, higher electron densities were characteristic of this mix. These two factors would lead to greater inversions. The observation of generally lower peak power amplitudes using the 1:2:8, helium-rich, CO_2-poor, mix substantiates this. The beneficial gas-cooling properties of helium are seen to be of little importance.

An increase in P_p with applied field strength was reported. As the field strength increased, so would the electron number density and temperature. The rate of $CO_2(001)$ direct excitation as compared to $CO_2(100)$ increases with T_e, as can be deduced noting the variation of the pertinent inelastic scattering

Lifetimes on the order of 10^2 milliseconds at pressures of a few torr have been observed [14]. $N_2(v=1) \rightarrow CO_2(001)$ selective energy transfer times, indicative of its resonant nature, are substantially less. Average values of 4 milliseconds at 1 torr to 10 microseconds at 50 torr have been reported [14]. Selective excitation, then, cannot be ruled out through time delay arguments alone. Yet, in several instances, time delays of less than 10 microseconds were seen. Also, the peak power amplitudes associated with the 1:4:4, N_2-rich mix were substantially less than values observed using 1:2:4. At higher E/N ratios substantially less $N_2(v = 1\text{-}4)$ species are produced by electronic excitation [7]. In fact, it is suspected that in high E/N systems, the parasitic process $CO_2(001)$ $N_2(v=1)$ may decrease the inversion [9]. Lastly, other observations have led to the conclusion that there was very little CO_2 present in its vibrational ground state within 2 microseconds after the current pulse began. Thus, selective excitation is not considered to have been an important inversion production mechanism under the conditions of the work performed. On the other hand, the longer time delays and lower powers observed using 1:4:4 as compared to 1:2:4 lend evidence to the importance of the selective de-excitation processes.

Variations in P_p and t_d led to conclusions about the dominant inversion mechanism. The hypotehsis formed must explain the observations yet to be analyzed, or at least be consistent with other explanations.

The time delay was observed to be generally longer when using the 1:2:8 mixture. Secondly, as the applied field was increased, t_d decreased. This behavior, as illustrated in Figure 15 has been observed by others working with TEA systems [20]. These variations can be explained as the variations in P_p were explained. The peak power output of the laser is proportional to the gain while the time delay is inversely proportional to gain. This effect is generally substantiated by the data. The fact that no trend was seen in the

Pulse decay was not always exponential. One may deduce that decay times were not indicative of only cotlisional decay of the upper laser level. This effect was more generally noted for the lower output experiments. Saturation, stimulated emission and some selective excitation may also have effected the pulse decay observed.

The fact that t_f and t_h decreased as pressure increased is not inconsistent with what has been hypotehsized. The rates of collisional processes increase with pressure. The saturation intensity would be expected to decrease with pressure in the device used. Evidence of this is obtained from the variation of t_d. One or both of these processes could account for the variation of t_f and t_h seen, therefore.

Optimum Pulse Rate.--The optimum pulse rate, w_o, has already been defined as that pulse rate at which maximum peak laser power was observed, having specified the other three independent parameters. These values correspond to the peaks and dips illustrated in Figures 17 and 17, respectively. Their variation can be explained using hypotheses heretofore presented.

Values of w_o were generally higher for the helium-rich mixture. This is consistent with the results reported by Alimpev et al. [19]. The optimum pulse rate is determined by CO concentration. Helium was found to cause a decrease in the production rate of carbon monoxide in repetitively pulsed systems. This also explains why operation at substantially higher pulse rates was possible using the 1:2:8 mixture. The decreases in w_o with increases in the applied field strength are explained noting that these increases would cause an increase in carbon monoxide production.

The fact that there was upper limit on the useable pulse rate range is attributed to the presence of both CO and other impurity species, expecially negative ions. Arching would be accompanied by a drastic decrease in the electron temperature and substantial increase in gas temperature. This would negate any inversion process.

pressure variation of P_p, while t_d increased with pressure, is attributed to a lack of data at 0.6" and 1.0" Hg. The time delay would be expected to increase with pressure (at constant field strength) under the marginal inversion conditions hypothesized. Increasing the pressure would decrease the electron temperature which would lead to an increase in the rate of $CO_2(100)$ population as compared to that of the upper level.

A comparison between Figures 16 and 17 is consistent with comparisons among the other data. The time delay decreased with pulse rate to a certain minimum and then increased until no lasing could be detected. This is expected from the inverse proportionality between t_d and peak laser power, using the explanation concerning the pulse rate variation of P_p.

Laser Pulse Shape.--For laser devices operating at near saturation intensities, that is, systems in which relatively few CO_2 molecules are in the inverted situation, it is difficult to specify the significance of the laser pulse rise and decay time. The variation of gain with time in such systems is determined by stimulated emission, diffusion, and collision processes.

The pulse rise times observed in conjunction with this work were fairly constant over all the determinations made. Being in the range of between 2 and 4 microseconds, they were always considerably shorter than decay times. At the onset of lasing, they were not greater than the lower laser level collisional lifetimes experimentally determined by others. Diffusion processes being relatively slow, this points out that stimulated emission processes initially had little effect on the inversion. One would deduce, then, that the power output rise time was indicative of the $CO_2(100)$ collisional decay rate. One would expect the rise times to be considerably longer than observed if recombination/cascade effects were the dominant inversion production mechanisms.

Conclusions

The parametric operational study of the high power laser device constructed was invaluable in the determination of the dominant processes affecting 10.6 micron gain. It was concluded that the primary inversion mechanism was direct electronic excitation of CO_2 to its upper laser level via inelastic scattering. The dominant inversion destruction processes was the production of CO (at the expense of CO_2), a species that competed with un-dissociated CO_2 for vibrational excitation. Discharge constriction instabilities were attributed to the buildup of impurities with increasing pulse rate, field strength and pressure.

These observations having been made, certain improvements in the laser system are warranted. These improvements should be followed by more detailed experiments in the same areas covered. A substantial increase in output power would be expected with increases in the gas flow rate. Since diffusion processes are relatively unimportant in fast flow, pulse discharge laser devices, the water cooling jacket could be removed. This would help alleviate the high voltage breakdown problems encountered. Larger diameter laser optics should also be installed so that the whole cavity cross section is used.

Having made these improvements, more detailed experiments at low energies as well as much higher energies should be performed. Particular attention should be paid to the variation of peak power and time delay with the pulse rate. Relatively little work has been reported in these areas in conjunction with the use of axially pulsed laser devices. More sophisticated experiments in which the gas flow rate is made an independent parameter would be helpful in the determination of optimum operational conditions, and dominant inversion mechanisms.

Nuclear Reaction Product Preionization Experiment

Positive results from this experiment would prove the feasibility of a definite alternative to electro- and photo-ionization "double discharge" CO_2 laser devices. The pronounced success of conventional preionization schemes is favorable when considering the possibility of the successful enhancement of a CO_2 laser using nuclear reaction product preionization.

To review, the major reason that the efficiency of high power CO_2 lasers is so low in comparison to the theoretical quantum efficiency is the mismatch in the two electron energy distributions required. The distribution needed to sustain the electrical discharge conductivity is very different relative to the optimum distribution for inversion production. The latter is characterized by a much lower temperature than the former and the dissimilarity becomes more pronounced as the laser medium pressure is increased.

In pulsed systems, the possibility exists for "tuning" the electron energy distribution to the optimum T_e for inversion. This is accomplished by preionization methods (1) double voltage pulses, (2) electron beam interaction, (3) photo cathode and/or photoionization processes. One generates an electron population which can quickly thermalize. Thermalization is controlled by the application of a lower potential such that the decay in electron energy is limited to the optimum T_e for inversion production.

There are practical problems involved with the double discharge methods used. Larger and larger high voltage power supplies are needed to keep up with the desired increase in medium density (pressure) in the double voltage pulse scheme. The production of a uniform discharge is difficult, also. With respect to the second method, large volume laser devices require large area e-beam accelerators to produce a uniform current over the medium volume. Pressure differentials across gun windows can be a limiting factor also.

Extra-high voltage engineering problems become significant as higher primary electron energies are needed for higher pressure operation. The relatively high ionization potentials of the important gases ($\sim$10 eV) require multiple photon collisions for preionization, a problem pertaining to the third method mentioned. UV photons penetration depths (<1 mm at 1 atmosphere) become too small as pressures are increased also.

The proposed alternative is to increase the CO_2 laser efficiency by using a radioactive (β,γ active) laser cathode. In corporation of such a device is relatively simple from an engineering standpoint. High primary particle energies make direct ionization possible. Most importantly, this method would be expected to work better at higher pressures, not worse as the three conventional schemes metnioned (in the regime where engineering problems become limiting or where penetration depths become very small).

The experiment undertaken was at low pressure because of the characteristics of the laser device used. However, positive results in this regime should be scalable to higher pressures. Observations made during the operational study of thepreviously described CO_2 laser supported the proposal alternative. The laser peak power and the discharge current increased with pulse rate. This was attributed to residual ionization and electron multiplication (near the cathode) processes. The use of an activated cathode would lead to an increase in the residual charged particle population. As it was concluded that the CO_2 molecules were pumped primarily by direct electronic impact, an activated cathode employment should lead to larger peak powers at a specified laser tube voltage, as compared to the conventional mode of laser operation.

To check this hypothesis, the operational characteristics of the CO_2 laser previously described were recorded as a function of certain sets of pressure, mixture, applied voltage and pulse repetition rate. This would be used as "baseline data" against which the output of the laser using a radioactive

cathode would be compared. Specifically, the optimum mixture ratio and pressure were used and never changed during the experiment. A mixture of CO_2:He, 1:4 was used at a pressure of 10 torr. The output of the laser was recorded as a function of applied voltage (50, 60, 800 and 100 kV) and pulse repetition rate (dependent on voltage).

Once the baseline data was recorded,the construction of the radioactive cathode was completed. A duplicate of the normal cathode, as shown in Figures 7 and 8, was made--the only difference being that the stainless steel pins were removable from the duplicate. The removed pins were activated in the University of Florida Training Reactor at a power of 100 kw for 10 minutes. Safe radiological procedure and limited the amount of activation of the cathode. Upon removal from the reactor, the pins caused a field of 7R/hr and 1 foot from there surface. Substantial 1 β-emission was detected also.

The activated pins were transferred to a hot cave and then inserted into the cathode housing using remote manipulators. The assembled cathode was then rushed to the laser device (located approximately 3 miles from the nuclear reactor). Using several people for short lengths of time, the cathode was installed in the laser.

Decay of the stainless steel radioactivity was more rapid than anticipated. Immediately after cathode insertion, the first experimental observations were made and recorded. At this point in time the cathode was causing a field of 150 mR/hr at one foot distance. The next day, the observations were repeated using a field of 2.5 mR/hr at one foot. On the third day, the observations were made again using 1.9 mR/hr at one foot.

The reduced data showed no trends. For this reason the data is not tabulated here. The lack of useable results from the experiment was attributed to three factors. First, the reaction product flux from the cathode was too low. Secondly, the output power of the CO_2 laser was found to be a sensitive

function of the applied electrical field. However power supply control was limited to approximately ±3 kV tolerances on reproducibility due to several system features. Therefore duplication of any set of specific laser parameters was difficult. Finally, the laser gas pressure was probably too low to cause a measurable effect under the above two circumstances. This possibility was realized at the beginning of the experiment, because of the longitudional electrode configuration of the laser, homogeneous discharge maintenance was not possible at higher pressures.

The basic hypotheses surrounding this preionization experiment were not disproven. Careful construction and employment of a transverse electrode, high pressure CO_2 laser should confirm the ideas expressed concerning nuclear reaction product preionization. The construction of a TEA CO_2 laser is planned as a future project.

References

1. R. DeYoung, Electrode Configuration Study for High Power CO_2 Laser Systems, M.S.E. Thesis, University of Florida, December 1970.

2. G.J. Denenberg, E.L. Roy, W.B. McKnight, "Performance of High-Voltage Axially Pulsed CO_2 Lasers," IEEE Journal of Quantum Electronics, Preprint, February 1972.

3. W.B. McKnight, G.J. Dezenberg, U.S. Army Missile Command, private communication.

4. A.E. Hill, "Role of Thermal Effects and Fast Flow Power Scaling Techniques in CO_2-N_2-He Lasers," Applied Physics Letters, Vol. 16, No. 11, p. 423, June 1, 1970.

5. G.J. Dezenberg, E.L. Roy, W.B. McKnight, Performance of High Voltage Axially Pulsed CO_2 Lasers, U.S. Army Missile Command Report No. RR-TR-71-1, April, 1971.

6. D.C. Smith, "Velocity Dependence on the Gain of a CO_2 Laser," IEEE Journal of Quantum Electronics, Vol. QE-4, No. 11, p. 948, November 1968.

7. W.L. Nighan, W.J. Wiegand, M.C. Fowler, R.H. Bullis, Investigation of the Plasma Properties of High Energy Gas Discharge Lasers, UARL Final Report K-920833-5, June 29, 1971.

8. W.J. Wiegand, "The Influence of Plasma Generated Impurities on Molecular Gas Discharges," Presented during 24th Annual Gaseous Electronics Conference, Gainesville, Florida, October 1971.

9. P.D. Tannen, "Influence at Contaminants on the CO_2 Laser," Presented during 24th Annual Gaseous Electronics Conference, Gainesville, Florida, October 1971.

10. J.M. Austin, A.L.S. Smith, "Analysis of Positive Ions in CO_2 Gas Laser Systems," Journal of Physics D, Applied Physics, Vol. 5, p. 468, 1972.

11. W.L. Nighan, "Electron Energy Distributions and Collision Rates in Electrically Excited N_2, CO and CO_2," Physical Review A, Vol. 2, No. 5, p. 1989, November 1970.

12. A.V. Phelps, "Rotational and Vibrational Excitation of Molecules by Low-Energy Electrons," Reviews of Modern Physics, Vol. 40, No. 2, p. 399, April 1968.

13. A. Stamoatovic, G.J. Shulz, "Excitation of Vibrational Modes Near Threshold in CO_2 and N_2," Physical Review, Vol. 188, No. 1, p. 213, December 5, 1969.

14. C.K.N. Patel, "Vibration Energy Transfer--An Efficient Means of Selective Excitation in Molecules," in Physics of Quantum Electronics Conference Proceedings, ed. by P.L. Kelley, B. Larx and P.E. Tannerswald, New York, McGraw-Hill, 1966.

15. P.K. Cheo, "Effects of CO_2, He, and N_2 on the Lifetimes of the 00°1 and 10°0 CO_2 Laser Levels and on Pulsed Gain at 10.6 μ," Journal of Applied Physics, Vol. 38, No. 9, p. 3563, August, 1967.

16. P.O. Clark, M.R. Smith, "Pulsed Operation of CO_2-N_2-He Lasers," Applied Physics Letters, Vol. 9, No. 10, p. 369, November 15, 1966.

17. W.B. McKnight, "Excitation Mechanisms in Pulsed CO_2 Lasers," Journal of Applied Physics, Vol. 40, No. 7, p. 2810, June 1969.

18. A.M. Danishevskii, I.M. Fishman, I.D. Yaroshetskii, "Investigation of the Laser Effect in CO_2 During Pulsed Excitation," Soviet Physics JETP, Vol. 28, No. 3, p. 421, March 1969.

19. S.S. Alimpev, N.V. Karlov, Yu. B. Konev, G.P. Kuz'min, R.P. Petrov, "Influence of Dissociation on the Inversion on a CO_2 Laser with Pulse Pumping," JETP Letters, Vol. 9, No. 7, p. 223, April 5, 1969.

20. J. Reid, B. Garside, E. Ballik, "Effects of Time-Delayed Amplification in TEA CO_2 Lasers," IEEE Journal of Quantum Electronics, Vol. QE-8, No. 5, p. 449, May 1972.

MEASUREMENT OF THERMODYNAMIC PROPERTIES OF UF_6 AND UF_6/He MIXTURES

by

David E. Sterritt

ABSTRACT

The theoretical and experimental efforts are described aimed at determining the specific heat of UF_6 the ratio of specific heats of UF_6 and the viscous coupling constant of UF_6/He mixtures as a function of temperature. Experimental data was taken with a ballistic piston compressor and analysis by a computer program which simulates the movement of the piston and calculates changes in the state of the gas.

MEASUREMENT OF THERMODYNAMIC PROPERTIES OF UF_6 AND UF_6/He MIXTURES

Introduction

Experiments with a ballistic piston compressor were made to investigate certain thermodynamic properties of gaseous UF_6. Measured gas pressures, volumes, and temperatures were analyzed with a computer program employing a numerical optimization scheme to arrive at the desired properties. The thermodynamic properties deduced include the UF_6 constant volume specific heat and specific heat ratio, and the viscous coupling constant for UF_6/He mixtures at temperatures up to 1,500°K.

The ballistic compressor shown schematically in Figure 1 consists of four main parts: the reservoir, the piston release section, the tube, and the high pressure test section.

In operation the chamber behind the plunger of the piston release section is pressurized so that the plunger moves to the forward (left) position and seals the reservoir from the tube. The tube is then filled with the test gas. Next, the reservoir is filled with driver gas to the pressure necessary to produce the desired maximum pressure in the test gas. The compressor is fired by releasing the pressure behind the plunger in the piston release section. The reservoir pressure drives the plunger to the rear and the reservoir gas rushes behind the piston driving it swiftly down the tube.

Diagnostics

Pressure.--The pressure of the mixture of uranium hexafluoride and helium

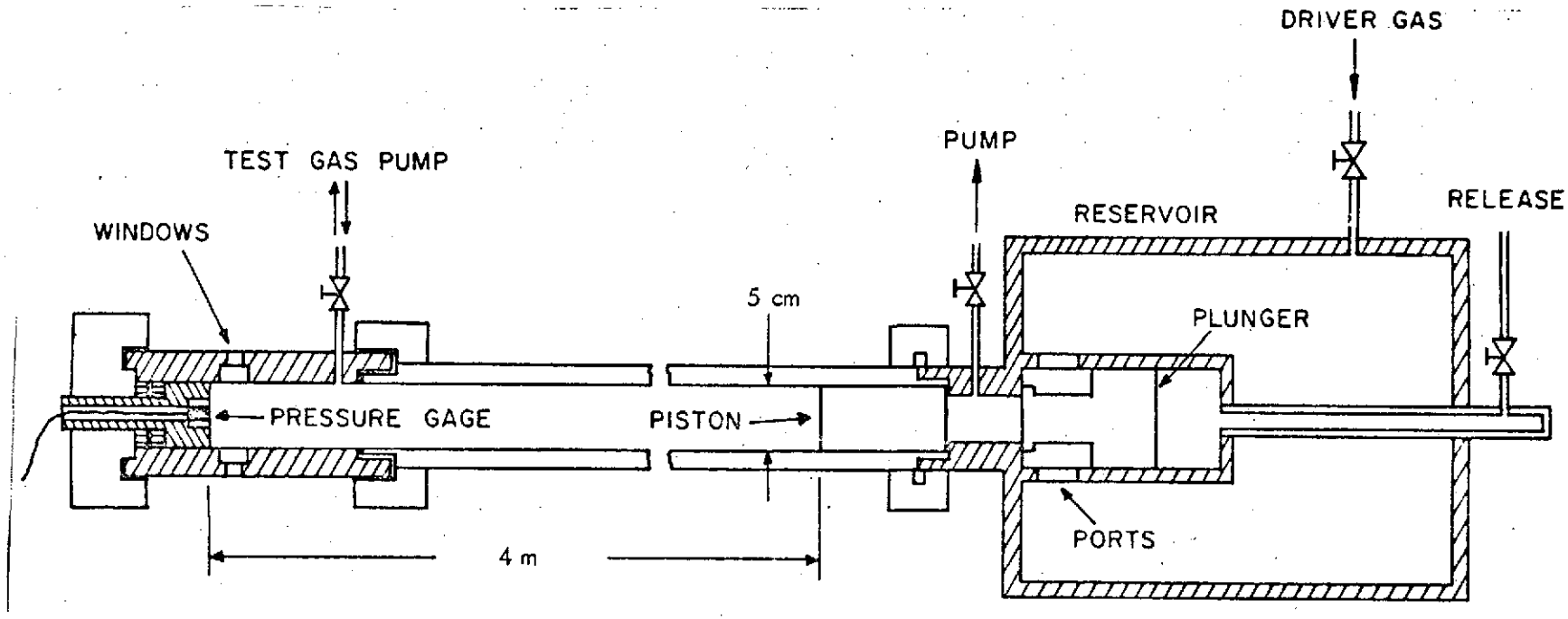

Figure 1. Schematic diagram of ballistic piston compressor.

is measured continuously during the compression cycle with a quartz crystal piezoelectric transducer. The signal from the pressure transducer is amplified and photographed on an oscilloscope. Reference signals of zero and maximum pressure are also photographed.

Volume.--The volume of the test gas is measured with a magnetic transducer which senses the position of the steel piston body.

Temperature.--The temperature of the test gas is measured by the brightness-emissivity method.

Figure 2 shows the data acquisition system. Data is collected for 10 ms during the period of maximum compression. The data acquisition system is triggered by a R.F. signal generated by the magnetic tranducer's amplifier.

Theory

The rapid compression of the real gas in a ballistic piston compressor is a complicated process, and can be approximated only very roughly by the compression of an ideal gas in an apparatus characterized by no heat or mass loss.

In spite of the rapidity of the compression process (0.1 seconds typical), a non-negligible quantity of heat is lost by the test gas to the compressor walls, thus rendering the compression process decidedly non-adiabatic. In addition, the pressure differential across the piston results in some gas leakage across the piston during the compression cycle. Reservoir gas leaks past the piston into the test gas during the piston acceleration, and from the test gas into the reservoir gas during piston deacceleration.

Analysis of these non-ideal phenomena is done by means of a computer program which simulates the movement of the piston and calculates changes in the state of the gases.

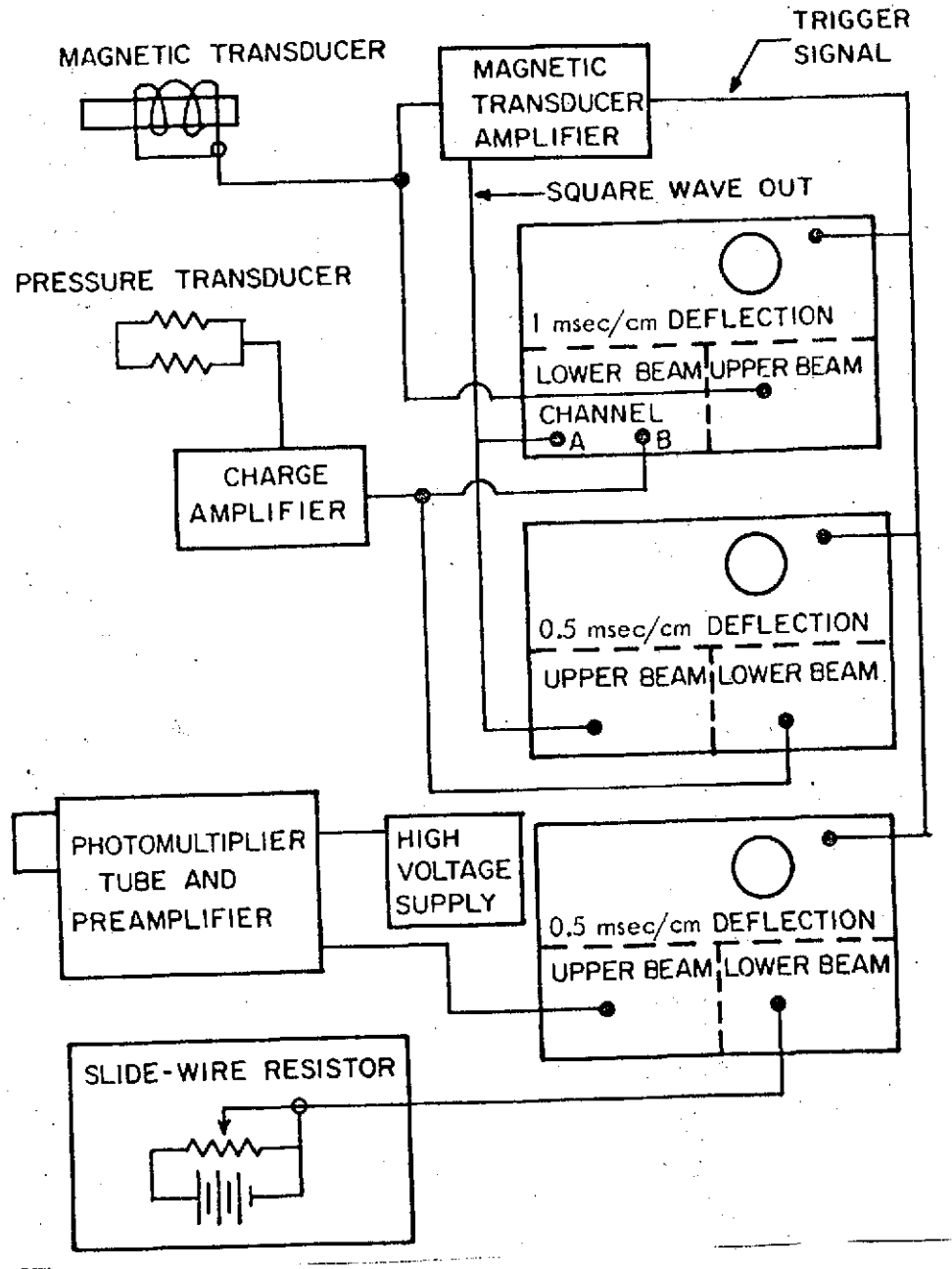

Figure 2. Block diagram of the data acquisition system.

Heat loss is calculated in cylindrical coordinates:

$$\frac{\partial T}{\partial t} = \alpha\left(\frac{\partial^2 T}{\partial r^2} + \frac{1}{r}\frac{\partial T}{\partial r}\right) ,$$

where α is the thermal diffusivity of the compressor walls. Gas leakage past the piston is calculated:

$$\frac{\partial n}{\partial t} = \frac{\pi\rho}{m_a} r_o(r_o - r_p)\left[\frac{1}{8\eta}\frac{\partial P}{\partial \ell}(r_o - r_p)^2 + V\right] ,$$

where n is moles of leaking gas, ρ the gas density, r_o the tube radius, η the gas viscosity, V the piston velocity. The piston gap $(r_o - r_p)$ is the clearance between the piston and tube walls.

Numerical simulation results in a tabulation of the position of the piston and the state of the gases approximately each microsecond. Also, at each tabulation, changes in test gas composition due to leakage and heat loss are performed.

Analysis of experimental measurements of pressure, volume and temperature consists of matching the simulated calculation to experiment. Those thermodynamic parameters which give accurate reproduction of experimental data on the computer also then accurately characterize the experimental gas mixture through a process of optimization, many experiment simulations are done by the computer, adjusting thermodynamic parameters of the unknown constituent of the test gas, until reasonable agreement between calculated simulation and experiment is achieved.

Experimental Results

A number of compressor firings were made and the results analyzed by the BCCC program. All shots were made with an initial test gas pressure of one atmosphere. Maximum test gas pressures and temperatures ranged from 175 to 350

atmospheres, and 750 to 1,500°K. The UF_6 concentration in the UF_6/He test gas mixture was varied from 1.3% to 6.5%.

The specific heat, $c_v(UF_6)$, was found to be the thermodynamic parameter most sensitive of all the parameters being optimized. This made it possible to determine the temperature dependence of $c_v(UF_6)$ with considerable accuracy throughout the complete temperature range of these experiments. The analytical form of the temperature dependence of $c_v(UF_6)$ established by Kirshenbaum from thermodynamic functions and the vapor pressure-temperature relationships of the condensate [1], i.e.,

$$c_v(UF_6)/R = C_1 + C_2T + C_3T^{-2} , \tag{1}$$

was adopted to represent the first three terms ("low temperature" part) of a four term representation of $c_v(UF_6)$ valid over the entire temperature range of this investigation. The fourth ("high temperature") term derived in this investigation,

$$C_4T(1 - e^{C_5T^2}) , \tag{2}$$

introduces the high temperature contributions to the heat capacity, and, in addition, compensates for the inaccuracy introduced by the use of the Kirshenbaum equation at temperatures beyond its range of validity. Evaluation of the coefficients C_4 and C_5 by the optimization procedure described earlier in this paper results in the expression,

$$c_v(UF_6)/R = 15.33 + 3.99 \times 10^{-3}T - 1.615 \times 10^{5}T^{-2} - 2.214 \times 10^{-3}T(1 - e^{-5 \times 10^{-7}T^2}) . \tag{3}$$

Equation (3) is a monotonically increasing function of temperature up to the 1,500°K limit of the experimental measurements on which it is based. This is the behavior predicted by statistical thermodynamics for a gas consisting of polatomic nonlinear molecules in thermal equilibrium. This observation suggests that indeed the ballistic piston test gas compression rate of these experiments is sufficiently slow to give true equilibrium values of $c_v(UF_6)$. This is in contrast to the anomalous decrease in specific heat with increasing temperature measured in a shock-tube by Dmitrievskii et al. [2], where their observations are ascribed to non-equilibrium vibrational excitation of the UF_6 in a two-stage process characterized by two significantly different vibrational relaxation times.

Agreement of equation (3) with the results of three separate $c_v(UF_6)$ determinations by Kirshenbaum [1], Gaunt [1], and Bigeleisen et al. [4], in the temperature interval in which these three separate determinations are in close agreement with each other, 200 to 500°K, is about 1%. Further, agreement with the results of the three studies cited above justifies a high degree of confidence in its accuracy up to 1,500°K.

The ratio of specific heats of UF_6 was calculated and is shown in Figure 3 for temperatures up to 1,500°K and for pressures from 0.1 to 100 atmospheres. Van der Waals constants derived from the triple point were used. The dashed part of the curves in Figure 3 are not physically realized because UF_6 is not a vapor at these conditions. Agreement is good with both the low temperature experimental values of c_p/c_v reported in DeWitt [5] and with the high temperature calculated values of Hassan and Deese [6].

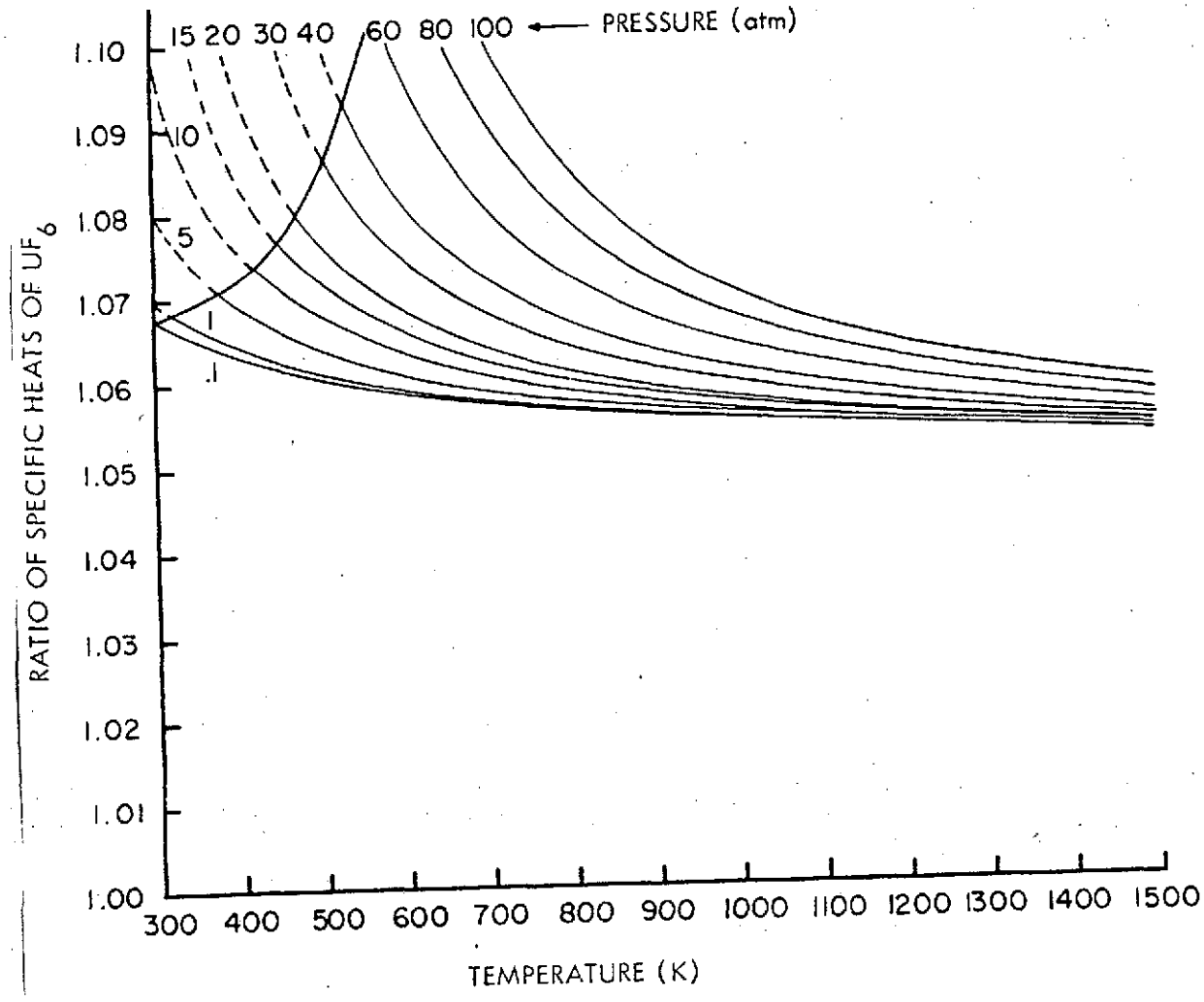

Figure 3. Measured values of the specific heat ratio of UF_6 as a function of temperature.

References

1. I. Kirschenbaum, Physical Properties of Uranium Hexafluoride, SAM Labs. (A-753 and Addendum I) (October 26, 1943).

2. V.A. Dmitrievskii, V.I. Fedulov and V.F. Nikolaeva, "Shock-Tube Investigations of Properties of Sulfur and Uranium Hexafluorides," Sov. Phys. JETP, 34, 759 (1972).

3. J. Gaunt, "The Infrared Spectra and Molecular Structure of Some Group 6 Hexafluorides," Trans. Faraday Soc., 49, 1122 (1953).

4. J. Bigeleisen, M.J. Mayer, P.C. Stevenson, and J. Turkevich, "Vibrational Spectrum and Thermodynamic Properties of Uranium Hexafluoride Gas," J. Chem. Phys., 16, 442 (1948).

5. R. DeWitt, Uranium Hexafluoride: A Survey of Its Physico-Chemical Properties, GAT-280, Goodyear Atomic Corporation (1960).

6. H.A. Hassan and J.E. Deese, Thermodynamic Properties of UF_6 at High Temperatures, North Carolina State University, Raleigh, North Carolina (1973).

NUCLEAR WASTE DISPOSAL UTILIZING A GASEOUS CORE REACTOR

by

Richard R. Paternoster

ABSTRACT

A feasibility study was undertaken of a gaseous core nuclear reactor designed to produce power to also reduce the national inventories of long-lived reactor waste products through nuclear transmutation. Neutron-induced transmutation of radioactive wastes can be an effective means of shortening the apparent half life.

NUCLEAR WASTE DISPOSAL UTILIZING A GASEOUS CORE REACTOR

Introduction

A major objection to the increased use of nuclear electric-power generation stems from envisioned difficulties related to the disposal and management of hazardous radioactive wastes. The vast majority of radioactive wastes are short-lived and easily managed with present waste disposal management techniques. However, several isotopes present in nuclear fission reactor wastes have half-lives of several thousands to several millions of years. These problem wastes are the main point of focus in the debate over disposal of nuclear wastes.

Ultimate disposal of the extremely long-lived wastes could reduce the waste disposal problem to humanly controllable time scales. Removal of long-lived wastes from the total accumulated waste would be the first step in this direction. Separation of iodine-129, the trans-uranium actinides, and other long-lived isotopes could be accomplished at several different stages in the waste disposal cycle. This could mean extraction at the fuel reprocessing site, after a five to ten year cool-down period, or after a 20 to 30 year decay interval. These separated long-lived wastes would be disposed of by methods which would completely remove them from the biosphere and hence any further consideration. Extraterrestial transport of nuclear wastes (ETT) may become feasible in light of recent advances in the space program. Ultimate disposal into deep space or the sun is a remote possibility. The only other presently known method of ultimate disposal is through the process of neutron-induced nuclear transmutation. Induced nuclear transmutation of radioactive wastes converts long-lived problem wastes into relatively harmless short-lived or stable isotopes.

TRANSMUTATION OF RADIOACTIVE WASTES

The concept of neutron-induced transmutation of radioactive wastes was first suggested by Steinberg et al. [1] as a means of effectively shortening the half-lives of waste Kr^{85}, Sr^{90}, and Cs^{137}. This would be accomplished in a neutron flux through the reactions

$$Kr^{85}(n,\gamma)Kr^{86}(\text{stable})$$

$$Sr^{90}(n,\gamma)Sr^{91} \xrightarrow[9.48\ hr]{\beta^-} Y^{91} \xrightarrow[58.6\ d]{\beta^-} Zr^{91}(\text{stable})$$

$$Cs^{137}(n,\gamma)Cs^{138} \xrightarrow[32.2\ m]{\beta^-} Ba^{138}(\text{stable}) .$$

In examining the neutron capture cross sections for those reactions they concluded that neutron fluxes approaching 10^{16} n/cm^2sec would be necessary for shortening the half-lives appreciably. They further suggested that the most logical approach would be through the use of dual-purpose facilities for power production and waste transmutation. In such a scheme the major cost of waste burning, namely the cost of producing neutrons, is written off against the cost of electric power generation.

Wolkenhauer [2] has studied transmutation of high-yield fission products Sr^{90} and Cs^{137} in a controlled thermonuclear reactor (CTR) blanket. Gore and Leonard [3] have also studied transmutation of massive loadings of Cs^{137} in CTR blankets with special flux trap designs. Cs^{137} represents the most difficult case for this technique because it has the lowest thermal neutron capture cross section of the moderately long-lived fission products. These schemes appear attractive since the CTR power plant operating on a deuterium-tritium fuel cycle would produce an excess of neutrons. Within a few decades such systems may be found technically and economically feasible.

Claiborne [4] has considered disposal by transmutation of transuranium actinide wastes. Most of those long-lived alpha emitters have appreciable neutron capture and/or fission cross sections. Table 1 gives the capture and fission cross sections at thermal and resonance energies used by Claiborne. Actinide transmutation occurs by direct fission such as

$$Am^{242m}(n,f)$$

and

$$Am^{244}(n,f) ,$$

or by neutron capture followed by fission such as

$$Am^{241}(n,\gamma)Am^{242}(n,f)$$

and

$$Am^{243}(n,\gamma)Am^{244}(n,f) .$$

In this scheme, those long-lived actinides are continuously recycled back into power reactor fuel elements and in this manner burned out. At fluxes presently available in power reactors (10^{13} - 5 x 10^{13} n/cm^{2}sec) this would be a somewhat slow process spanning over several decades. Furthermore, serious problems arise in handling and safeguarding the recycled actinides during fabrication of fresh fuel elements.

Requirements for Transmutation of Radioactive Waste

Given a high enough neutron flux or a long enough period of irradiation any isotope with a non-zero neutron capture cross section can be transformed into other isotopes. However, the transmutation of radioactive waste imposes a number of constraints upon the process.

TABLE 1. THERMAL CROSS SECTIONS AND RESONANCE INTEGRALS FOR CAPTURE AND FISSION IN THE TRANSPLUTONIUM ACTINIDES

Nuclide	Thermal Cross Sections (barns)		Resonance Integrals (barns)	
	Capture	Fission	Capture	Fission
$_{95}Am^{241}$	925	3.1	2150	0
$_{95}Am^{242m}$	2000	6000	0	0
$_{95}Am^{242}$	0	2900	0	0
$_{95}Am^{243}$	105	.5	1500	1.5
$_{95}Am^{244}$	0	2300	0	0
$_{95}Am^{245}$	0	0	0	0
$_{96}Am^{242}$	30	5	0	0
$_{96}Am^{243}$	200	600	500	1850
$_{96}Cm^{244}$	10	1.2	650	12.50
$_{96}Cm^{245}$	343	1727	120	1140
$_{96}Cm^{246}$	1.3	0	121	0
$_{96}Cm^{247}$	60	120	500	1060
$_{96}Cm^{248}$	3.6	0	170	0
$_{96}Cm^{249}$	2.8	50	0	0
$_{96}Cm^{250}$	2	0	0	0
$_{97}Bk^{249}$	1450	0	1240	0
$_{97}Bk^{250}$	350	3000	0	0
$_{98}Cf^{249}$	450	1690	1.5	2920
$_{98}Cf^{250}$	1900	0	11600	0
$_{98}Cf^{251}$	2850	3750	1600	5400
$_{98}Cf^{252}$	19.8	32	44	110
$_{98}Cf^{253}$	12.6	1300	0	0
$_{98}Cf^{254}$	50	0	1650	0

The selection of prospective candidates for waste transmutation must begin with the radioactive wastes themselves. Reaction rates for neutron-induced transmutation processes can be specified in terms of neutron capture and/or fission cross sections. Unfortunately, high-yield fission product wastes have small neutron capture cross sections. An example is the capture cross section for the (n,γ) reaction in 10.7 year half-life Kr^{85}. At the time of Steinberg's study [1], the thermal neutron capture cross section of Kr^{85} was believed to be 15 barns. Using this figure it was concluded that disposal by transmutation at Kr^{85} could be economically and technically feasible. A recent measurement [5] of this cross section found it to be 1.66 ± 0.20 b. Thus, an order of magnitude increase in the fluence is required to reach feasible transmutation levels.

Another criterion for neutron-induced transmutation of radioactive waste is isotropic purity. If maximum utilization of available neutrons is to be achieved isotopic impurities of a given waste isotope must be eliminated or reduced to lowest possible content. In the case of Kr^{85} transmutation, three stable krypton isotopes, Kr^{83}, Kr^{84}, and Kr^{86} are present with Kr^{85} in fission wastes. The low concentration of Kr^{85} in krypton wastes (7.2 percent) and its low capture cross section compared with Kr^{83} ($\sigma_c \simeq 2.5$ barns) makes enrichment of Kr^{85} necessary.

A final requirement for successful transmutation of radioactive waste is that the end product nuclide of the transmutation process be no more hazardous than the initial waste product. The ideal end product of a transmutation process would be a stable nuclide with a zero neutron capture cross section. A nearly ideal nuclide in this respect is waste I^{129}($t_{1/2} = 15.9 \times 10^6$ years). The transmutation reactions in this case are

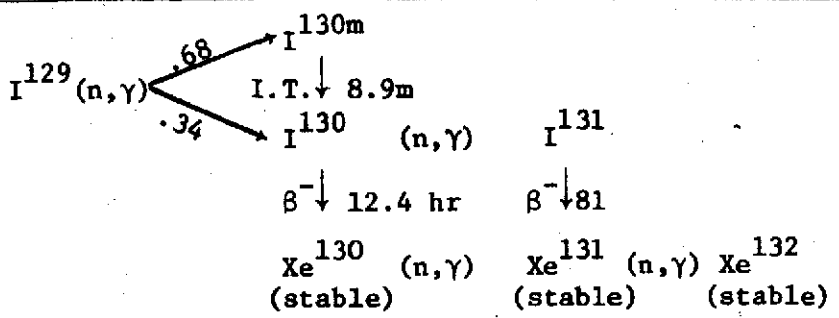

Thus even with several reaction paths the vast majority of I^{129} will be converted to stable isotopes of xenon. The situation is more complex in the case of actinide waste transmutation. In a sustained irradiation of waste actinides, such as curium, quantities of higher actinides, such as berkelium and californium will inevitably be formed. These higher actinides are generally alpha emitters with varying half-lives.

Transmutation Systems and Waste Disposal

The transmutation of I^{129} is first examined in the following. After a 160-day decay period, the short-lived iodine isotopes I^{128}, I^{130}, I^{131}, I^{132} and I^{133} decay away leaving stable I^{127} and the 15.9×10^6 year half-life, I^{129}. The spent fuel from present day LWRs contains about 40 grams/MTU of I^{127} and 231 grams/MTU of I^{129} at 160 days after discharge and 33,000 MWD/MTU burnup. These two isotopes constitute roughly 0.78 percent of the total fission product wastes with the I^{129} isotope being about 85 percent of this amount.

The proposed means for disposal of I^{129} by induced nuclear transmutation is by neutron capture to I^{130} which beta decays with a 12.4 hour half-life to stable Xe^{130}. The thermal neutron capture cross section for the (n,γ) reaction in I^{129} is 28 barns and the resonance integral is 50.4 barns. The remaining 15 percent of LWR iodine wastes is stable I^{127} with a thermal neutron absorption cross section of 6.2 barns and a resonance integral of 177 barns.

A schematic of the proposed system is shown in Figure 1. The 85 percent I^{129}-15 percent I^{127} mixture available directly from the fuel reprocessing plant as liquid I_2 would be enriched to 95 percent I^{129} in an isotope enrichment facility. A laser isotope separation facility would be ideally suited for such a small scale operation. The enriched I^{129} would be inserted in the core of the power-burner reactor in a suitable concentration. The I^{129} upon capturing a neutron and decaying to stable xenon isotopes, primarily Xe^{130} could be harmlessly vented to the atmosphere or sold commercially.

The specification of I^{129} enrichment is optional, but desirable from the standpoint of maximum neutron utilization for I^{129} burning. If 100 kg of unenriched iodine waste (85 percent I^{129}-15 percent I^{127}) is initially loaded for transmutation and exposed to a thermal neutron fluence such that 50 kg of I^{129} are transmuted, then about 2.6 kg of stable I^{127} are also transmuted to stable Xe^{127}. Irradiating 95 percent I^{129} enriched iodine in the same fluence results in the transmutation of 55 kg of I^{129} and only 0.9 kg of I^{127}.

The actinide transmutation system would involve loading of several waste isotopes simultaneously for transmutation. The actinide wastes considered here are the isotopes of americium and curium. The amounts of the significant isotopes present in LWR fuel wastes following a ten year decay period are shown in Table 2. The two prevalent isotopes are Am^{241} and Am^{243}. The most important isotope present in curium wastes is the 18.1 year half-life Cm^{244}. A decay interval of ten years after discharge from the reactor is reasonable to allow the wastes to cool down. Following this cool-down period the wastes would be loaded into the power-burner reactor for transmutation. After irradiation the transmuted waste would be removed from the reactor and stored to allow decay of short-lived actinides. Following this cool-down period the fission product wastes would be chemically removed and the remaining

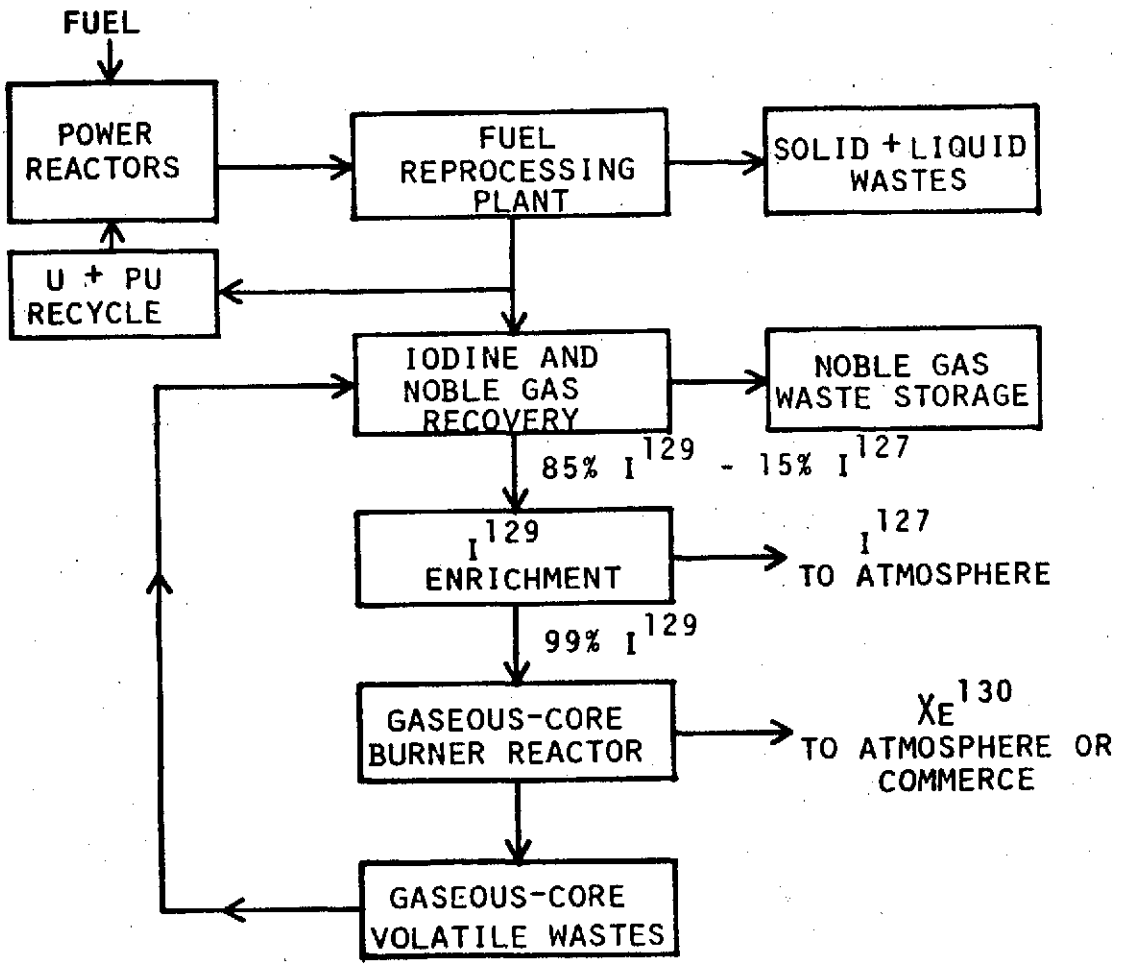

Figure 1. Pathway for I^{129} Waste Transmutation in the Gaseous-Core Reactor.

TABLE 2. RELATIVE AND ABSOLUTE AMOUNTS OF AMERICIUM AND CURIUM ISOTOPES PRESENT IN AMERICIUM AND CURIUM WASTES FROM ATLANTIC 1 REFERENCE LWR FUEL AT TEN YEARS AFTER DISCHARGE AT 33,000 MWd/MTU BURNUP

Isotope	Concentration in Spent Fuel Grams/MTU	Grams in Spent Fuel Load	Percent of Isotope Present in Element
Am^{241}	48.3	4166.84	32.37
Am^{242m}	.92	79.37	.62
Am^{242}	1.10×10^{-5}	.001	Insignificant***
Am^{243}	100	8627.0	67.01
Am^{244}	Insignificant*	Insignificant**	Insignificant***
Am^{245}	Insignificant*	Insignificant**	Insignificant***
Total Am	149.22	12873.21	100
Cm^{242}	2.21×10^{-3}	.191	Insignificant***
Cm^{243}	.0679	5.86	.28
Cm^{244}	22.1	1906.57	89.98
Cm^{245}	2.14	184.62	8.72
Cm^{246}	.251	21.65	1.02
Cm^{247}	3.31×10^{-3}	.286	Insignificant***
Cm^{248}	2.29×10^{-4}	.0198	Insignificant***
Cm^{249}	Insignificant*	Insignificant**	Insignificant***
Cm^{250}	Insignificant*	Insignificant**	Insignificant***
Total Cm	24.56	2119.20	100

*Denotes $\leq 10^{-5}$ grams/MTU.
**Denotes $\leq 10^{-3}$ grams.
***Denotes $\leq 0.1\%$.

actinides would be recycled into the next loading of waste. A schematic of the actinide transmutation system is shown in Figure 2.

THE GASEOUS-CORE NUCLEAR REACTOR CONCEPT

Gaseous-fueled, externally moderated cavity reactors have been under theoretical investigation in the United States since about 1954. The primary motivation for developing the gaseous-core reactor has been for high specific-impulse nuclear rocket propulsion. The two configurations that have received the most attention are: (1) the open cycle concept, in which the fissioning fuel is partially confined in the core by vortex-generated hydrodynamic forces, and (2) the closed cycle or nuclear light bulb concept, where the fuel is physically contained within a thin, radiation-transparent wall and recirculated for removal of fission product poisons. Uranium-235 fueled core regions ranging from 0.5 to four meters in diameter surrounded by reflector-moderator regions of practical thickness require minimum critical masses ranging from one to thirty kilograms. The critical particle densities of fissionable nuclei correspond to molecular densities of gases at less than atmospheric pressure.

Of the possible gaseous fuels enriched uranium hexafluoride is the most obvious first choice. It sublimes at 54.6°C at atmospheric pressure and remains completely in the gaseous state at temperatures below 2000°K [7]. Three gaseous-core experimental facilities have been constructed to date. A 1.5 kW(t) $U^{235}F_6$ fueled research reactor was constructed in the USSR in the late 1950s [8]. Two gaseous-core research reactors have been constructed in the United States. The most recent was a spherical gas-core critical experiment [9,10] performed in early 1970 at the National Reactor Testing Station.

The gaseous-core reactor concept has found little terrestial application to date. A recent patent disclosure [11] proposes a UF_6 fueled reciprocating

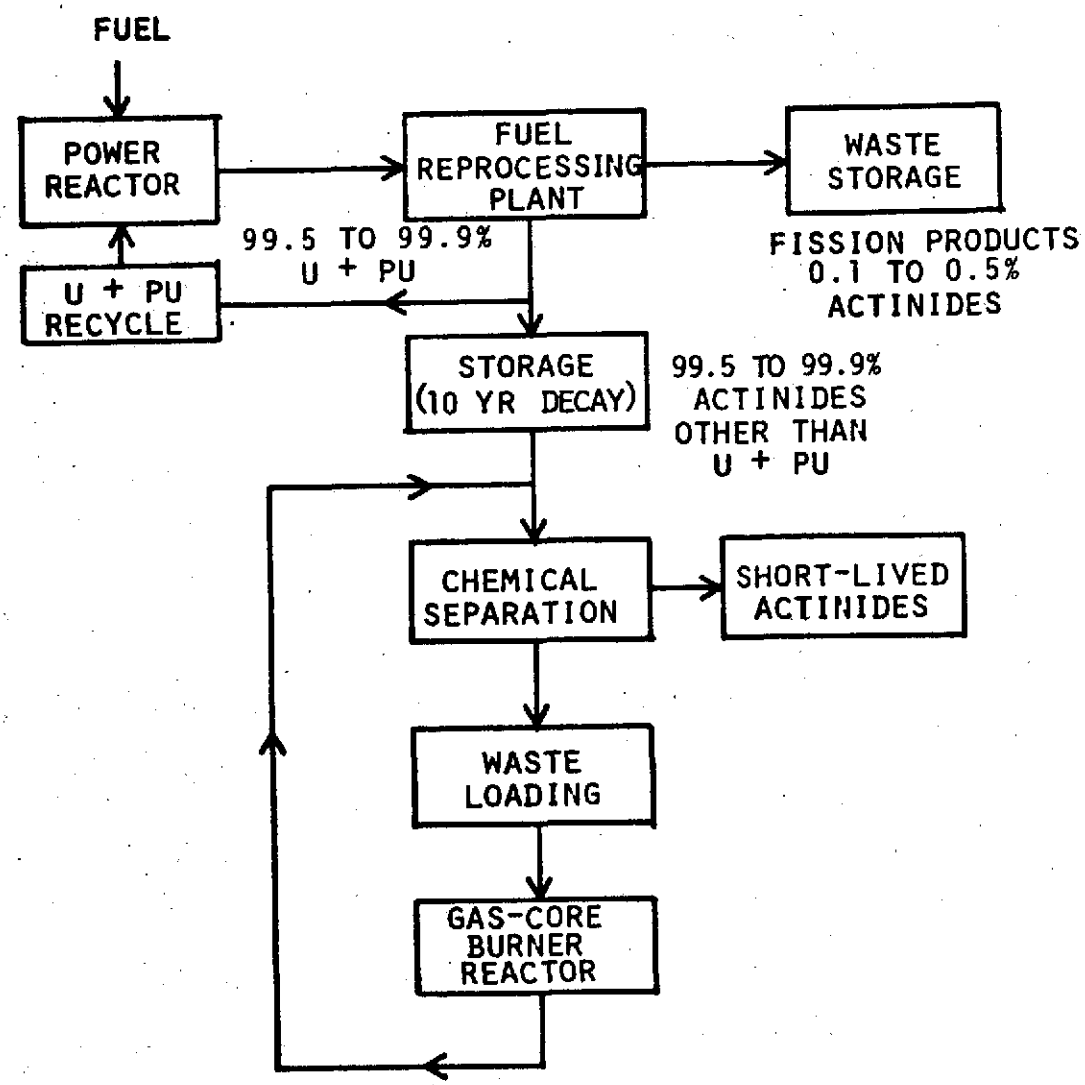

Figure 2. Pathway for Actinide Waste Transmutation in the Gaseous-Core Reactor.

engine. This pulsed nuclear reactor concept is analogous to the internal combustion engine; only the working fluid is a UF_6-He mixture and the spark plug is an artificial neutron source. A detailed analysis [12] of the concept concludes that efficiencies greater than 40 percent are attainable. An 8400 MW(e) MHD power plant design has been proposed [13] which takes advantage of the high temperatures generated in the fissioning uranium plasma. This analysis concluded that large commercial power plants using a gaseous-core nuclear heat source coupled to the MHD generator could have thermal efficiencies in excess of 70 percent. Another design study by Gritton and Pinkel [14] indicates that attractive power levels in reactors of practical size can be obtained with gas pressures and wall temperatures within the potential capability of known structural materials. For a spherical gas core reactor with a radius of 152.4 cm to generated about 4000 MW(t) would require a uranium partial pressure of about 11 atmospheres. Practical heat removal considerations with water and lithium as coolants limit power output to 200 to 1500 MW(t), respectively, for a static fuel configuration.

The Dual Purpose Gaseous-Core Power-Production, Waste Transmutation Facility

The design of such a dual purpose facility would ideally combine both the economic production of electric power with attractive rates of transmutation for radioactive waste disposal operations. This means high efficiencies and high neutron fluxes are necessary.

Figure 3 shows a schematic cross section of the proposed gaseous-core reactor. The fuel is UF_6 enriched to 6 percent U^{235}. The interior core region is four meters in diameter surrounded by a reflector-moderator of D_2O with a thickness of 500 cm. The D_2O is encased in an outer reflector of 500 cm

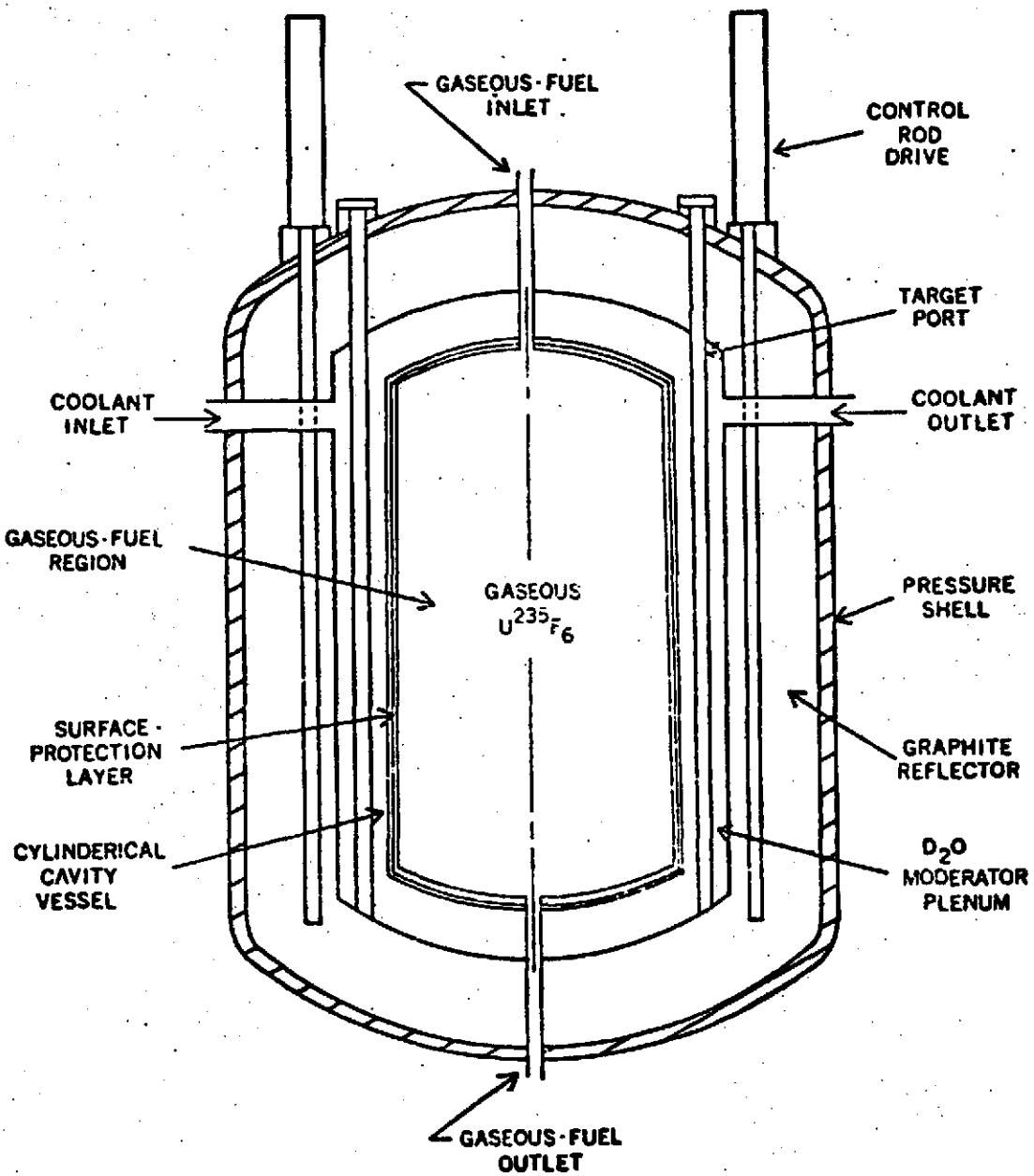

Figure 3. Gaseous-Core Power-Burner Reactor.

of reactor grade graphite. The additional outer graphite reflector is provided to return as many of the neutrons to the core as possible.

Figure 4 shows a possible flow diagram for the UF_6 gaseous-core reactor. Fuel flows through the core, and is heated internally by fission energy. The gaseous UF_6 leaves the reactor at 1800°K and 800 psi and enters the regenerator where it gives it some of its sensible heat to an intermediate helium coolant loop. The UF_6 then goes through the primary heat exchanger giving up the remainder of its sensible heat and its latent heat to the helium working fluid. From there the UF_6 liquid at 600°K enters a sump tank. Here all the volatile fission products are removed. These include Kr. Xe, fluoride compounds of iodine, and several others. Nonvolatile fission products could be removed by an on-line reprocessing stream utilizing the fluoride volatility process [15]. From the sump tank the liquid UF_6 is pumped through an evaporator at 800°K and returned to the core.

Electric power could be produced if the helium working fluid was expanded in a turbine and recirculated back to the heat exchanger. Assuming the waste heat from the UF_6-He cycle was rejected to the surroundings at 100°F (43°C) and ideal Carnot efficiency of 82.4% is obtained. This simple calculation neglects all thermodynamic irreversibilities and heat losses. The point is, however, that this high efficiency is the result of the high temperatures produced in the gaseous-core nuclear reactor. If 75% of the ideal Carnot efficiency could be achieved in practice (typical in power plant design), a system efficiency of about 65% would result. Furthermore, if 15% of the reactor power is used to circulate the gaseous fuel and working fuel this leaves an overall plant efficiency of 50%. A power plant with this efficiency would reduce the amount of heat wasted to the environment by about a factor of two over present-day power plants.

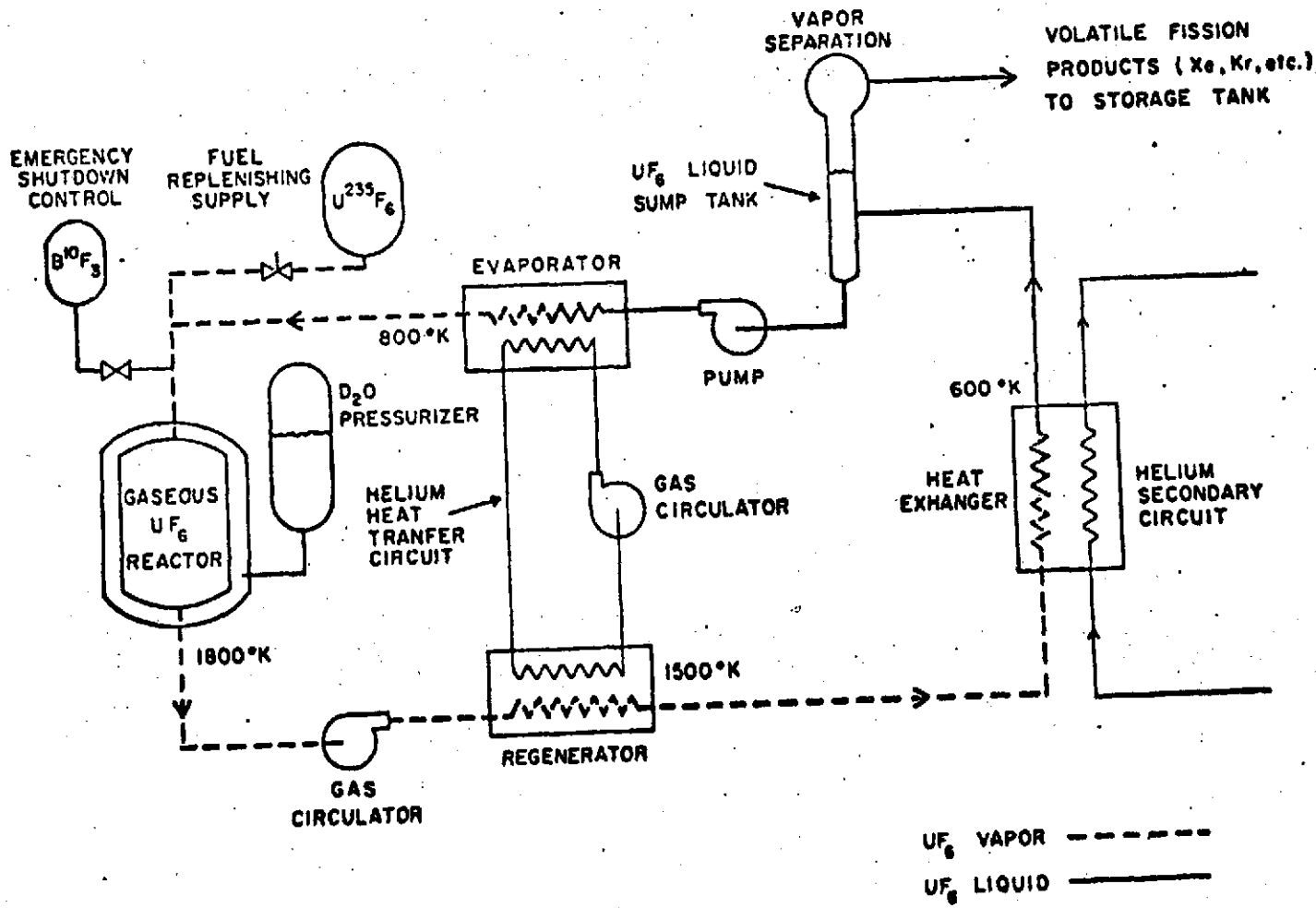

Figure 4. Schematic Diagram of Gaseous-Core Circulating Fuel System

The two meter radius core reflected by 0.5 meters of D_2O requires a minimum of 14 kg of U^{235} to maintain criticality in the cold, clean condition. Due to the buildup of fission product poisons at hot, operating conditions, additional fuel must be added to compensate for this negative reactivity effect. Thus, a mass of 140 kg of $U^{235}F_6$ (in 6% enriched UF_6) is maintained in the core at any particular instant in time. Control of excess reactivity is by means of adjustable control rods located in the graphite reflector and by the addition of burnable poisons in the D_2O. Fine reactivity control would ideally be through the use of these burnable poisons; specifically radioactive waste products such as I^{129}, continually dissolved and burned in the D_2O. The control rods would then only be used for startup and shutdown control. Further reactivity control would be aserted through the addition of burnable radioactive wastes in the 16 target ports. These ports, located a distance of 12 cm into the D_2O reflector-moderator, would be used to load and transmute actinide wastes which are not suitable for dissolution in the moderator. The large negative temperature coefficient associated with the gaseous fuel density, and the Doppler coefficient of the 6 percent enriched fuel should make the reactor both very easy to control and inherently safe. Emergency shutdown control is provided by injection of high-pressure, gaseous $B^{10}F_3$ (thermal neutron absorption cross section, 3813 barns) directly into the core.

Let us now consider the waste transmutation aspects of the proposed facility. Mention has been made of loading radioactive waste iodine-129 in the D_2O reflector-moderator and actinide wastes in the target ports of the reactor. Waste I^{129} could be loaded continuously at the same rate at which it burned up and removed from the reactor. Actinide transmutation would involve batch loading and subsequent recycle after an appropriate burnout period.

The question remains of how much radioactive waste can be loaded into the reactor. Here one would like to load the largest amount possible without poisoning the reactor out of operation. Radioactive iodine-129 added to the D_2O will primarily affect the thermal utilization factor, f. Using the known fuel composition and reactor configuration, values of f were computed for the feasible concentrations of I^{129} added to the D_2O. A maximum concentration of 2600 ppm of I^{129}, or about 425 kg, can be added to the D_2O before the reactor becomes subcritical.

The insertion of actinides into the core of the reactor will have two complicating effects; the addition of fuel (and hence neutrons) in the form of fissile $Am^{242}{}_m$, Cm^{243}, Cm^{245}, etc., and the addition of neutron-absorbing fission products during the course of neutron exposure and actinide burnup. Claiborne [4] has concluded that the effect of recycling 99.5 % of the waste actinides back into light water reactor fuels is minimal. A maximum average reactivity decrease of about 0.8 percent is attained in about five cycles through the reactor. This reactivity decrease can be counteracted by only about a 2% increase in the fissile material, which would amount to increasing the fuel enrichment about 0.1%.

Many of the actinides have substantial thermal fission cross sections, shown in Table 1 and hence, can achieve criticality if assembled in sufficient amounts. The only significant transplutonium actinide nuclides for which criticality in a thermal system could occur are Cm^{244} that contains fissile Cm^{245} and Cf^{252} that contains sufficient target precursor, Cf^{251}. Because of the very low potential critical mass of Cm^{245} ($\sim$42 g) and Cf^{251} ($\sim$10 g) the possibility of thermal criticality must be anticipated and included in the design. The published data of Clark [18] indicates that concentrations of 15 g/liter for Cm^{245} and 6 g/liter for Cf^{251} may achieve criticality in a homogeneous mixture.

Advantages and Disadvantages of the Gaseous Core Power Reactor Concept

Compared with conventional solid-core nuclear reactors the gaseous core power reactor would have several advantages. These advantages and disadvantages derive mainly from the fact that the fuel is in the gaseous state. A basically simpler internal reactor core without the need for fuel pins, cladding and spacers is possible. Elimination of fuel element fabrication costs, UO_2 to UF_6 conversion charges would result in considerable savings in the monetary and energy cost of power production. Continuous replenishing of fissile fuel and continuous removal of fission product poisons would give rise to the possibility of continuous operation with increased fuel and neutron economy. Due to its inherent low inventory of U^{238} and its high neutron flux, less actinide waste is generated by the UF_6 gas core reactor. Operating nuclear characteristics of the gas-core reactor were simulated with the ORIGEN computer code [19]. Figure 5 shows the buildup of fission product and actinide waste in the UF_6 reactor and in a typical LWR of equal power output as a function of time. After three years of continuous operation the UF_6 reactor contains about one order of magnitude less of long-lived actinide waste than the LWR. This behavior is due to the steady-state nature of refueling operations, as opposed to the "batch" fuel loading technique of present day LWRs. In addition, with continuous fuel (U^{235}) addition and removal of xenon and other volatile fission product poisons, fuel burnups of 250,000 to 300,000 MWd/MTU were obtained in the computer results. The practical disadvantages of the UF_6 gas-core reactor are primarily due to the inevitable dissociation of the fuel and its associated fluoride compounds. Specifically, they are: fuel dissociation, corrosion-limited lifetime of core and primary system components, and accountability of heavy-element by-product fluorides

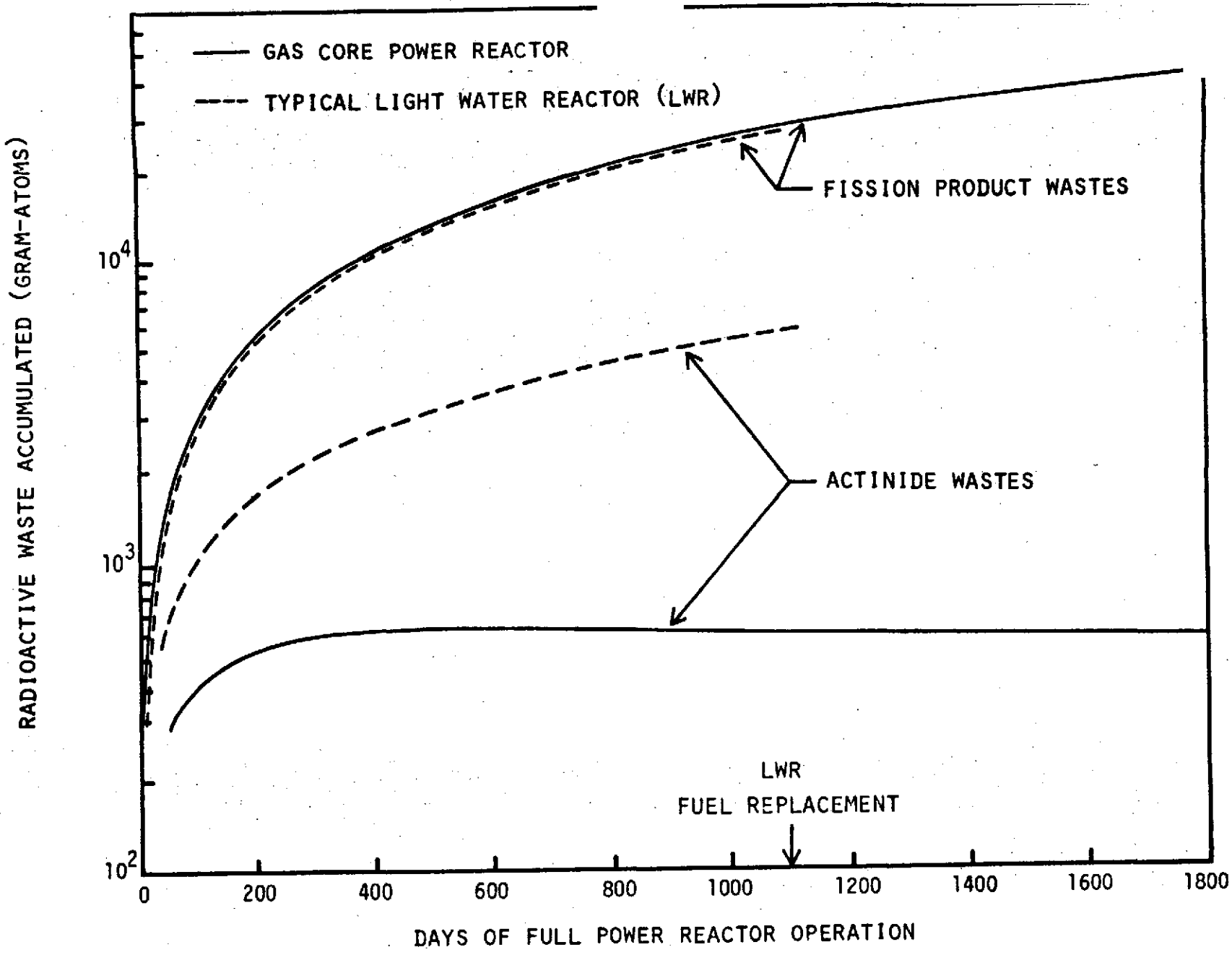

Figure 5. Comparison of Radioactive Waste Production of 3425 Mw(t) Fission Power Reactors.

in the circulating fuel system produced at high power operation. Here there is considerable experience in handling liquid fluoride salts from the Molten Salt Reactor (MSR) program. Also experience in handling UF_6 at the gaseous diffusion plants should prove extremely useful.

RESULTS AND CONCLUSIONS OF THE TRANSMUTATION STUDIES

Transmutation Rates and Reactions

The UF_6 gaseous-core reactor was chosen for this study as a neutron source because of its obvious potential for producing high neutron fluxes and generating useful power simultaneously. A reference reactor design was produced which could satisfy both of these requirements. The reactor power specified was 3425 Mw(t) which resulted in an average thermal neutron flux across the core of 6.44×10^{14} n/cm^2-sec. The ORIGEN computer code [19] was then used to study the transmutation rates of several waste isotopes present in the discharged fuel from reactors of the current LWR-type.

The waste isotopes chosen for the study were: I^{129}, Am^{241}, Am^{242m}, Am^{243}, Cm^{243}, Cm^{244}, Cm^{245}, and Cm^{246}. The amounts of the initial waste loading were determined from the composition of 20 discharged LWR fuel loads stored for a decay interval of ten years. The composition of the Am and Cm waste loading is the same as that given in Table 2. The quantities of I^{129}, Am and Cm used in the study are approximately equivalent to the waste product in 60 reactor years of operation.

In calculating rates of transmutation it is necessary to characterize the neutron energy spectrum of the reactor and the cross section dependence on spectrum for the particular target material. Thus the reaction rate depends not only on the magnitude of the neutron flux but also the shape of the neutron energy spectrum. The contribution of resonance energy neutrons to the reaction

rate is expressed by the ratio of resonance-to-thermal neutron fluxes, ϕ_{res}/ϕ_{th}.

The rates of waste transmutation were found to strongly depend on the value of ϕ_{res}/ϕ_{th}. The transmutation rate curves for I^{129} are shown in Figure 6 for three values of ϕ_{res}/ϕ_{th} in the range of interest. In this calculation the thermal neutron flux was 6.44×10^{14} n/cm^{2}sec and the initial loading is 400 kG of I^{129} (the waste I^{129} accumulated from 60 reactor-years of LWR operation). The effective neutron capture cross sections of I^{129} for the values of ϕ_{res}/ϕ_{th} = 0.058, 0.29 and 0.58 were calculated to be 20.6, 32.3 and 46.9 barns, respectively.

For the specified neutron flux of 6.44×10^{14} n/cm^{2}sec, transmutation rates of 68 kG/yr, and 77.6 kG/yr were calculated using the values of ϕ_{res}/ϕ_{th} = 0.058, 0.29, and 0.58, respectively.

The calculations for actinide transmutation were performed in a similar manner. The calculated transmutation rate curves of americium wastes for ϕ_{res}/ϕ_{th} = 0.058, 0.29, and 0.58 are shown in Figures 7, 9, and 11, respectively. The same curves for curium wastes are shown in Figures 8, 10, and 12 respectively. It should be remembered in examining these curves that the Am and Cm wastes were irradiated at the same time in the neutron flux. Furthermore, these curves are the total waste composition of the initial waste loading plus the actinide by-product waste produced by fuel burnup in the UF_6 gaseous core reactor. It was felt that this would more realistically take into account the waste produced in affecting the transmutation process itself.

The curves presented in Figures 7 through 12 can be better understood with the aid of the cross section data presented in Table 3. The capture-to-fission ratio, $\alpha = \sigma_\gamma/\sigma_f$, is important in actinide transmutation. The relative probability that a compound nucleus decays by fission is $1/(1 + \alpha)$, and the relative probability that it decays by emission of capture γ-rays is $\alpha/(1 + \alpha)$.

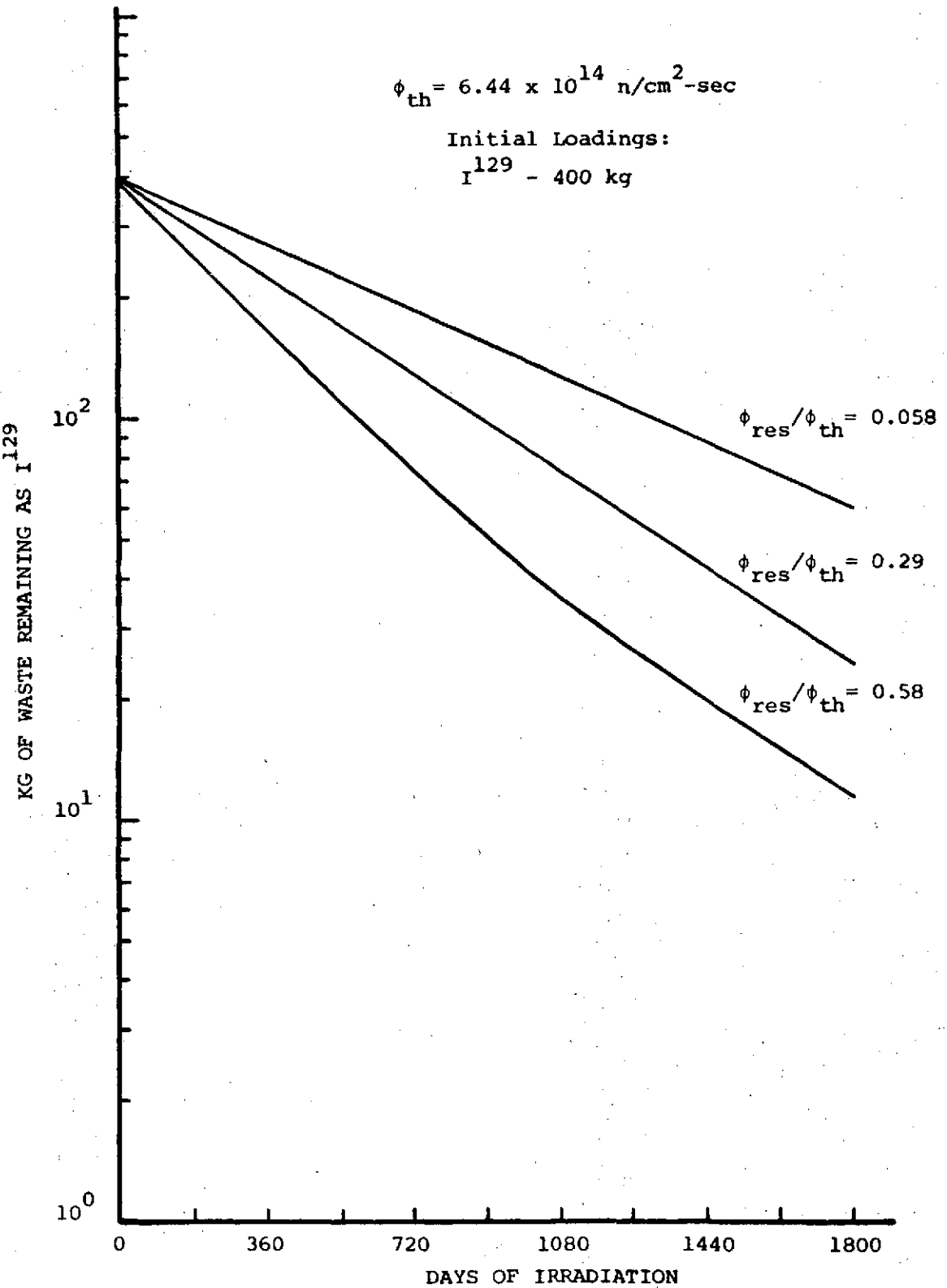

Figure 6. I^{129} waste transmutation versus irradiation time for ϕ_{res}/ϕ_{th} = 0.058, 0.29, 0.58.

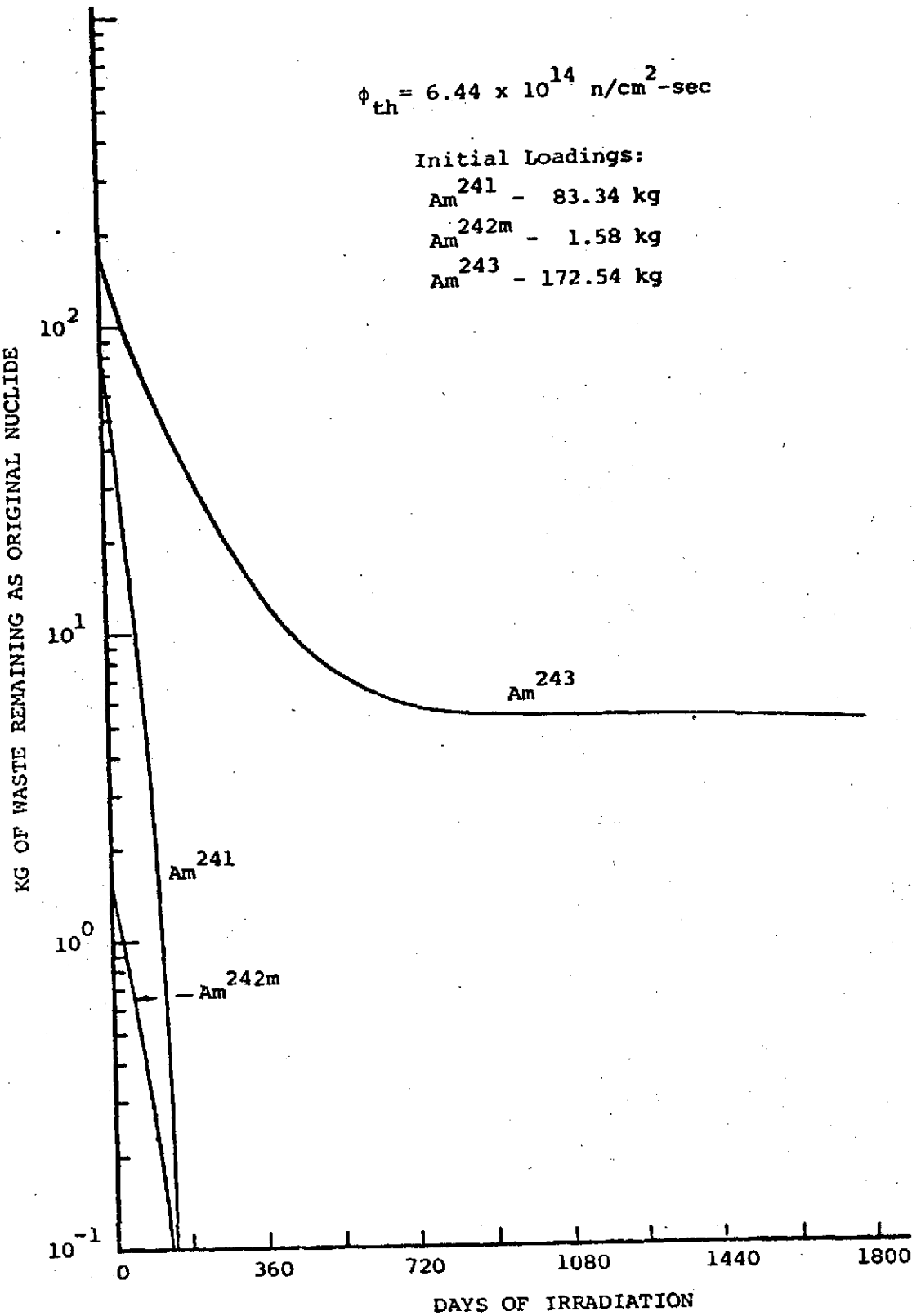

Figure 7. Americium waste transmutation versus irradiation time for ϕ_{res}/ϕ_{th} = 0.058.

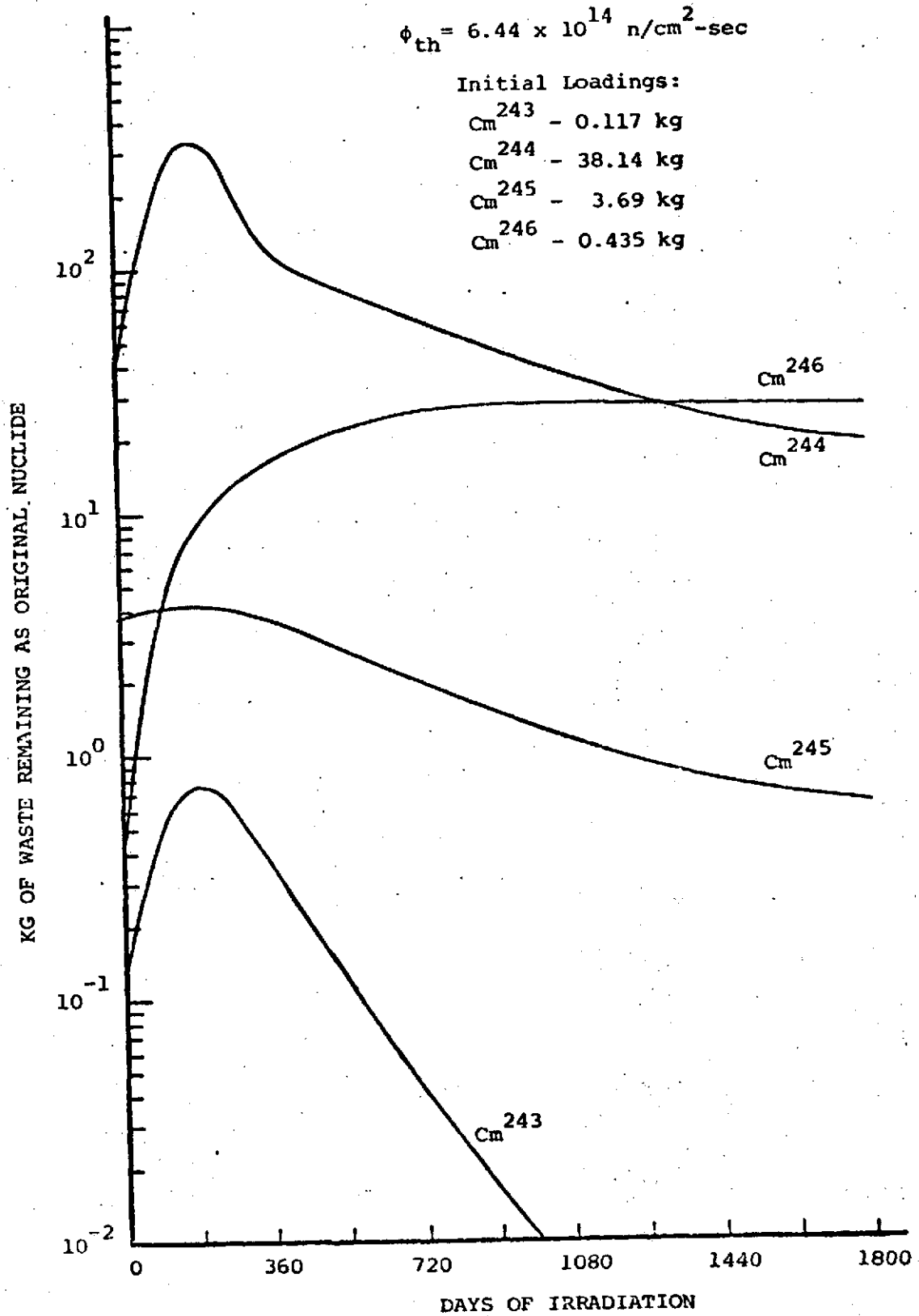

Figure 8. Curium waste transmutation versus irradiation time for ϕ_{res}/ϕ_{th} = 0.058.

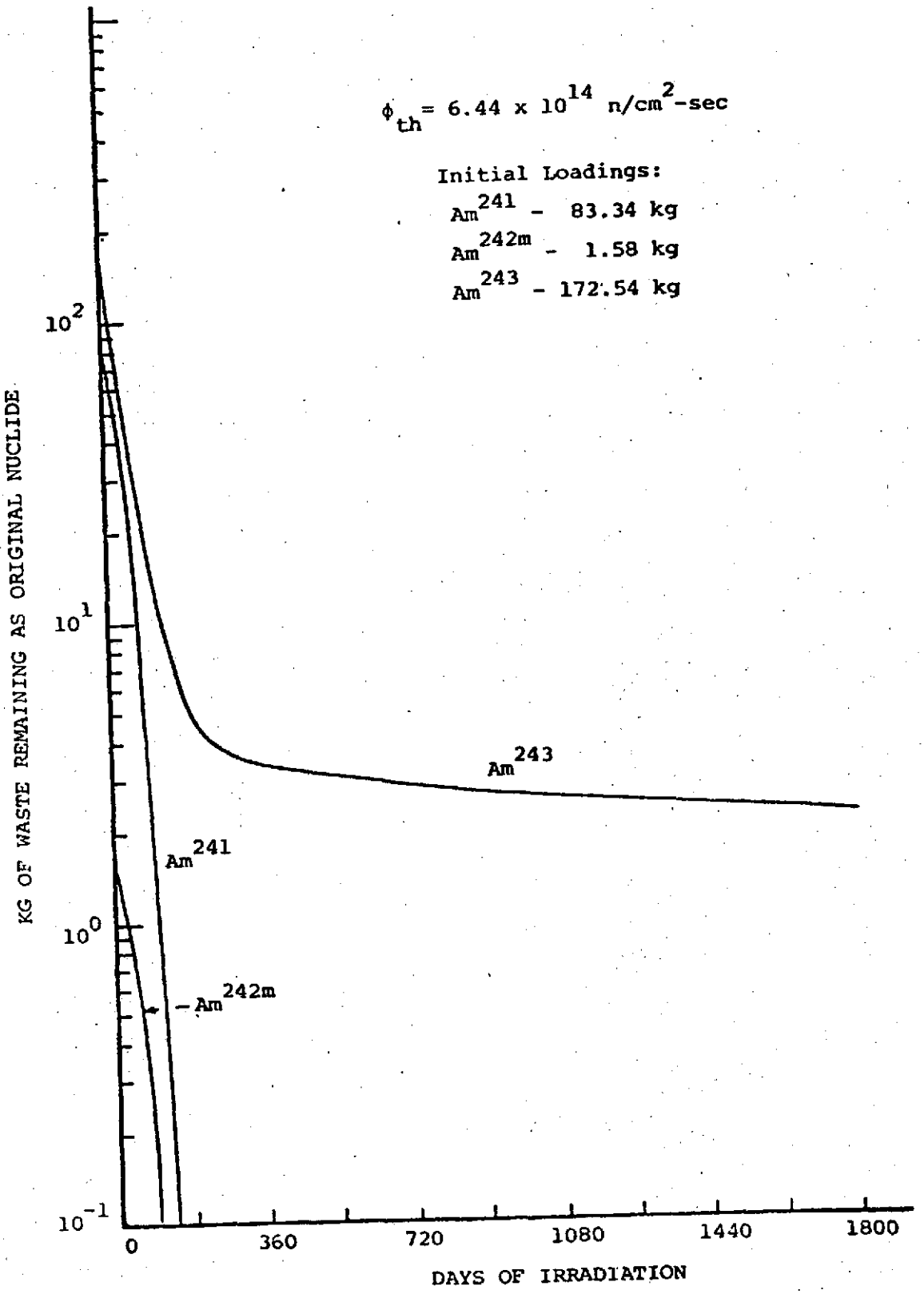

Figure 9. Americium waste transmutation versus irradiation time for ϕ_{res}/ϕ_{th} = 0.29.

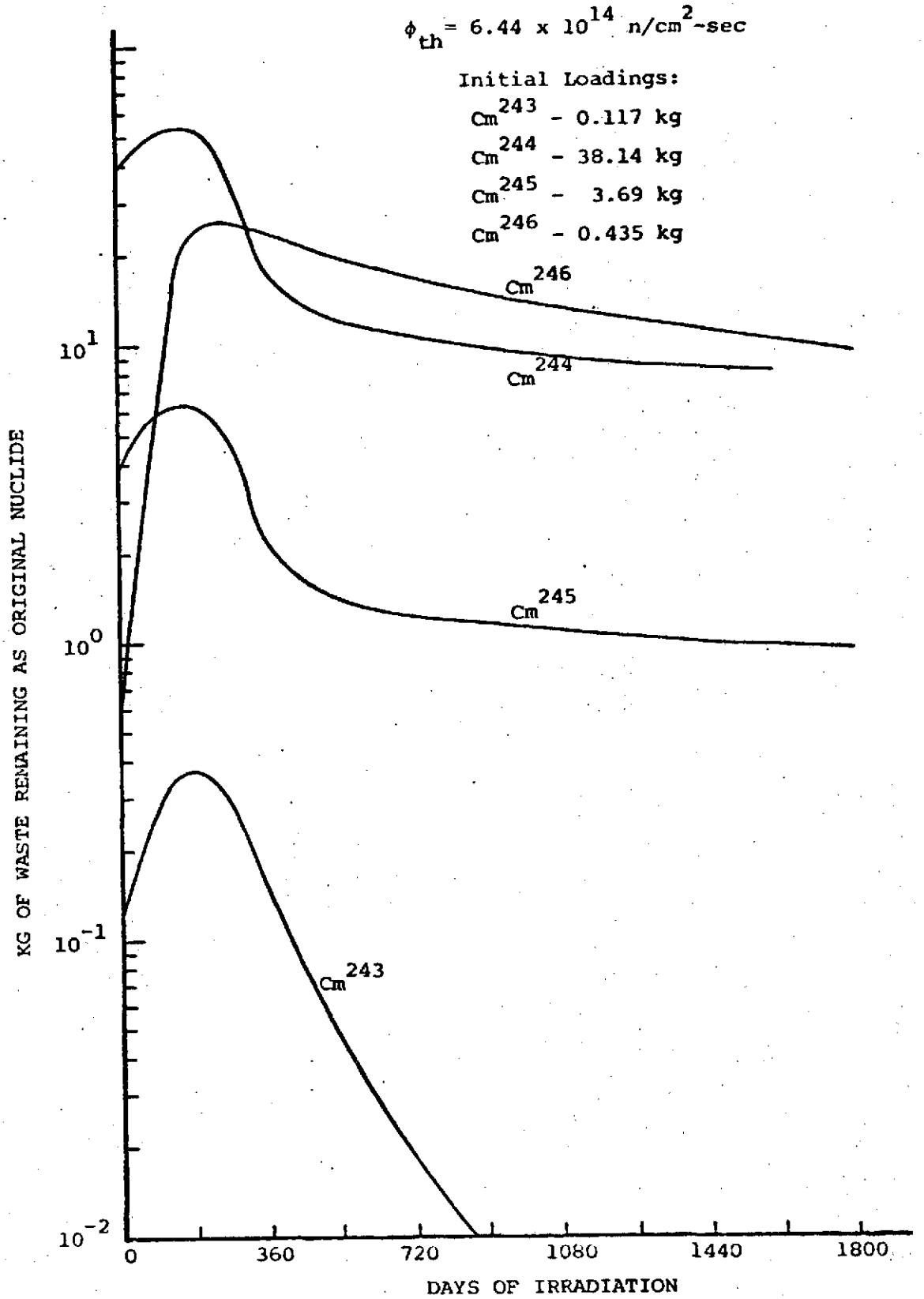

Figure 10. Curium waste transmutation versus irradiation time for ϕ_{res}/ϕ_{th} = 0.29.

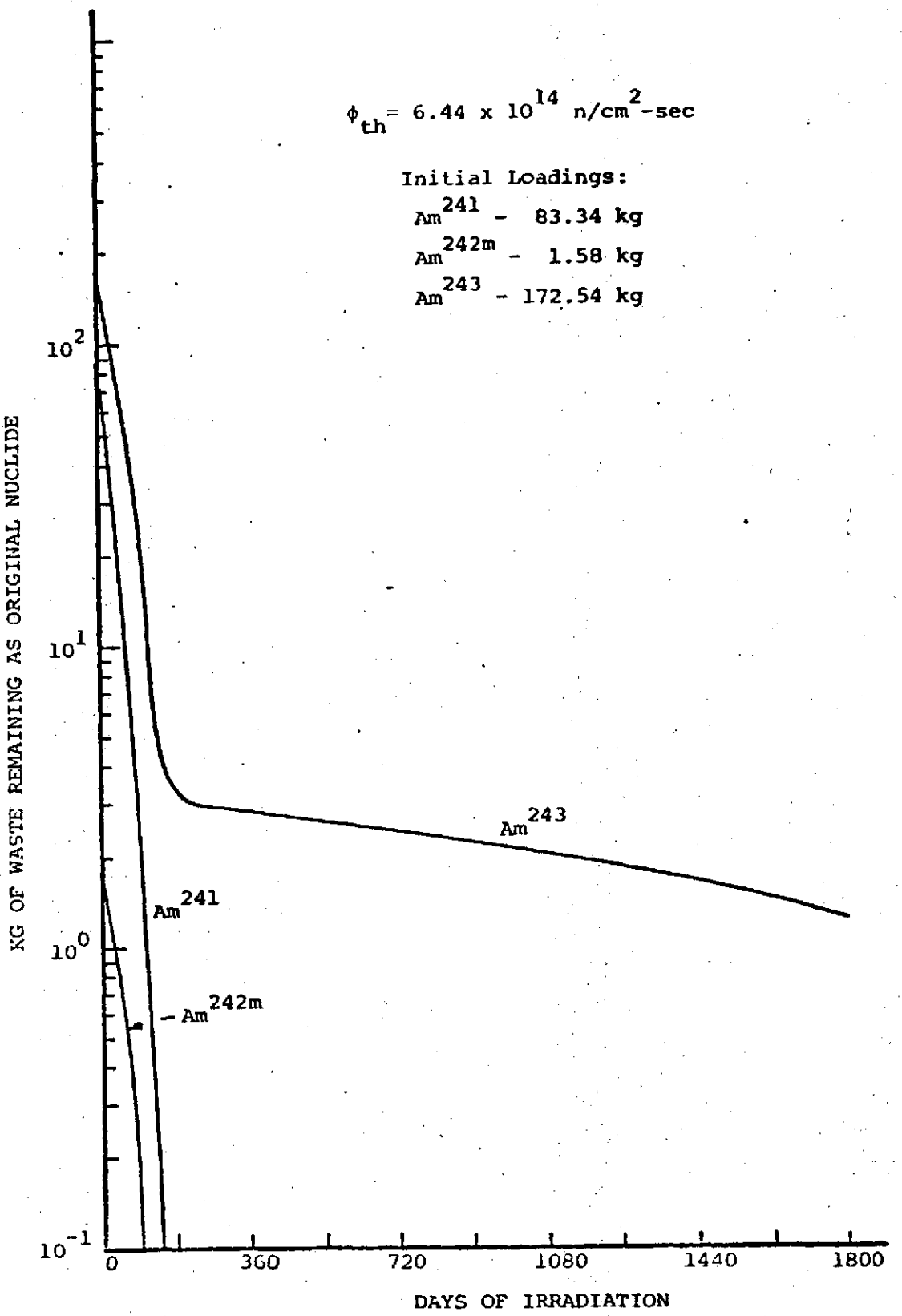

Figure 11. Americium waste transmutation versus irradiation time for ϕ_{res}/ϕ_{th} = 0.58.

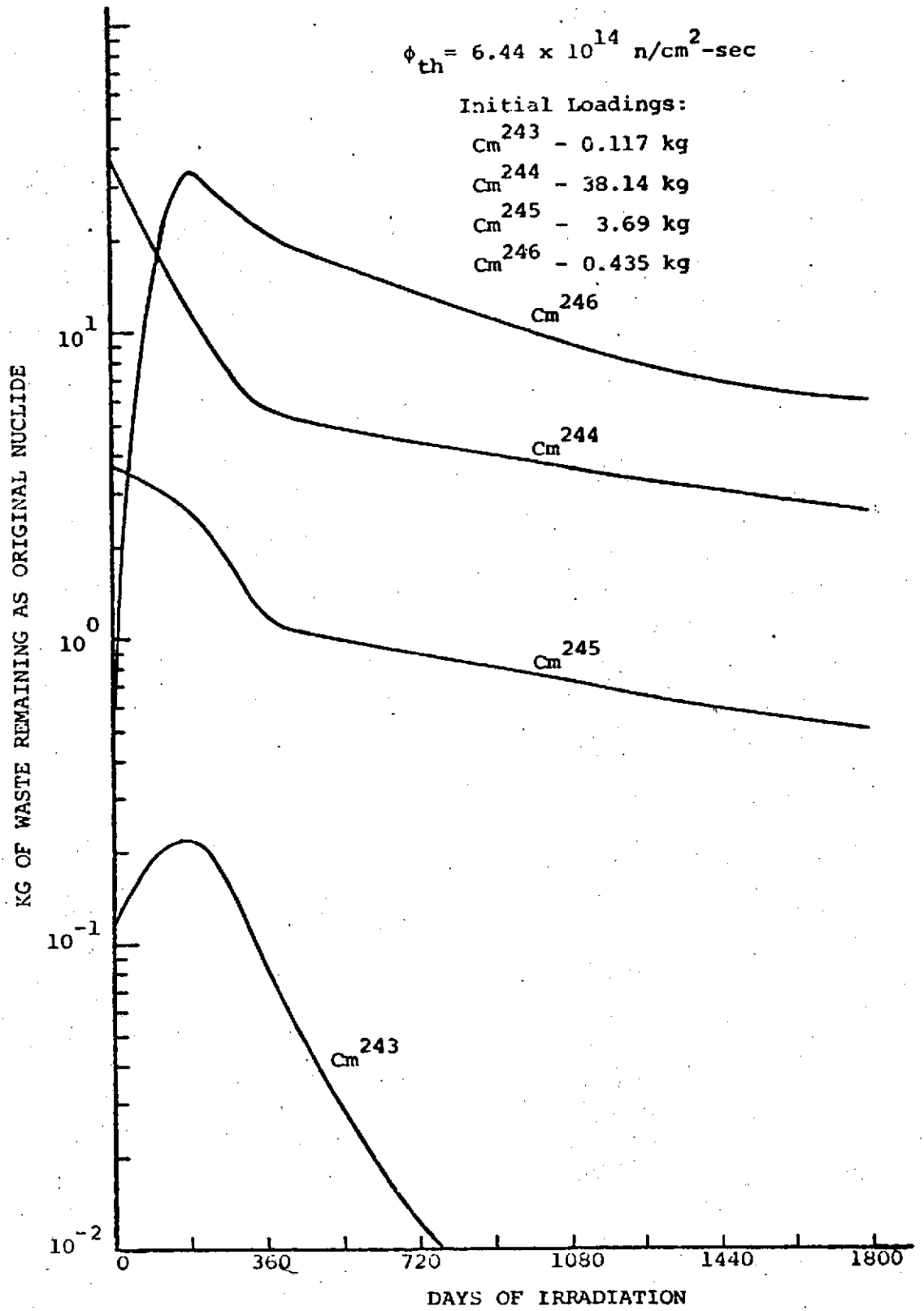

Figure 12. Curium waste transmutation versus irradiation time for ϕ_{res}/ϕ_{th} = 0.58.

TABLE 3. EFFECTIVE (n,γ) AND (n,f) CROSS SECTIONS (in barns) FOR Am AND Cm WASTE ISOTOPES FOR THREE VALUES OF RES = 0.058, 0.29, AND 0.58

Nuclide	RES = 0.058			RES = 0.20			RES = 0.58		
	σ_γ^{eff}	σ_f^{eff}	α	σ_γ^{eff}	σ_f^{eff}	α	σ_γ^{eff}	σ_f^{eff}	α
Am^{241}	707	4.17	169.5	1210	4.17	290.2	1830	4.17	438.8
Am^{242m}	1260	3780	0.33	1260	3780	0.33	1260	3780	0.33
Am^{243}	153	0.37	413.5	501	0.72	695.8	936	1.15	813.9
Cm^{243}	155	485	0.32	271	914	0.30	416	1450	0.29
Cm^{244}	44	1.48	29.7	195	4.38	44.5	383	8.01	47.8
Cm^{245}	223	1150	0.19	251	1420	0.18	286	1750	0.16
Cm^{246}	7.81	0	--	35.9	0	--	71	0	--

Thus a high value of α means a low probability of fission following neutron absorption, and conversely, a low value of α means a high probability of fission.

From the data in Table 4 the major reaction paths can be identified. The major reactions for the americium isotopes are

$$Am^{241}(n,\gamma) \begin{cases} \rightarrow Am^{242m}(n,f) \\ \rightarrow Am^{242}(n,\gamma)Am^{243} \end{cases}$$

and

$$Am^{243}(n,\gamma)Am^{244}(n,f) \ .$$

The saturation behavior of Am^{243} is due to by-product Am^{243} produced by successive (n,γ) reactions in the U^{238} present in the fuel of the reactor. The major reaction paths at the curium nuclides is not so readily identifiable. It can be said, however, that successive (n,γ) reactions on the curium isotopes are responsible for the production of significant amounts of nuclides with mass number greater than 244. The production curves for significant transmutation by-products with $A \geq 247$ is shown $\phi_{res}/\phi_{th} = 0.29$ and 0.58 in Figures 13 and 14, respectively. The by-product production curve for $\phi_{res}/\phi_{th} = 0.058$ has been omitted because the quantities of these isotopes produced in this case is at least two orders of magnitude lower than in the others.

The Effect of Transmutation on the Hazard Potential of Radioactive Wastes

The relative inhalation hazard (RIHH) and the relative ingestion hazard (RIGH), are quantative measures of the potential danger which could result from release of radioactive wastes into the environment. The success of a particular transmutation scheme can be judged in terms of the overall reduction in the values of the RIGH and RIHH following transmutation.

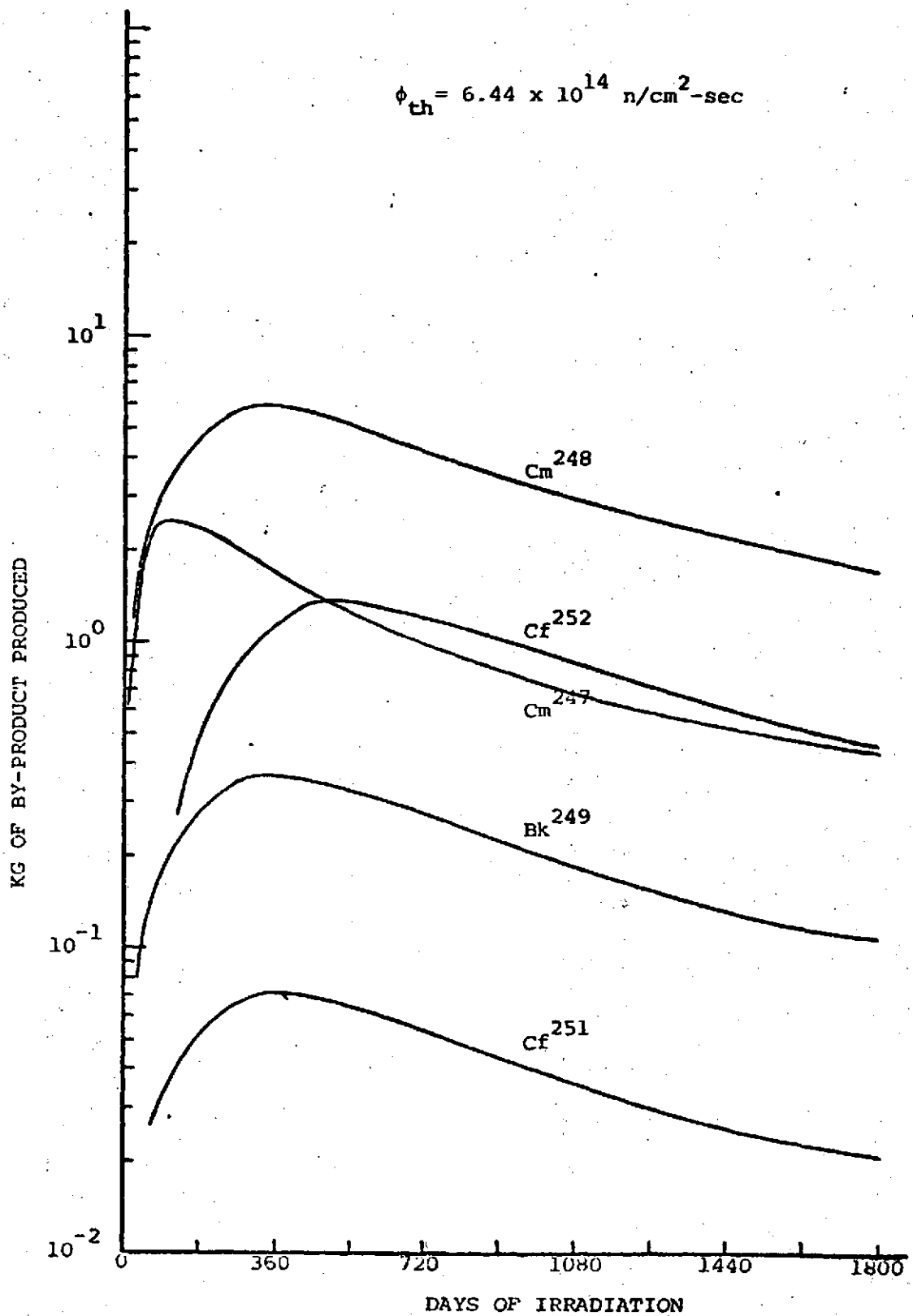

Figure 13. Transmutation by-product production versus irradiation time for ϕ_{res}/ϕ_{th} = 0.58.

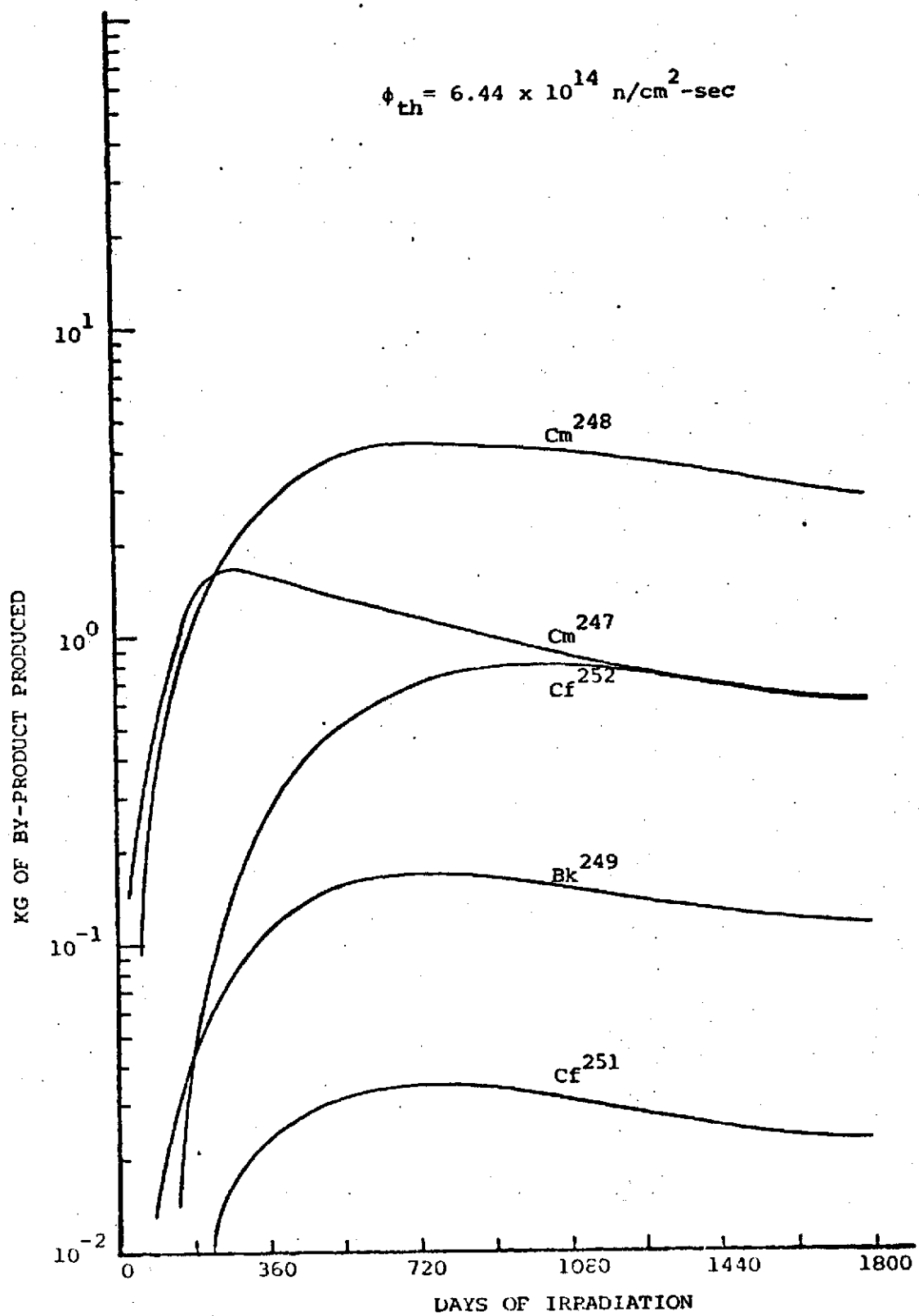

Figure 14. Transmutation by-product production versus irradiation time for ϕ_{res}/ϕ_{th} = 0.29.

The effect of transmutation on the nuclide RIHH and RIGH of I^{129} is shown in Figure 15. The first section of the abscissa of this figure represents the reduction in the hazard measure due to the five year irradiation at $\phi_{th} = 6.44 \times 10^{14}$ n/cm^{2}sec for the three values of ϕ_{res}/ϕ_{th}. No significant reduction in the hazard measure occurs after irradiation due to the 15.9×10^6 year half-life of I^{129}. The top curve in this figure shows the hazard measure of I^{129} with no transmutation after fuel reprocessing. In the case of I^{129} the curves shown represent the total hazard measure since no by-products with significant radioactivity are made from the initial loading of I^{129}.

Figures 16 and 17 show the effect of transmutation on the total actinide RIHH and RIGH, respectively. The first section of the abscissa of these figures represents the reduction in the total actinide hazard measure resulting from transmutation of the quantities of americium and curium waste described in Figures 7 through 12. The three lower curves in Figures 16 and 17 are the hazard measure of the transmuted actinides (including by-products) plus the hazard measure of the burned nuclear fuel with 99.5 percent of the U and Pu removed at the end of the five year irradiation. The upper curve in both figures represents the hazard measure of all actinides (with 99.5 percent of the U and Pu removed) generated in 60 reactor-years of LWR operation. The differences in the shape of these curves represent the varying isotopic compositions of the irradiated and unirradiated wastes.

Economic Considerations for Transmutation of Radioactive Wastes

The cost of neutron-induced transmutation of radioactive waste is primarily the cost of producing neutrons. The major factors which govern the cost of neutrons are: reactor fuel and associated costs; plant depreciation including interest charges; and salaries, taxes, maintenance and general

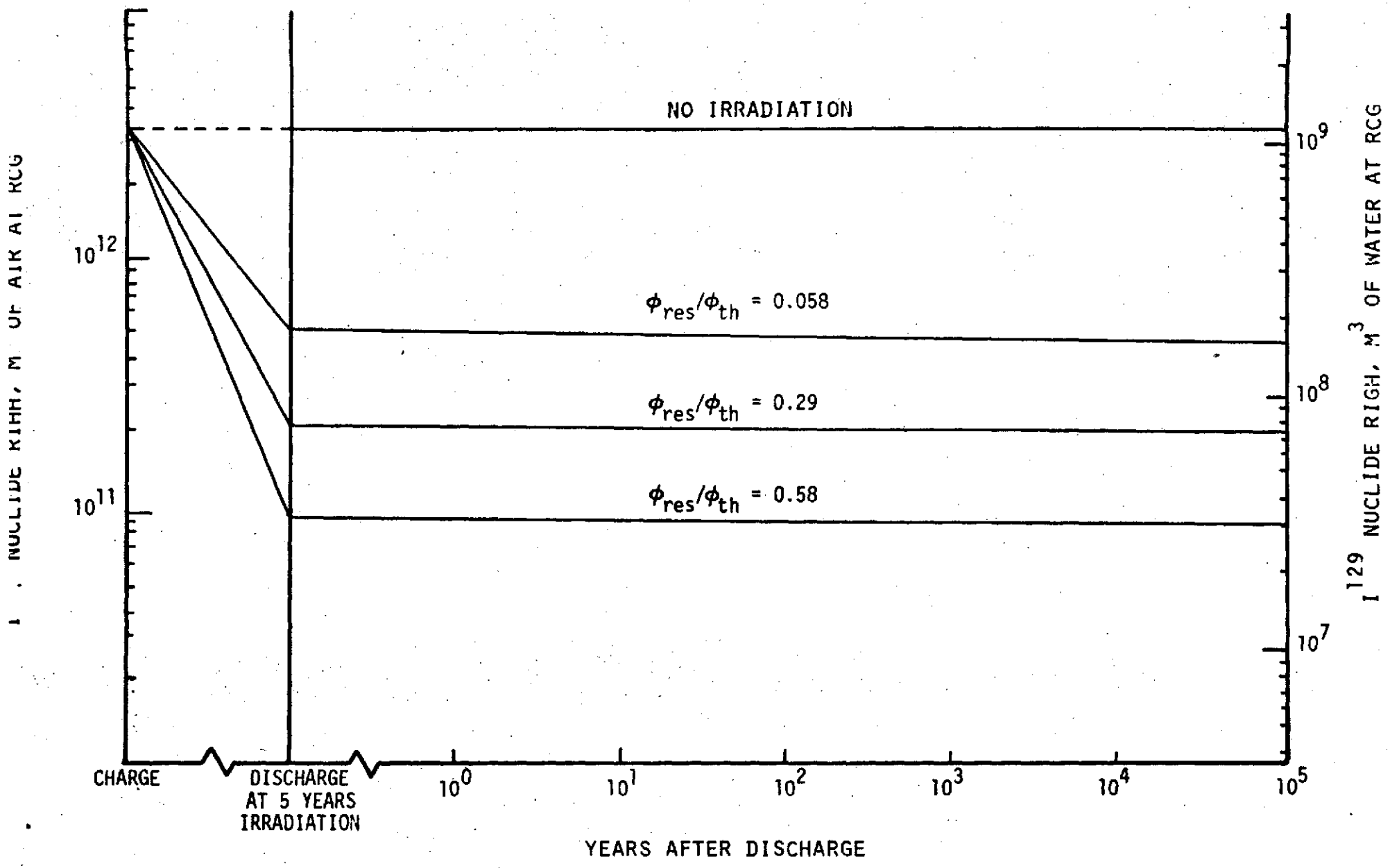

Figure 15. Iodine-129 Hazard Reduction Following Transmutation.

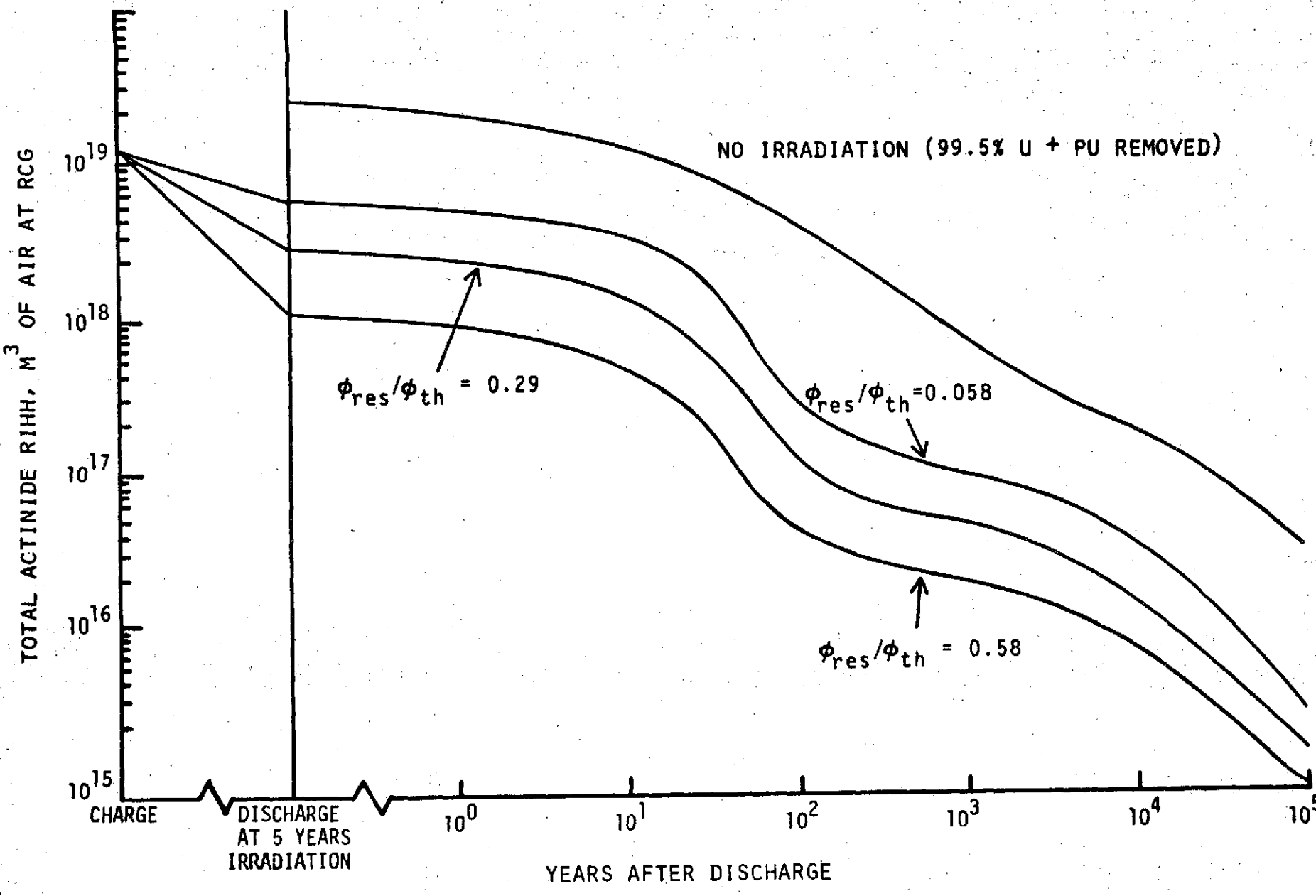

Figure 16. Total Actinide RIHH Reduction Following Transmutation of Am and Cm Wastes.

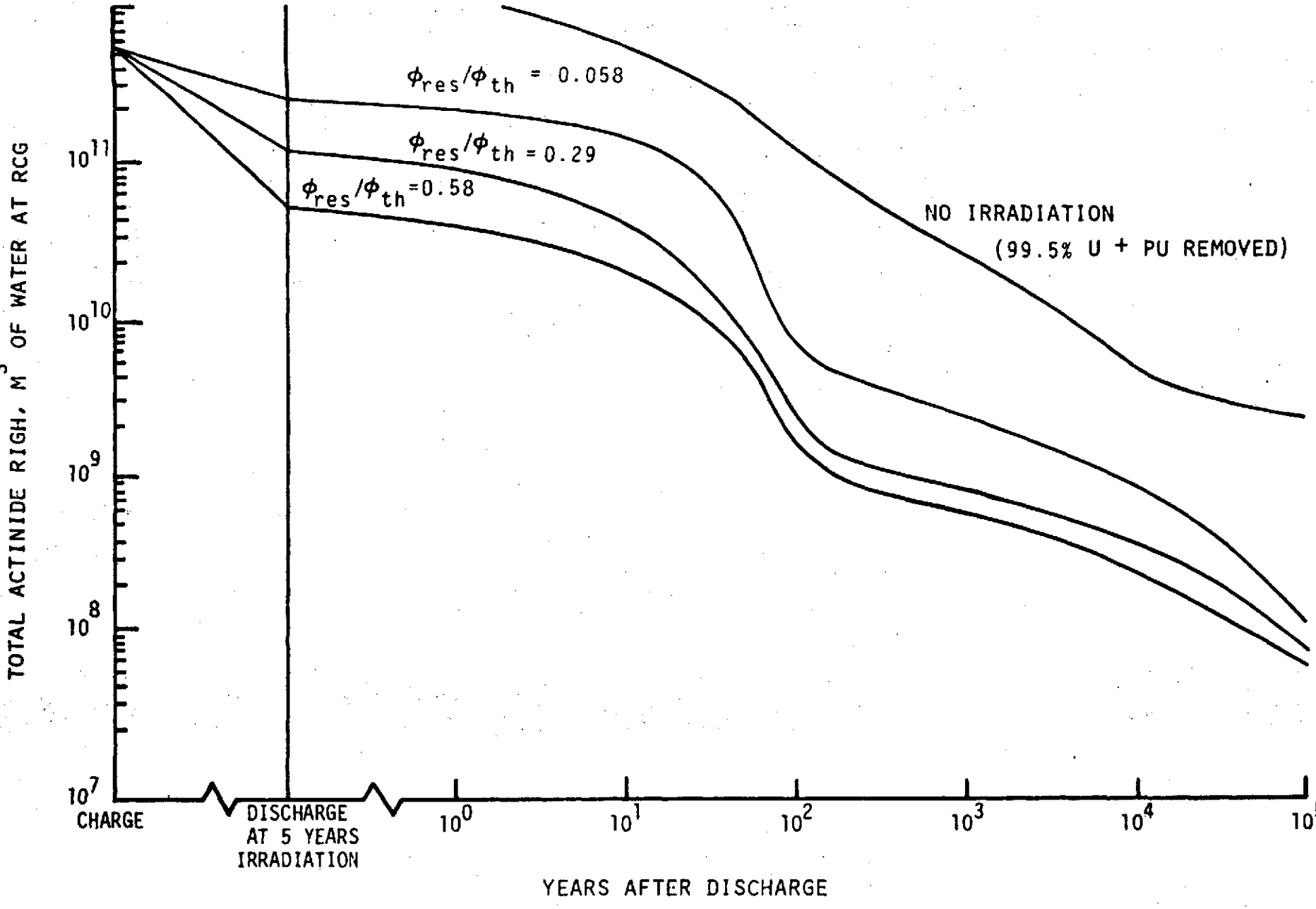

Figure 17. Total Actinide RIGH Reduction Following Transmutation of Am and Cm Wastes.

operating costs. The cost of transmutation would also be a function of plant output because the sum of the plant costs listed above would remain fairly constant over a wide range of output, with fuel costs being the major variant. Plant output is determined by: reactor power, operating efficiency, and neutron utilization.

For large-scale transmutation of radiactive wastes in the 1980s and beyond, the price of target material will be determined primarily by costs associated with chemical separation from power reactor fuel residues. Estimates of unit recovery costs extrapolated to the mid-seventies for actinide targets and fission products are listed below [20]:

Comparison of Chemical Recovery Costs

Actinide Targets		Fission Targets	
$Am^{241,243}$	∿\$31/g	Cs^{137}	∿\$10/g
$Cm^{242,244}$	∿\$81/g	Sr^{90}	∿\$16/g
		I^{129}	∿\$10/g

As available quantities increase in the late seventies, and if a need for recovery of these materials is established, unit recovery costs could be reduced further.

Aside from developmental costs, several economic factors are in favor of the UF_6 gaseous-core reactor for use as a duel-purpose power reactor-transmutation facility. Fabrication of power reactor fuel elements accounts for about 40 percent of the total fuel cost [21] and chemical processing for about another 15 percent. Elimination of fuel fabrication costs and reduction in chemical processing costs could lower fuel costs by 45 to 50 percent of the UF_6 reactor. Increased operating efficiency resulting from continuous operation and increased neutron utilization resulting from continuous removal of

fission product poisons could result in lower neutron costs than other reactor concepts. If salable power is generated in the reactor the assigned neutron cost could be lower still.

Conclusions and Recommendations

This study has attempted to ascertain the feasibility of nuclear transmutation in a UF_6 gaseous-core reactor. Some specific conclusions were obtained in the limited time available. Transmutation of I^{129} by a five-year exposure to a thermal neutron flux of 6.44×10^{14} $n/cm^2 sec$ results in nearly order-of-magnitude reductions in the waste inventory of this nuclide. This reduction in inventory results in an order of magnitude decrease in the hazard potential of fission product waste I^{129}. A five-year transmutation of americium and curium wastes produces order-of-magnitude decreases in the overall hazard potential of actinide wastes generated in 60 reactor-years of LWR operation. The actinide results are in approximate agreement with those obtained by Claiborne [8]. It was found in this study that increased values of the resonance-to-thermal flux ratio, ϕ_{res}/ϕ_{th}, resulted in increased rates of transmutation and increased reductions in hazard potential for both I^{129} and the actinides. A rough breakdown of transmutation costs seems to indicate that the UF_6 reactor could be competitive with other transmutation reactor concepts.

Any study which attempts to determine the feasibility of a concept generally raises more questions than it answers. Several questions were raised during the course of this study.

> Would recycling previously transmuted wastes accomplish further decreases in the hazard measure of actinide wastes?
>
> What is the effect of varying the irradiation time on the inventory or hazard potential of actinide wastes, i.e., would three years irradiation accomplish the same effect as five years irradiation?

The technique of induced transmutation requires further study. Other long-lived isotopes should be examined for feasibility for the transmutation process. One such isotope which may prove feasible is 2.13×10^5 year Tc^{99}. It is present in significant quantities in fission product wastes and has a 22 barn thermal neutron capture cross section and a 92 barn resonance integral. Further investigation into the process of neutron-induced transmutation may lead to realization of a practical method for disposal of long-lived radioactive wastes.

LIST OF REFERENCES

1. M. Steinberg, G. Wolzak and B. Manowitz. Neutron Burning of Long-Lived Fission Products for Waste Disposal," BNL-8558, Brookhaven National Laboratory (1964).

2. W.C. Wolkenhauer. "The Controlled Thermonuclear Reactor as a Fission Product Burner," BNWL-1695 Battelle Pacific Northwest Laboratories, pp. 33-52 (1972).

3. B.F. Gore and B.R. Leonard, Jr. "Transmutation of Massive Loadings of Cesium-137 in the Blanket of a Controlled Thermonuclear Reactor," Nucl. Sci. Eng., Vol. 53, pp. 312-323 (1974).

4. H.C. Claiborne. "Neutron-Induced Transmutation of High-Level Radioactive Waste," ORNL-TM-3964, Oak Ridge National Laboratory (1972).

5. C.E. Bemis, Jr., R.E. Druschel, J. Halperin and J.R. Walton. "Thermal-Neutron Capture Cross Section and Resonance Integral for 10.7-Year Krypton-85," Nucl. Sci. Eng., Vol. 47, p. 371 (1972).

6. J.D. Clement and J.R. Williams. "Gas-Core Reactor Technology," Reactor Tech., Vol. 13, p. 266 (1970).

7. H.A. Hassan and J.E. Deese. "Thermodynamic Properties of UF_6 at High Temperatures," N.C. State University, Raleigh, N.C. (1973).

8. K. Kikoin et al. "Experimental Reactor with Gaseous Fissionable Substance (UF_6)," Soviet J. At. Energy, Vol. 5, p. 1167 (1958).

9. J.H. Lofthouse and J.F. Kunze. "Spherical Gas-Core Reactor Experiment," NASA-CR-72781, National Aeronautics and Space Administration (1971).

10. J.F. Kunze, J.H. Lofthouse and C.G. Cooper. "Benchmark Gas-Core Critical Experiment," Nucl. Sci. Eng., Vol. 47, pp. 59-65 (1972).

11. R.T. Schneider and M.J. Ohanian. Patent Disclosure, University of Florida (January 1970).

12. E.T. Dugan and N.J. Diaz. "Pulsed-Gaseous-Core Reactor Power Plants," Presented at 1974 ANS Winter Meeting, Washington, D.C., October 27-31, 1974.

13. J.R. Williams and S.V. Shelton. "Gas-Core Reactors for MHD Power Systems," Research on Uranium Plasmas and Their Technological Applications, NASA-SP-236, pp. 3430350 (1970).

14. E.C. Gritton and B. Pinkel. "The Feasibility of the Gaseous-Core Nuclear Reactor for Electric-Power Generation," RM-5721-PR, The Rand Corporation (1969).

15. S. Lawroski. "Survey of Separations Processes," Proc. Second U.N. Conf. Geneva, Vol. 4, pp. 575-582 (1958).

16. G. Safonov. "Externally Moderated Reactors," R-316, The Rand Corporation (1957).

17. J.R. Lamarsh. Nuclear Reactor Theory. Addison-Wesley Publishing Company, Inc.: Reading, Mass., p. 283 (1966).

18. H.K. Clark. "Critical Masses of Fissile Transplutonium Isotopes," Trans. Amer. Nucl. Soc., Vol. 12, p. 886.

19. M.J. Bell. "ORIGEN--The ORNL Isotope Generation and Depletion Code," ORNL-4628, Oak Ridge National Laboratory (1973).

20. W.A. Rodger. "Multipurpose Plant for the Recovery of Neptunium and Other Isotopes," report prepared for New York State Atomic and Space Development Authority (1967).

21. G.W. Beeman, Nucl. News, Vol. 10, No. 2, p. 23 (1967).